ISTANBUL TECHNICAL UNIVERSITY ★ GRADUATE SCHOOL OF SCIENCE ENGINEERING AND TECHNOLOGY

NUMERICAL MODELLING ON BEHAVIOR OF FLEXIBLE UNDERGROUND PIPELINES UNDER SEISMIC LOADS

M.Sc. THESIS

Ehsan YAHYAVI ZANJANI

Department of Civil Engineering

Soil Mechanics and Geotechnical Engineering Programme

JUNE 2016

ISTANBUL TECHNICAL UNIVERSITY ★ GRADUATE SCHOOL OF SCIENCE ENGINEERING AND TECHNOLOGY

NUMERICAL MODELLING ON BEHAVIOR OF FLEXIBLE UNDERGROUND PIPELINES UNDER SEISMIC LOADS

M.Sc. THESIS

Ehsan YAHYAVI ZANJANI
(501111322)

Department of Civil Engineering

Soil Mechanics and Geotechnical Engineering Programme

Thesis Advisor: Y.Doç. Dr. Esra Ece BAYAT
Thesis Co.Advisor: Y.Doç. Dr. Hakki Oral ÖZHAN

JUNE 2016

İSTANBUL TEKNİK ÜNİVERSİTESİ ★ FEN BİLİMLERİ ENSTİTÜSÜ

SİSMİK YÜKLER ALTINDA GÖMÜLÜ ESNEK BORULARIN DAVRANIŞI ÜZERİNE SAYISAL MODELLEME

Yüksek Lisans Tezi

Ehsan YAHYAVI ZANANI
(501111322)

İnşaat Mühendisliği Anabilim Dalı

Zemin Mekaniği ve Geoteknik Mühendisliği Lisansüstü Programı

Tez Danışmanı: Y.Doç. Dr. Esra Ece BAYAT
Tez Eş Danışmanı: Y.Doç. Dr. Hakki Oral ÖZHAN

HAZİRAN 2016

Ehsan Yahyavi Zanjani a M.Sc. student of ITU Institute of Science student ID 501111322, successfully defended the thesis entitled "NUMERICAL MODELLING ON BEHAVIOR OF FLEXIBLE UNDERGROUND PIPELINES UNDER SEISMIC LOADS ", which he prepared after fulfilling the requirements specified in the associated legislations, before the jury whose signatures are below.

Thesis Advisor :   **Y.Doç. Dr. E. Ece BAYAT**   ....
Istanbul Technical University

Thesis Co.Advisor : **Y.Doç. Dr. Hakki. Oral ÖZHAN**   ....
Istanbul Kemerburgaz University

Jury Members :   **Prof.Dr. Mehmet BERİLGEN**   ....
Istanbul Yildiz Technical University

Doç. Dr. Aykut ŞENOL   ....
Istanbul Technical University

Y.Doç. Dr. Berrak TEYMÜR   ....
Istanbul Technical University

Date of Submission : 2 May 2016
Date of Defense   : 9 June 2016

To my dear family,

FOREWORD

I would like to take this opportunity to thank many people for their support and contribute toward the completion of this dissertation. First, I would like to express my sincere appreciation to my dear advisor, Dr. Esra Ece BAYAT, for her patience, motivation, enthusiasm, immense knowledge and continuous guidance and support throughout my program of study and this research work. Also my dear co-advisor Dr.Hakki ÖZHAN for providing proper condition to use the program and also for his consultants during the thesis proces.

My sincere gratitude goes to my committee members Prof.Dr. Mehmet BERİLGEN, Dr. Aykut ŞENOL and Dr. Berrak TEYMÜR. My sincere appreciation is to Prof.Dr. Mehmet BERİLGEN for technical support and providing the field work data in PLAXIS program and his support during the research period.

I would like to thank my parents, who support me not only during my dissertation but also during my whole life. Also I thank my brother and sister for their great love and encouragement. At the end, many thanks to my dear friend Mazdak SADEGHPOUR for his help and support.

June 2016   Ehsan YAHYAVI ZANJANI
                                                          (Geotechnical Engineer)

TABLE OF CONTENTS

ABBREVIATIONS

FEA	: Finite Element Analyses
FEM	: Finite Element Method
HDPE	: High Density Polyethylene
$\mathbf{K_1}$	: Lateral Soil Coefficient
L	: Longitudinal Length of the PGD Zone
$\mathbf{L_a}$	: Anchor Length
M	: Earthquake Magnitude
PGA	: Peak Ground Acceleration
PGD	: Permanent Ground Deformation
PGV	: Peak Ground Velocity
$\mathbf{P_{uplift}}$	: The Uplift Force per Unit Length
W	: Width of PGD Zone
$\boldsymbol{\delta}$	: Amount of PGD Movement
$\boldsymbol{\delta_f}$	: Fault displacement

LIST OF TABLES

LIST OF FIGURES

NUMERICAL MODELLING ON BEHAVIOR OF FLEXIBLE UNDERGROUND PIPELINES UNDER SEISMIC LOADS

SUMMARY

In this study, a numerical calculation on interaction between soil and flexible pipelines was performed. Properties of soil and pipe may cause significant effects on the movements of buried pipelines. Generally, Earthquakes damage the buried pipes and facilities in two forms: (1) Permanent Ground Deformation (PGD) and (2) Wave Propagation.

In this research the behavior of buried pipes under the harmonic and the earthquake loads using 2D finite element software PLAXIS by investigating acceleration, displacement, PSA (pseudo-acceleration response spectrum) and also axial force, bending moment and shear force in different soil conditions for the soils in the bottom layer of the pipe (bedding) and also the soil surrounding the pipe has been modeled and investigated.

In order to verify the results of PLAXIS, acceleration and displacement values computed by PLAXIS were compared by the same parameters generated by the 1D software DEEPSOIL in the equal condition of soil and depth and under the equal Harmonic Loads where the little difference in the results was due to the fact that DEEPSOIL is 1D and needs more input parameters than PLAXIS. In this study, a model with the dimension of 10m x 10m containing bedding soil with the thickness of 8.0 meters and trapezius-shape layer as the backfill surrounding the pips with the thickness of 2.0 meters and the bases of 1.5 m and 2.5 m at the top and the bottom respectively where two types of soil namely dense and loose were applied.

The material of the modeled pipe was Polyethylene with the diameter of 400 mm and the wall thickness of 12 mm at the depth of 2.0 m where for the more precise investigation of the pipe behavior under the dynamic loads, 3 points on the periphery of the pipe and 3 points on the model bedding (wave entrance) top of the model at the ground surface and also at the free field were considered.

It is concluded that the maximum horizontal displacement values for all soil position, (different bedding and backfill) are approximately the same. However, for the points located on the pipe, there is more displacement for the point located just on the bedding, compared with the points located in other positions.

The maximum horizontal displacement values for all soil position, (different bedding and backfill) are approximately the same. However, for the points located on the pipe, there is more displacement for the point located just on the bedding, compared with the points located in other positions, when the vertical displacement in loose sand is significant, regardless of the backfill materials (nearly four times more than dense value). It can be said that any increase in the bending moment, above the level of maximum allowable moment, can cause failure in the pipe. This is while axial force and shear force do not have significant effect in pipe failure.

The amount of strain as an important factor in the assessment of the behavior of the pipes buried under the effect of dynamic weights, based on the figures indicated in the PLAXIS application, the study can conclude that the level of horizontal and vertical strain in loose sand is higher than that of dense sand.

SİSMİK YÜKLER ALTINDA GÖMÜLÜ ESNEK BORULARIN DAVRANIŞI ÜZERİNE SAYISAL MODELLEME

ÖZET

Bu çalışmada, zemin ve esnek boru hatları arasındaki etkileşim üzerine bir sayısal analiz yapılmıştır. Zemin ve boru özellikleri, gömülü boru hatlarının hareketleri üzerinde önemli etkilere neden olabilir. Dinamik yüklemeye maruz boru hatlarının davranışını parametrik olarak incelemek için, gömülmüş Polietilen borularının harmonik ve deprem yükleri altındaki davranışlarını iki boyutlu (2D) PLAXİS sonlu elemanlar programı aracı ile ele alınmıştır. Sonuçlar tartışılmış ve tek değişkenli doğrusal ve doğrusal olmayan matematiksel modelleme ile çalışılmıştır. Zemin tipleri (gevşek ve sıkı kum), farklı depremler gibi faktörler ile irdelendi. Sonuçlar dikkate alındığında, bu faktörlerin (zemin cinsi ve boru özellikleri) dinamik yükler etkisinde boru hattının deplasmanına sebep olabilecek önemli öğeler olduğu sonucuna varılmıştır. Bazı önemli karşılaştırmalar ve sonuçlar verilmiştir.

Borunun altındaki zemin koşullarının ivme, akım değeri, sözde spektral ivme (pseudo spectral acceleration – PSA) ve eksenel ve kesme kuvvetleri incelenmiştir. Genel olarak deprem iki şekilde borularda ciddi hasarlar yaratmaktadır: birinci kalıcı zemin deformasyonları, ikincisi ise dalga yayılmasıdır. Literatürde ve analitik incelemelerde dalga yayılımından ortaya çıkan tesisatın kopma ve kırılması kalıcı zemin deformasyonları (PGD) ile karşılaştırıldığında elde edilen oranların arasında çok farklılık olmadığı belirtilmiştir. Geçmiş depremler boru hatlarının kalıcı zemin hareketleri tarafından tehdit altında bulunduğunu göstermiştir. Depremler sonucunda oluşan kalıcı zemin deformasyonları nedeniyle boru hatlarında önemli birçok hasar oluşmuştur. Maddi ve yaşamsal kaza riskini azaltmak amacıyla deprem nedeniyle oluşan kalıcı zemin deformasyonlarına maruz gömülü boru hatlarının davranışlarının incelenmesi gerekmektedir. Sonlu elemanlar yöntemi kalıcı zemin deformasyonlarına maruz boruların davranışını incelemek için yararlı olan yöntemlerden biridir.

O'Rourke (1999), 1971 yılında meydana gelen San Fernando depreminde oluşan yanal kalıcı zemin deformasyonlarını incelemiştir. Hamada ve O'Rourke (1992), 1964 yılında meydana gelen Niigata depreminde oluşan yanal kalıcı zemin deformasyonlarını incelemişlerdir. Yapılan bu çalışmalar sonucunda iki tip yanal kalıcı zemin deformasyonuna rastlanmış olup, gözlenen bu yanal kalıcı zemin deformasyonları dağılı yayılı kalıcı zemin deformasyonu ve bölgesel ani kalıcı zemin deformasyonu olarak sınıflandırılmışlardır. Dağılı yayılı kalıcı zemin deformasyonları sıvılaşmaya bağlı oluşan kalıcı zemin deformasyonu durumlarında, bölgesel ani kalıcı zemin deformasyonları ise zemin kayması durumlarında gözlemlenmektedir.

Literatürde yapılan çalışmalar incelendiğinde gömülü boru ile zemin arasındaki etkileşimin doğrusal olmayan yay elemanları ile modellendiği görülmektedir. Bu

çalışma kapsamında, boru ve zemin arasındaki etkileşim doğrusal olmayan davranışa sahip eksenel ve yanal bağlantı elemanları kullanılarak modellenmiştir. Bağlantı elemanlarının doğrusal olmayan davranışının modellenebilmesi için gerekli olan parametreler; maksimum zemin direnci ve maksimum elastik deformasyondur. Bu parametreler ALA (2001)'de önerilen bağıntılar yardımıyla hesaplanmıştır.

Plaxis programından elde edilen sonuçların doğrulanması için zemin türü, tabaka derinliği ve eşit harmonik yükü gibi parametreleri eşit koşullarda DEEPSOIL programı ile elde edilen sonuçlar karşılaştırılmıştır. İki programdan elde edilen sonuçların arasında çok az bir fark ortaya çıkmıştır, bu farklılık ise DEEPSOIL programının tek boyutlu olduğu ve PLAXİS programının iki boyutlu olmasından daha fazla verinin girilmesinden kaynaklanması olduğu söylenebilir, bu yüzden her iki programda elde edilen sonuçlar kabul edilmektedir.

Bu çalışmada iki modelleme yapılmaktadır. İki tabakadan oluşan ve 8.0 metre kalınlıkta olan 10m x 10m boyutunda dikdörtgen şeklinde boru altındaki zemin ve diğer modelleme ise 2.0 metre kalınlığında ve borunun alt ve üstünde bulunan 2.5m x 1.5m boyutlarında trapez bir modelleme kullanılmıştır. Zemin türü ise Gevşek Kum ve Sıkı Kum olarak seçilmiştir. Zemin davranışını modelleyebilmek için Hs Small modeli kullanılmıştır.

Modellemede kullanılan borunun özellikleri 400 mm çapında ve 12 mm kalınlığında olup yeryüzünden 2.0 m derinliğinde gömülmüş olan polietilen bir borudur. Deprem etkisini incelemek üzere borunun çevresinde 3 nokta belirlenmiş ayrıca borunun zeminle temas ettiği yatağın üzerinde ise deprem dalgalarının geleceği noktaya 3 ayrı nokta belirlenmiştir. Analizler harmonik yükler ve deprem yükleri altında gerçekleştirilmiştir. Harmonik analiz için ivme büyüklüğü $1m/s^2$ ve frekans 5Hz özelliklerine sahip olan harmonik yükü 10 saniyelik bir zaman diliminde sıkı kum tabakasının altında uygulanmıştır. Programdan edinilen sonuçlara bakıldığında borunun üzerinde, içinde ve dolgu tabakanın yüzeyinde ve de doğal zemin(free field) yüzeyindeki deprem ivmeleri çok farklılık göstermiştir. Bunun nedeni ise gelen dalganın enerjisinin üst tabakaya hareket ettiğinde azalması olarak düşünülebilir.

Borunun çevresindeki zeminin yumuşak olması nedeniyle buradaki enerjinin dağılıp tükenmesi yataktaki enerji değerinden daha fazla olması tespit edilmiştir bu yüzden deplasman değeri borunun çevresinden uzak noktalara göre daha fazla olmuştur. Harmonik yükün etkisi sonucu PSA değeri serbest noktalarda yatak noktalarıyla hemen hemen aynı değer bulunmuştur. Halbuki bu değer borunun çevresindeki noktalarda diğer noktalara kıyasen daha azdı.

İkinci analizde zemin ve boru arasındaki etkileşimi ve dolgu zeminin boruda etkisini araştırmak için Kobe depremindeki deprem yükünü (PGA= 0.76g) 48 saniye içerisinde dört değişik zemin türünde (gevşek ve sıkı yatak zemin, yumuşak ve ya sert dolgu) incelenmiştir. Elde edilen sonuçlara bakıldığında en yüksek ivme değeri sıkı yatak tabaka ve sert dolguda ve en düşük ivme ise gevşek yatak tabaka ve yumuşak dolguda belirtilmiştir. İvme gibi, PSA değeri de en yüksek ve en düşük değerleri sıkı ve gevşek zeminde ortaya çıkmıştır. Yatay deplasman zeminin tüm dört yönünde de aynı değerde olup dikey deplasmanda ise en yüksek değer gevşek kumda belirtilmiştir; bu değerin sıkı kumda gevşek kuma göre daha az olduğu da gözlenmiştir. Sonuç olarak gevşek kumda oturma oranı daha yüksek olup bu değerin yüksek olması borularda ciddi hasarlara yol açmıştır.

Boru ve borunun çevresindeki zeminde iki nokta ele alınarak iki nokta arasındaki göreceli deplasman sıkı kumda, gevşek kumdan daha yüksek olduğu gözlenmiştir bu

yüzden borunun hareketi çevresindeki zeminden fazla olup sonuçta boru daha ciddi hasar göreceği belirlenmiştir. Borunun dinamik yükler altındaki davranışlarını değerlendirilmesinde birim deformasyon parametresinin önemli bir ölçüt olduğundan ve Plaxis'de elde edilen sonuçlara göre yatay ve dikey eksenel birim deformasyon gevşek kumda sıkı kumdan daha fazla olduğu gözlenmiştir.

Tüm eksenel ve kesme kuvvetleri ve eğilme momenti değerlerine bakıldığında borunun deprem yükleri altında emniyet momentinden daha yüksek bir eğilme momente sahip olduğu ortaya çıkmıştır. Eğilme momentinin yüksek olması borunun kırılma ve bozulmasına sebep olmuştur. Halbuki kesme kuvveti ve eksenel kuvvetlerin değeri emniyet değerlerinden daha düşük bir değere sahip oldukları ve borunun kırılma ve kopmasında etkin bir rol oynamadıkları görünmüştür.

Eksenel birim deformasyon hesaplamaları için literatürde mevcut bağıntılar kullanılarak dalga yayılımı sonucu ortaya çıkan eksenel birim deformasyonlar hesaplanmıştır. Sonuçların Plaxis analiz sonuçları ile benzerlik gösterdiği görülmüştür.

1. INTRODUCTION

It is acknowledged that underground structures suffer less damage from earthquakes than structures on the ground surface. Recent earthquakes have damaged many lifeline structures. Buried gas and water pipelines are also no exceptions. The damage or disruption of buried pipelines due to earthquakes may severely affect civil lifeline structures since it may cause fires, economic losses, and disable of lifeline networks. There is substantial pipeline damage in past major earthquakes, such as 1906 San Fransisco Earthquake, 1933 Long Beach Earthquake, 1952 and 1954 Kern County Earthquakes, 1964 Nigata, 1971 San Fernando, 1979 Imperial Valley Earthquake, 1989 Loma Prieta Earthquake, 1994 Northridge Earthquake, 1999 Duzce Earthquake and 1999 Chi Chi Earthquake (O'Rourke and Lane, 1989; O'Rourke and Palmer, 1996). These earthquakes demonstrated that the permanent ground deformation (PGD) caused by earthquakes generated significant damages on buried pipelines. The principle form of permanent ground deformation caused by earthquake is observed as land sliding, surface faulting, lateral spreading and seismic settlement. Transverse permanent ground deformation includes land sliding and lateral spreading. O'Rourke and Tawfik (1983) and Hamada and O'Rourke (1992) observed two types of transverse PGD as spatially distributed transverse PGD and abrupt transverse PGD. Subsequently, the seismic analysis and behavior of buried pipelines have been investigated by many researchers. Most of the studies mainly deal with the numerical modeling of buried pipelines, soil-pipeline interaction, and earthquake induced pipeline stress. Finite Element Methods (FEM) is also helpful for executing rigorous analysis for seismic response analysis of buried pipelines.

Investigating geotechnical problems using FEM has been widely used in this research area for many years even though there are limitations for analyzing such problems accurately. However, linear and nonlinear problems such as prediction of settlement and deformation between buried pipelines and soil is highly amenable to solution by FEM. For this reason, PLAXIS, which is used for general Finite Element Analysis (FEA), was chosen in order to estimate failure aspects of buried pipelines.

The main purpose of this study is to understand failure aspects of flexible buried pipeline caused by earthquake through FEA. Most of the researches conducted on soil-pipe interaction are focused on steel pipes; however, there are a few studies on seismic behavior of underground pipelines with materials other than steel and in particular high-density polyethylene (HDPE). With HDPE pipelines now becoming the industry standard for natural gas and water distribution systems, a detailed investigation into the interaction of these types of pipes with the surrounding soil is needed to ensure that the response of both pipeline and soil components is properly understood during design. The aim of this study is to determine behavior of pipeline subjected to seismic loads. For this aim, the behavior of pipeline subjected to harmonic and earthquake load is investigated parametrically for different soil layers, flexible type of pipe, and material properties of backfill, using PLAXIS finite element software. The thesis is divided into five chapters. Following this introduction, chapter two presents the review of literature on the subject. The literature discussed includes a summary of earthquake effects, explaining the mechanism of earthquake-induced ground movements and their interactions with buried pipelines. This chapter constitutes a detailed treatment of the behavior of buried pipelines subject to ground shaking. Then, the Soil-Pipe interaction has been investigated.

Chapter Three gives the definition of the PLAXIS software and the use of H_s small model is presented. Also in this chapter a verification study between PLAXIS and DEEPSOIL is performed. In chapter Four, the dynamic analysis for buried pipeline in different soil has been computed. In continue, presents the results of the numerical modeling analysis.

Displacements, accelerations, spectral response acceleration of both pipeline and soil have been investigated for different values of seismic parameters and soil media. Chapter Five presents the main suggested conclusion of the research.

2. LITERATURE REVIEW

According to literature survey for large ground deformation response of pipelines shows that the study of aboveground pipelines for large ground motion hazards is relatively less reported compared to buried pipelines, also pipelines are usually buried (FEM-233, 1992). That is why in this report emphasize was given to buried pipelines and its performance. Seismic hazard of pipeline is well demonstrated and documented during past several earthquakes all over the world. Few of them are summarized below.

• The 1971 San Fernando earthquake, over 80 transmission line failures occurred in pipelines due to shaking that had oxy-acetylene welded joints while less than five occurred in pipelines with electric arc welded joints. For transmission lines subjected to permanent ground deformation, approximately 10 failures each occurred in oxy-acetylene and electric arc welded pipe. Failures in electric arc welded pipe occurred in areas with offsets of two meters while no failures occurred in another are subjected to two to three meters of displacement (USGS, 2008).

• In 1989 Loma Prieta earthquake had three failures of transmission lines and extensive pipe damage to cast iron distribution system in the San Francisco Marina District resulted in an extensive cast iron pipe replacement program using Polyethylene (USGS, 2008).

• In1994 Northridge earthquake there were 209 repairs required to metallic distribution lines and 27 to polyethylene lines (USGS, 2008).

• In addition, Tsai et al. (2000) reported that during 1999 Chi-Chi (Taiwan) earthquake 2000 mm diameter pipe destroyed by rupture of Chelungpu fault. The fault was steep reverse type and during earthquake fault offsets, around 4 to 10 m were observed along its length (Rajkumar and Ilamparuthi, 2008).

Permanent ground deformation was distinctive source for major pipeline damages, damage from ground waves has been also observed in pipelines, which were

weakened either by corrosion or by welds of poor quality, even though there are cases of combinations of these damage modes.

2.1 Permanent Ground Deformation (PGD) Hazard

As mentioned by O'Rourke and Liu (1999) pipelines can be categorized into two distinctive groups, continuous and segmented pipelines. For pipelines, seismic hazards can be classified as being either wave propagation hazards or Permanent Ground Deformation (PGD) hazard (O'Rourke and Liu, 1999). Permanent ground deformation (PGD) may arise because of landslides, creeping of land, liquefaction induce ground deformation, and abrupt surface shatter due to faulting. In literature PGD hazard generally referred hazard due to ground motion causes by landslide or liquefaction, discussed in subsequent topics. Hall and Newmark (1977) stated that there was no case of a modern buried welded steel pipeline failure because of ground shaking. However there are some examples of pipe damages due to wave propagation, which includes pipeline damage in Mexico City by 1985 Michoacán earthquake. O'Rourke and Liu (1999) suggested that PGD hazards are usually limited to small regions; their potential for damage is very high since they impose large deformation on pipelines. On other hand, the wave propagation hazards typically affect the whole pipeline network, but with lower damage rates.

It is not particularly meaningful to assign average proportions of damage to either permanent ground movement or seismic shaking. Both the forms of displacement often are interrelated so that a clear distinction cannot be made between damage caused by one or other. Nevertheless, it is important to recognize that permanent differential ground movements may accompany any earthquake and that the movements can assume a variety of patterns depending on local soil and other geological conditions. There for analysis can be simplified by assuming a one to one correspondence between pipeline and soil movement. The principal forms of permanent ground deformation (PGD) are surface faulting, land sliding, seismic settlement and lateral spreading due to soil liquefaction. Whether the buried pipeline fails when subjected to PGD depends, in part, on the amount and spatial extent of the PGD, which are introduced here.

2.1.1 Fault hazard

An active fault is a discontinuity between two portions of the earth crust along which relative movements can occur. The movement is concentrated in relatively narrow fault zones. Principal types of fault movement include strike and dip slip. In strike-slip fault the predominant motion is horizontal, which further divided as right lateral and left lateral (Figure 2.1). The lateral fault deforms a continuous pipe primarily in tension or compression depending on the pipe-fault intersectional angle. In dip-normal and dip-reverse faults, the predominant ground displacement is vertical. When the overhanging side of fault moves downwards, the fault is normal (Figure 2.1), which primarily deforms a pipe in tension. On other hand, when the overhanging side of fault moves relatively up, the fault is term as reverse fault (Figure 2.1), that deforms a pipeline in compression.
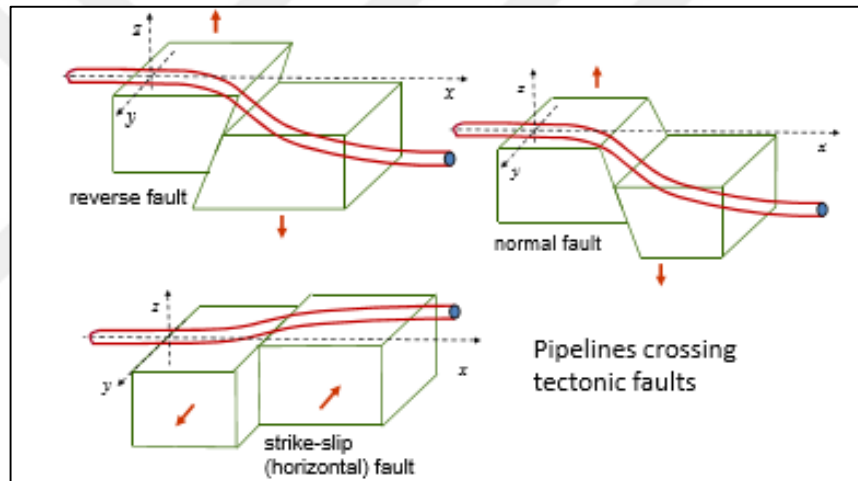
Figure 2.1: Schematic representation of pipeline configuration crossing faults (Jos, 2015).

The pioneering study of the pipe-fault crossing is done by Newmark and Hall (1975) which further modified by Kennedy et al (1977) and Wang and Yeh (1985) in which they proposed simplified analytical model for pipe strike-slip fault crossing.

2.1.1.1 Newmark and Hall

The considered model of Newmark and Hall (1975) is shown in Figure 2.2. To estimate axial tensile strain and to predict the pipeline's response crossing strike-slip fault. In this study, Newmark and Hall (1975) treated the pipeline like a cable. Total δ_f fault movement with pipe-fault intersection angle $\beta \leq 90°$ is considered which results in tensile strain in the pipe. The only force that acts on the pipeline is the

friction force at the pipe-soil interface along the longitudinal direction. As an initially step, a maximum axial stress value is assumed in the pipeline and length of the pipeline required for the zero frictional force condition is determine. This length is considered as anchor length (L_0) as shown in figure. For assumed stress-strain (elasto-plastic) relationship, stress induced deformation over L_0 is calculated. The physical deformation of pipe is estimated from fault geometry is then compared with deformation using pipeline fault geometry. Using new value of maximum axial strain, deformation is calculated until convergence of physical and calculated deformation attains. Since Newmark and Hall (1975) modeled the pipe as cable, which can carry only tensile strain. Hence, bending strength of pipe and lateral interaction at pipe-soil interface are totally ignored.
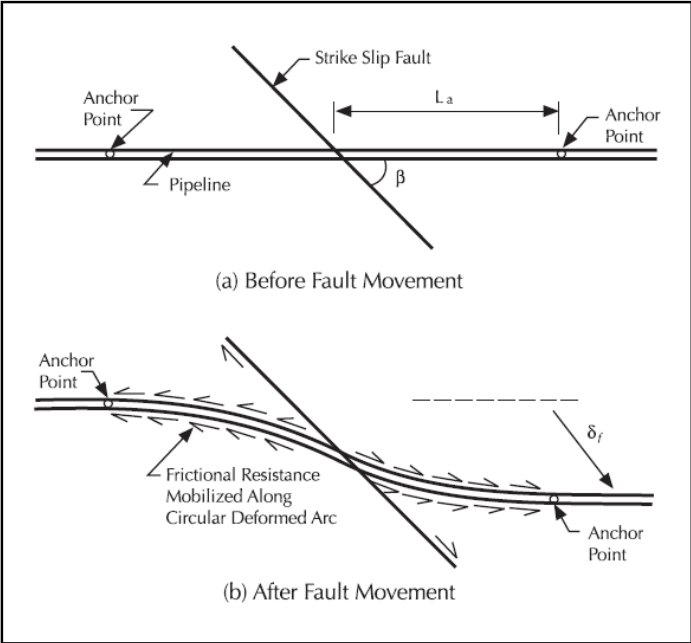
Figure 2.2: Pipeline crossing right lateral strike slip fault (Newmark and Hall, 1975)**.**

2.1.1.2 Kennedy et al.

Kennedy et al. (1977) improved the Newmark and Hall (1975) method for estimating the maximum axial strain in pipe by incorporates the effect of lateral soil interaction. In this method, it is assumed that pipeline would bend in circular arc of constant radii on both side of fault line as shown in Figure 2.3. For calculating radii of curvature, it is assumed that pipe as negligible bending stiffness, which is only possible for large fault movement when pipe material gets strain well beyond the yield point under

tensile strain. Rest of procedure is similar to that of Newmark and Hall (1975) method.
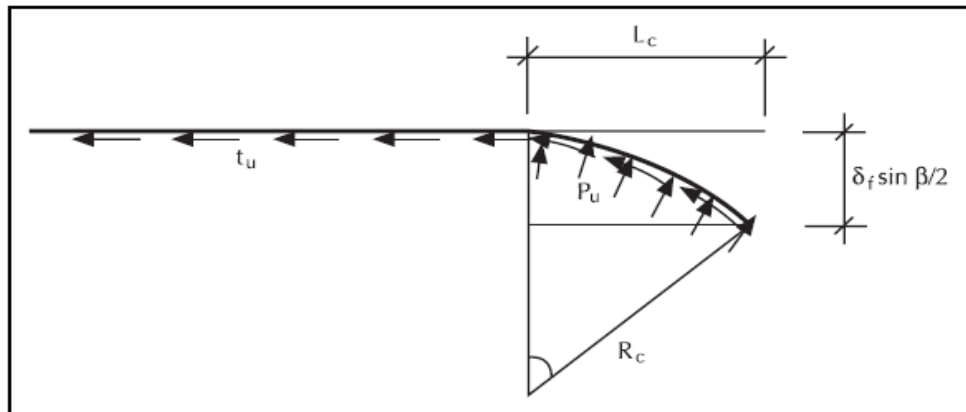
Figure 2.3: Kennedy et al. (1977) model with lateral soil pressure.

2.1.1.3 Wang and Yeh

In sequence of Newmark and Hall (1975) and Kennedy et al. (1977)'s work, Wang and Yeh (1985) introduced some additional modifications. In this method, total pipe length is divided in to three regions, with I and II region as curved of constant radius as shown in Figure 2.4.
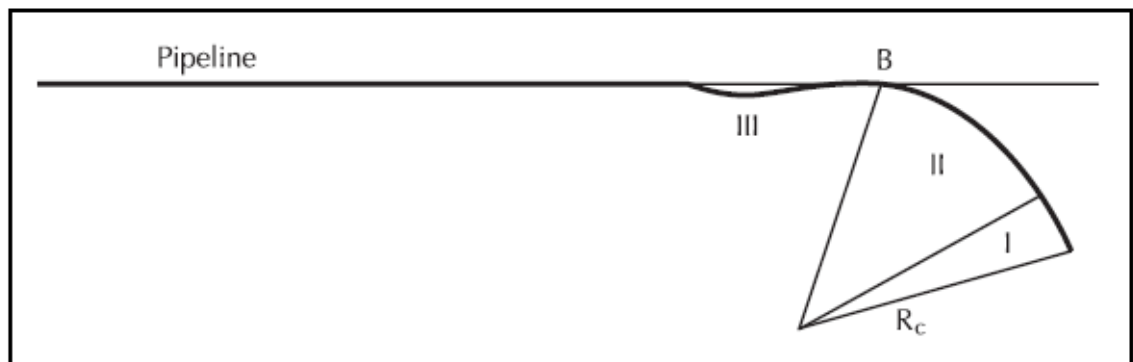
Figure 2.4: Three zone in Wang and Yeh (1985) model.

The radius of curvature calculated from force and deformation compatibility. It was also assumed that strain in region II and III are elastic while the strain in region I is inelastic. For straight portion in region III, they used the theory of beam on elastic foundation. In a method they notify that maximum bending strain is in the region II and crucial combination of axial and bending strain will develop at point B (Figure 2.4) hence concluded that the pipe would fail at point B, which seems counterintuitive since one expects tensile ruptures at or very near to the fault crossing.

7

2.1.1.4 Wells and Coppersmith

It is possible to estimate fault displacement PGD_F in terms of earthquake moment magnitude using empirical relations, e.g. Wells and Coppersmith (1994). Subsequently, the axial strain induced by the fault movement in the pipeline wall can be computed analytically, following the procedure in Kennedy et al. (1977). For the case of horizontal faults (Figure 2.5), using the horizontal ground-induced displacement PGD_{FH} the maximum axial strain is:

$$\varepsilon = \frac{PGD_{FH}}{L_H} \cos\theta + \left(\frac{PGD_{FH}}{3L_H} \sin\theta\right)^2 \tag{2.1}$$

Where θ is the angle between the fault plane and the pipeline axis, L_H is the distance between the fault and the "anchor point", estimated by the following expression:

$$L_H = \sqrt{(F_Y/k_H)\,\sin\theta} \tag{2.2}$$

Where k_H is the horizontal soil stiffness and F_Y is the plastic axial force. In the case of an oblique fault, with simultaneous fault movement PGD_{FV} in the vertical direction, one may write the following equation for the axial strain in the pipeline,

$$\varepsilon = \frac{PGD_{FH}}{L_H} \cos\theta + \left(\frac{PGD_{FH}}{3L_H} \sin\theta\right)^2 + \left(\frac{PGD_{FV}}{3L_V}\right)^2 \tag{2.3}$$

Where L_V is the distance between the fault and the "anchor point" in the vertical plane, estimated from equation (2.2) using the vertical soil stiffness k_V.
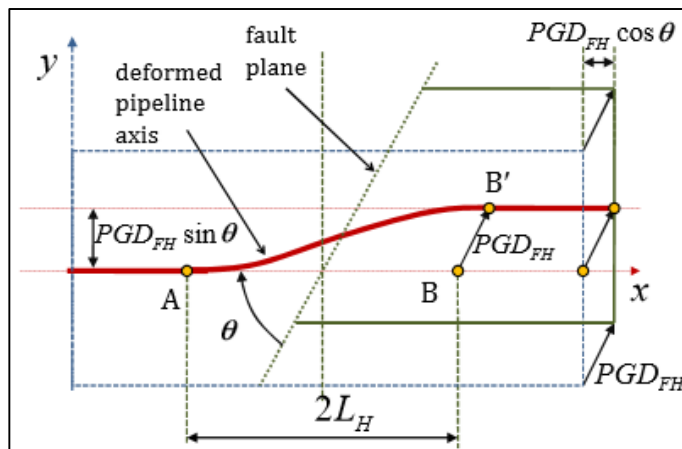
Figure 2.5: Pipeline deformation crossing a horizontal fault at angle θ (Wells and Coppersmith, 1994).

2.1.1.5 Takada et al.

Takada et al. (1998) discretized pipeline by four nodes thin shell element with elasto-plastic material characteristic and soil as nonlinear springs. One end of the springs are connected to the nodes of shell elements and the another ends are given forced displacement to simulate the fault movements (Figure 2.6). Total model length L = 30D is considered, where D is diameter of the pipe, analysis performed for 1m normal and reveres fault displacements. In this work, both geometric and material nonlinearities were considered. Results are compared for normal and reverse fault motions. It is found that because of the local buckling in reverse fault motion, high strains are developing near the fault region. Parametric study has done for both normal and reverse faulting to finding the effect of soil rigidity, in which observed that the pipeline is more susceptible to the reverse fault than normal fault, but as the increment of the soil stiffness, normal and reverse fault have the same effect on the pipeline. The effects of the fault angle and diameter-to-thickness ratio are also considered. Post yielding results, of Takada et al. (1998) model do not matches with experimental results. This model cannot ensnare actual behavior of soil during large deformation and failure of the soil this might have resulted in higher estimation of plastic strains.
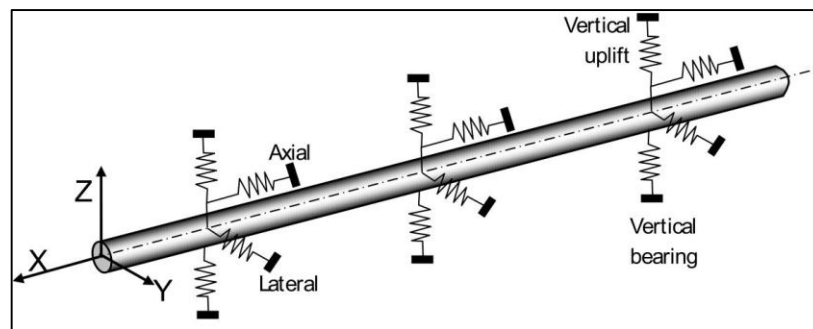
Figure 2.6: Pipe as shell element and soil as spring model (Takada et al., 1998).

2.1.1.6 Liu et al.

To reduce the memory and calculation time requirement, Liu et al (2004) developed shell finite model with an equivalent boundary condition for estimating the response of a buried pipeline under fault movement (Figure 2.7). In this study, only the pipeline segment near fault is modeled with plastic shell elements. The material property of pipe segment far away from the fault is considered as elastic and nonlinear spring elements at equivalent boundaries are obtained, applied to two ends

of shell model. The inelastic property of equivalent boundary spring is derived by considering axial strain in the pipe similar like Newmark and Hall (1975) assumption. From static and sliding friction force equation they developed force per unit deformation, which is, consider as inelastic property of equivalent boundary spring. Then results of 60 m model are compared with 300 m and 180 m fixed boundary model that coincided. However, Liu et al. (2004) derived equivalent boundary condition but did not clarified minimum requirement of length for shell model pipeline.
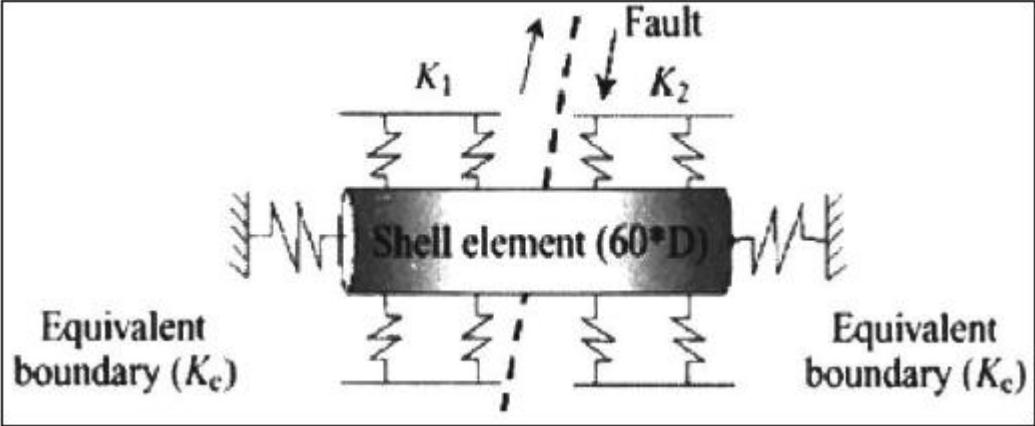
Figure 2.7: Liu et al. (2004) equivalent boundary model.

2.1.1.7 Karamitros et al.

Karamitros et al. (2007) newly introduced a number of refinements in the method proposed by Wang and Yeh (1985). Previous method overlooked the effect of axial force on bending stiffness. Karamitros et al. (2007) suggested most unfavorable combination of axial and bending would not necessarily take place at the end of high curvature portion but within the zone, closer to the fault crossing point. As first step analysis like Wang and Yeh (1985), Karamitros et al. (2007) treated the straight end segments AA' and CC' (Figure 2.8) as beams on elastic foundation in order to obtain the relation between shear force, bending moment and rotation angle at points A and C. In step two, they consider the boundary conditions determined in first step, and then segments AB and BC are analyzed according to the elastic-beam theory in order to derive the maximum bending moment. In third step, axial force on the pipeline, at the intersection with the fault trace (point B), are obtained by equalizing the required and the available pipeline elongation. In fourth step, bending strains are calculated, considering geometric second-order effects. In fifth step, the maximum pipeline

10

strain is computed from the demand for equilibrium between the externally applied axial force and the internal stresses developing on the pipeline cross-section. Finally, given the stress and strain distribution within the cross-section, an updated secant Young's modulus is computed and steps 2–6 are repeated until convergence is accomplished.

The results compare using hybrid shell-beam finite element model with total 1000 m pipe length. In which 50 m long cylindrical shell and 450 m beam is taken. To simulate soil pipeline interaction effects, each node of the model was connected to axial, transverse horizontal and vertical soil springs, modeled as elastic-perfectly plastic elements.
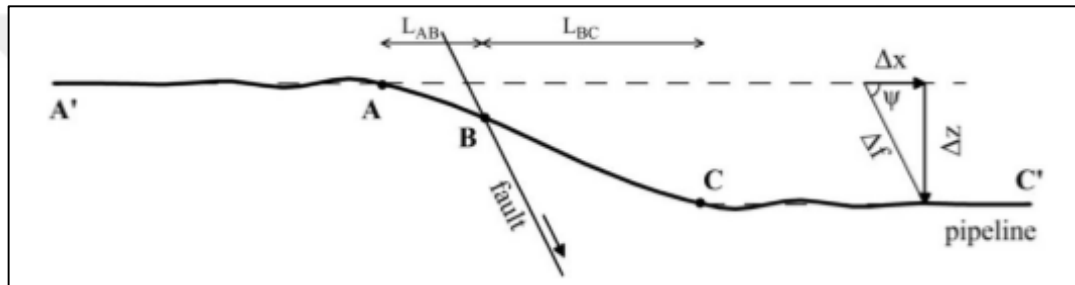
Figure 2.8: Segments partitioning of the pipeline in Karamitros et al. (2007) model.

Though this method refine the actual method proposed by Kennedy et al. (1977) and Wang and Yeh (1985) but could not able to overcome basic limitation of actual method that is restricted applicability to strike-slip fault motion, where pipeline should be strictly in tension.

In addition to above, analytical models there are several numerical models proposed, which includes beam on nonlinear Winkler foundation. In which pipe modeled with beam/shell elements and soil with springs (Radan, 2000). Nodes of the shell elements of the pipe are attached to soil that is modeled as springs (Takada et al., 1998; Liu et al., 2004; Karamitros et al., 2007) comprehensively explained in IITK-GSDMA (2007).

2.1.2 Landslide hazard

Landslides are permanent mass movements of the ground that may be triggered by rains, floods, seismic shaking, and other natural causes as well as human-made causes, such as grading, terrain cutting and filling, excessive development etc. Based on soil movements, geometry of soil movement and the types of material involved

11

O'Rourke and Liu 1999 categorized landslide as slides, rock falls and topples, spread, and slump-flow (Figure 2.9). Lateral spreading is considered liquefaction induced phenomenon, discussed in subsequent subsection.

Depending up on the type, landslide can produce diverse effect on the pipeline. Rock fall and rock topple (a), which can cause damage to aboveground pipelines by direct impact of falling rocks. This type of landslide has relatively little effect on buried pipelines. Another form landslide which has adverse effect on pipeline is earth slump or earth slide (b). This usually occurs along natural slopes, embankments, river channels; often pipeline runs through such regions.
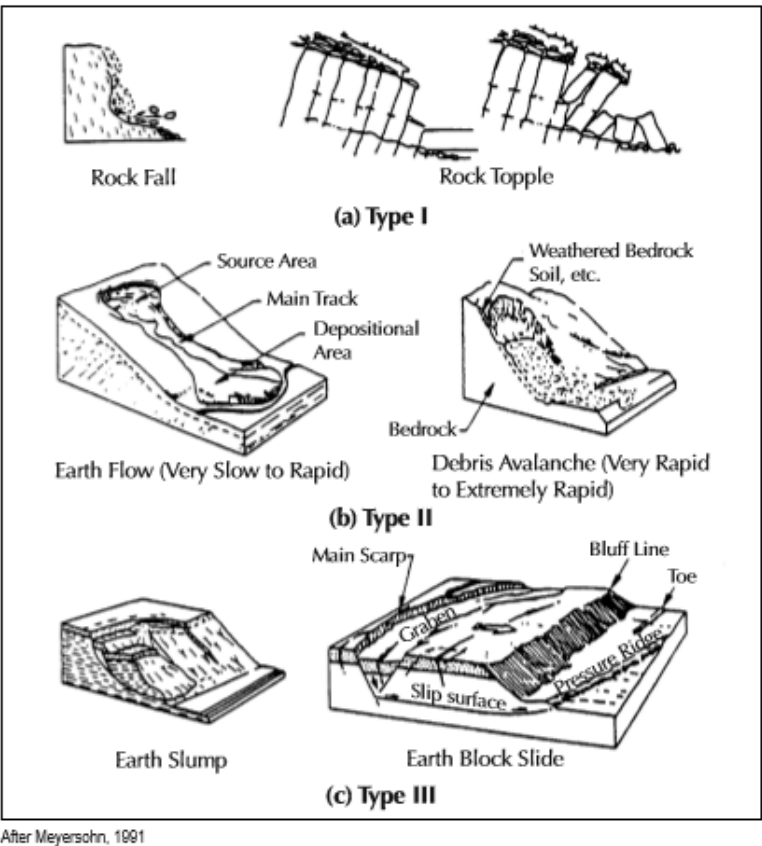
Figure 2.9: Type of ground failure associated with landslide (O'Rourke and Liu 1999).

2.1.3 Liquefaction hazard

Seismic shaking to a loose saturated sandy soil deposited usually results in loss of shear strength is known as liquefaction, which in turn results in the flow or lateral movement of liquefied soil. Small component of vertical soil movement is often accompanied with liquefaction induced lateral spreading and disregarded herein. There are two possibilities as regard of pipeline response to liquefaction-induced

lateral spreading. In first case such as at the Ogata Primary School site during the 1964 Niigata event, the top surface of the liquefied layer is essentially at the ground surface. For the first case, a pipeline is subjected to horizontal force due to liquefied soil flow over and around the pipeline as well as uplift or buoyancy forces. In second case such as at Mission Creek site during the 1906 San Francisco event, the top surface of the liquefied layer is located below the bottom of a typical pipeline. That is, the pipeline is contained in a non-liquefied surface soil layer that rides over the liquefied layer. For second case, the pipeline is subject to horizontal forces due to non-liquefied soil-structure interaction but not subject to buoyancy effects (O'Rourke and Liu, 1999). Pipeline response in a non-liquefied surface soil layer is considered for this study.

O'Rourke and Liu (1999) suggested four geometric characteristics of a lateral spread that influence pipeline response in horizontal plane. In reference to Figure 2.10, these are the amount of PDG movement δ, the transverse width of the PGD zone W, the longitudinal length of the PGD zone L, and the pattern or distribution of ground movement across and along the zone. Depending on whether the lateral spread takes place parallel or perpendicular to the pipeline axis, the PGD is classified as longitudinal or transverse PGD respectively (Figure 2.11). Under longitudinal PGD, a corrosion-free continuous pipeline may fail at welded joints, may buckle locally (wrinkle) in a compressive zone, and/or may rupture in a tensile zone. When the depth is very shallow, the pipeline may buckle globally (beam buckling) in a compressive zone.

To accommodate the transverse ground movement due to transverse PGD a continuous pipeline stretch and bends, this result in an axial tension (stretch due to arc length effect) and flexural (bending) strain of failure mode in continuous pipeline. That is, if the axial tension strain is low, the pipe wall may buckle in compression due to excessive bending or if axial tension is not small, the pipe may rupture in tension due to the combined effect of axial tension and flexure. O'Rourke and Liu, 1999 cited example of 1971 San Fernando event, continuous pipe failure due to PGD. The transverse component of PGD was approximately 1.7 m caused multiple breaks. Also at some location required repair within PGD zone. The records indicate that three repairs near the eastern boundary of the soil movement were due

to tensile failure and two other repairs near the western boundary were due to compressive failure.
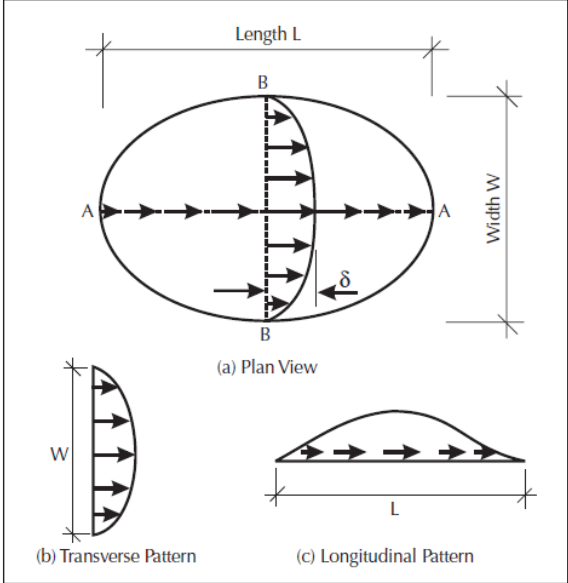
Figure 2.10: Characteristic of a lateral spread (O'Rourke and Liu, 1999).
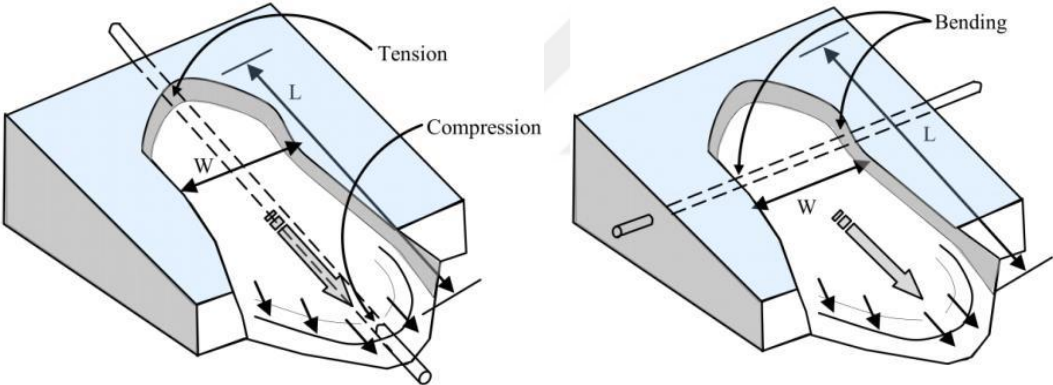
Figure 2.11: Longitudinal and transverse pipe-PGD crossing (IITK-GSDMA, 2007).

2.1.3.1 O'Rourke and Liu

To suggest damage of the pipeline subjected to the longitudinal PGD during 1994 Northridge California event, O'Rourke and Liu proposed failure criterion (O'Rourke and Liu, 1994). For the analysis purpose, two cases were considered. In first case amount of ground movement assumed large and strain of pipe considered the function of the PGD zone width. While other case zone width assumed large and pipe strain is assumed as a function of ground movement. In both tension and compression, strain is varying linearly up to peak strain point. Critical pipe length is determined from the friction force and ground movement. For the above assumption

14

peak strains are compared with the criterion given by the Newmark and Hall (1975) for pipe failure in tension and compression.

To find the response of continuous pipeline subjected to transverse PGD many researchers have developed numerical model using finite element technique also used different pattern to idealize PGD briefly described below.

2.1.3.2 Finite Element Models

Certain researchers (Suzuki et al., 1988; Kobayashi et al., 1989; Liu and O'Rourke, 1997) used finite element approaches to evaluate response of buried pipelines subjected to spatially transverse PGD.

2.1.3.3 O'Rourke and Lane

O'Rourke and Lane (1989) approximated PGD pattern by the beta probability density function (Figure 2.12) given by

$$Y(x) = \delta \ [s/s_m]^{r'-1}[(1-s)/(1-s_m)]^{\tau-r-1} \tag{2.4}$$

Where $s_m = 0.5, r' = 2.5 \ and \ \tau = 5.0$.

In this model, O'Rourke and Lane (1989) assumed pipeline is anchored at a distance *La* from the margin of the PGD boundary. The anchor point was taken the point where the bending strain of the pipe is less than 1×10^{-5}. The pipe consider for the analysis was API X-60 grade, 0.61m in diameter with 0.0095m wall thickness and buried at 1.5m. O'Rourke and Lane (1989) studied the effect of δ on maximum tensile strain by varying width of PGD zone as 10, 30, and 50m.
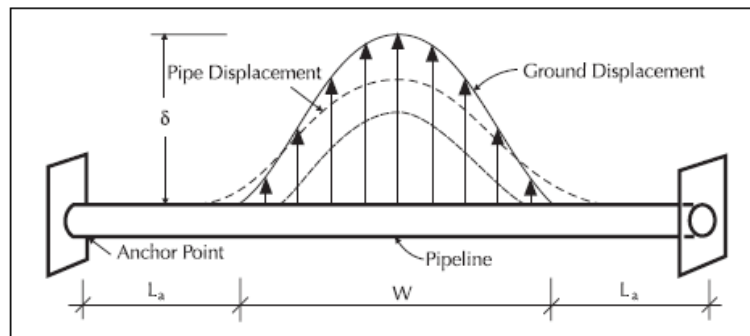
Figure 2.12: O'Rourke and Lane (1989) model.

2.1.3.4 Suzuki et al

Suzuki et al. (1988) and Kobayashi et al. (1989) expressed the pattern of transverse ground displacement by the cosine function raised to the *n* power as given below.

$$y(x) = \delta \left[\cos\frac{\pi x}{w}\right]^n \qquad (2.5)$$

2.1.3.5 Liu and O'Rourke

Liu and O'Rourke (1997) predicted the spatially distributed transverse permanent ground deformation by using the following function:

$$y(x) = \frac{\delta}{2}\left[1 - \cos\frac{2\pi x}{w}\right] \qquad (2.6)$$

Where x is the non-normalized distance from the margin of the PGD zone. When n is equal to 2 in the Suzuki et al. (1988) and Kobayashi et al. (1989)'s function, O'Rourke's function takes the same shape of the Suzuki et al. (1988) and Kobayashi et al. (1989)'s models.

The maximum soil deformation occurs at the center of PGD zone and the soil deformation is accepted as zero at the margins. These assumptions are valid for all patterns.

2.1.3.6 O'Rourke

O'Rourke (1989) developed a simple analytical model for pipeline response to spatially distributed transverse PGD. He considered two types of response as shown in Figure 2.13. For a wide width of PGD zone, the pipeline is relatively flexible and its lateral displacement is assumed to closely match that of soil. For this case, the pipe strain was assumed to be mainly due to the ground curvature (i.e. displacement controlled). For a narrow width, the pipeline is relatively stiff and the pipe lateral displacement is substantially less than that of the soil. In this case, the pipe strain was assumed to be due to loading as the soil-pipe interface (i.e. loading controlled).

For the wide PGD width/flexible pipe case, the pipe is assumed to match the soil deformation given.

$$y(x) = \frac{\delta}{2}\left[1 - \cos\frac{2\pi x}{w}\right] \qquad (2.7)$$

For the wide PGD width/flexible pipe case, the pipe is assumed to match the soil deformation given.

$$\varepsilon_b = \pm \frac{\pi^2 \delta D}{w^2} \qquad (2.8)$$

In this model, the axial tensile strain is based solely upon the arc-length of the pipe between the PGD zone margins. Assuming the pipe matches exactly the lateral soil displacement, the average axial tensile strain, ε_a is approximated

$$\varepsilon_a = \left(\frac{\pi}{2}\right)^2 \left(\frac{\delta}{w}\right)^2 \qquad (2.9)$$

For the narrow width/stiff pipe case, the pipe is modeled as a beam, built at each margin (i.e. fixed-fixed beam), subjected to the maximum lateral force per unit length Pu at the pipe-soil interface. For this case, the axial tension due to arc-length effects is small and neglected. Hence, the maximum strain in the pipe is given by

$$\varepsilon_b = \pm \frac{P_{u}\,w^2}{2\pi EtD^2} \qquad (2.10)$$
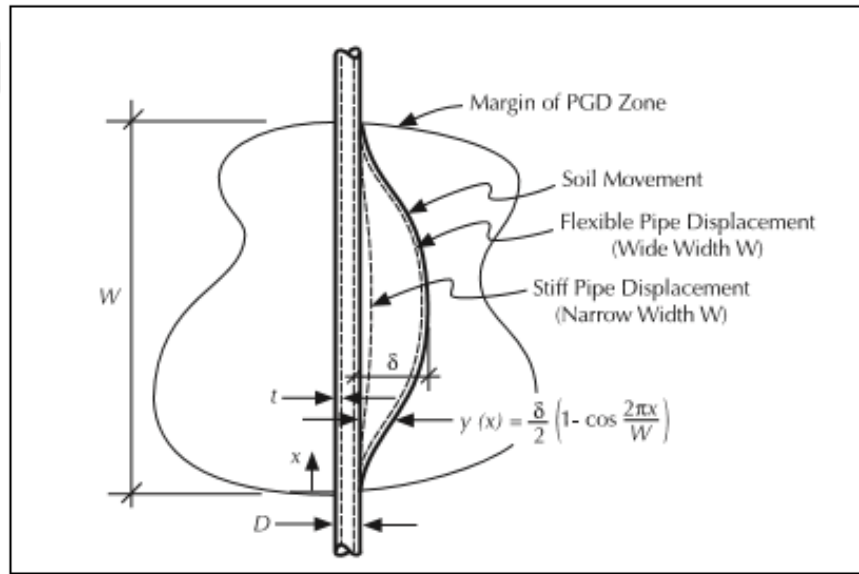
After M. O'Rourke, 1989

Figure 2.13: O'Rourke's analytical model for pipeline subject to spatially distributed transverse PGD (O'Rourke, 1989)

2.2 Wave Propagation Hazards to Continuous Pipeline

It appears that Eguchi was the first to separate wave propagation damage and PGD damage (Wai-Fah and Charkes, 2003) in his study to correlate pipeline repair rate

with Modified Mercalli Intensity (MMI). In which only wave propagation damage correlated with MMI. Ground deformations and displacements, rather than inertial forces caused by ground accelerations are the major cause of earthquake damage to pipelines. The ground strains caused by seismic wave propagation do not result in large permanent deformations (FEM-233, 1992). There have been some events, such as 1999 M 7.4 Kocaeli, M 7.2 Duzce, Turkey earthquakes, substantial water supply damage occurred in many cities. For example, the entire water distribution system in Adapazari was damaged. The water service could not be restored until many months after the earthquake (Toprak and Taskin, 2006). In addition to above there are some more events for which wave propagation was the predominant hazard such as 1964 Pugel Sound, 1969 Santa Rosa, 1983 Coalinga and 1985 Michoacan earthquakes (O'Rourke and Liu 1999). Either wave propagation hazards mostly occur in water supply (segmented pipeline) or in pipeline which were weakened either by corrosion or by welds of poor quality (FEM-233, 1992). There are no written cases of newer continuous pipeline failure due to wave propagation hazards.

The peak ground motion parameters (acceleration and velocity) as well as the appropriate propagation velocity characterize the wave propagation hazard for a particular site. There are two types of seismic waves, body waves and surface waves. Body waves propagate through the earth, while surface waves travel along the ground surface. Seismic faulting while, for the simplest case, surface waves are generated by the reflection and refraction of body waves at the ground surface generates body waves. Body waves include compression waves (P waves) and shear waves (S waves). In compression waves, the ground moves parallel to the direction of propagation, which generates alternating compression and tensile strain. For S-waves, the ground moves perpendicular to the direction of propagation. The situation for surface waves is somewhat more complex. Rayleigh and Love waves are the two main types of surface waves generated by earthquakes. For the Love waves (L waves), the particle motion is along a horizontal line perpendicular to the direction of propagation, while for Rayleigh waves (R waves) the particle motion traces a retrograde ellipse in a vertical plane with the horizontal component of motion being parallel to the direction of propagation. For both L and R waves, the amplitude of motions decreases with depth below the ground surface. Note that if R waves are present, they occur after the arrival of the direct body waves. That is, P waves arrive

at a site first, followed by S waves. If surface waves are present, they typically arrive after the body waves.

In general, the axial strain induced in a straight continuous pipeline depends on the ground strain, the wavelength of the travelling waves, and the interaction forces at the pipe–soil interface. For small to moderate ground motion, one may simply assume that pipe strain is equal to ground strain. However, for large ground motion, slippage typically occurs at the pipe–soil interface, resulting in pipe strain somewhat less than the ground strain.

Since pipelines are typically buried horizontally 1 to 3 m below the ground surface, both body and surface waves are of interest. The following sections focus on the techniques for estimating effective propagation velocity for body and surface waves.

2.2.1 Body Waves

For body waves, we consider herein only S-waves since S-waves carry more energy and tend to generate larger ground motion than P-waves. For the S-wave, the horizontal propagation velocity, that is the propagation velocity with respect to the ground surface, is the key parameter. For vertically incident S-waves, the apparent propagation velocity is infinity. However, there is typically a small angle of incidence in the vertical plane leading to non-zero horizontal ground strain. O'Rourke and Ayala (1993) have studied the apparent horizontal propagation velocity, C, for body waves. They developed an analytical technique, utilizing all three components of motion at the ground surface and a ground motion intensity tensor, for evaluating the angle of incidence of S-waves. The apparent propagation velocity for S-waves is then given by:

$$C = \frac{C_S}{\sin \gamma_s} \tag{2.10}$$

Where γ_s is the incidence angle of S-waves with respect to the vertical and Cs is the shear wave velocity of the surface soils.

2.2.2 Surface Waves

For surface waves, we only consider R-waves since L-waves generate bending strains in buried pipelines, which, particularly for moderate pipe diameters, are significantly less than axial strain induced by R-waves. As indicated previously, R-

waves cause the ground particles to move in a retrograde ellipse within a vertical plane. The horizontal component of the ground motions for R waves is parallel to the propagation path and thus will generate axial strain in a pipe lying parallel to the direction of wave propagation. Since R-waves always travel parallel to the ground surface, the phase velocity of the R-waves, C_{ph} is the apparent propagation velocity.

Note that the phase velocity is defined as the velocity at which a transient vertical disturbance at a given frequency, originating at the ground surface, propagates across the surface of the medium. The phase velocity is a function of the variation of the shear wave velocity with depth, and, unlike body waves, is also a function of frequency. For R-waves, the wavelength λ, frequency f and the phase velocity C_{ph} are interrelated by:

$$C_{ph} = \lambda \text{f} \tag{2.11}$$

The variation with frequency is typically quantified by a dispersion curve. Analytical and numerical solutions are available in the technical literature to generate dispersion curves for layered soil profiles.

O'Rourke and Palmer (1996) developed a simple procedure for determining the dispersion curve for layered soil profiles in which the shear wave velocity increases with depth. Figure 2.13 presents a normalized dispersion curve for a uniform layer of thickness, H_s with shear velocity C_L and Poisson's ratio, v_L over a half space with shear velocity C_H and Poisson's ratio, v_H. The curves are for two values of the shear velocity ratio. The dispersion relationship is not strongly affected by the densities of the layer and half space and those parameters are excluded from Figure 2.14.

Considering first the simplest case of a uniform layer over a half space, they found that at low frequencies ($H_s f / C_L \leq 0.25$), the wavelength is large compared to the layer thickness, and the phase velocity is slightly less than the shear wave velocity of the stiffer half space. That is, the R-wave is not greatly affected by the "thin" layer. Conversely, at high frequencies ($H_s f / C_L > 0.5$), the wavelength is comparable to or smaller than the layer thickness, and the phase velocity is slightly less than the shear wave velocity of the layer. The dispersion curve for an arbitrary single layer over a half space can be approximated by:

$$C_{ph} = \begin{cases} 0.875 C_H, & \dfrac{H_s f}{C_L} \leq 0.25 \\[2mm] 0.875 C_H - \dfrac{0.875 C_{H-} \ C_L}{0.25} \left(\dfrac{H_s f}{C_L} - 0.25 \right), & 0.25 \leq H_s f/C_L \leq 00.50 \\[2mm] C_L, & \dfrac{H_s f}{C_L} \geq 0.50 \end{cases} \qquad (2.12)$$

Where f is the frequency in Hz.
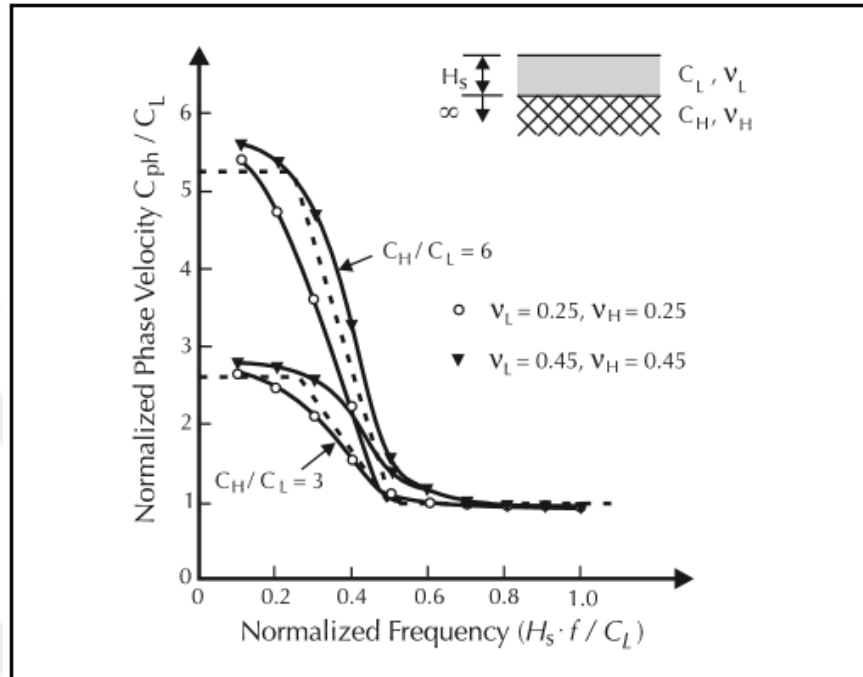
Figure 2.14: Normalized dispersion curve for single layer over half space.

2.2.3 Wavelength

For typical soil profiles, in which the material stiffness increases with depth, the propagation or phase velocity of the fundamental R-waves is an increasing function of the wavelength. That is, long wavelength waves travel faster than short wavelength waves. Hence, the effective propagation velocity for strain calculations with stations separated by a distance L_s could very well be related to the phase velocity of R-waves having a wavelength λ proportional to L_s.

A precise analytical relationship between separation distance, L_s and the appropriate wavelength, λ, is complicated by the fact that the displacement amplitudes associated with various wavelengths are not constant. However, a reasonable starting point might be $2L_s < \lambda < 4L_s$. As pointed out by Takada et al. (1998), ground motion of two points due to a wave with $\lambda = 2L_s$ would be out-of-phase by 180°, leading large relative displacements and strains. Similarly, ground motion at two points due to a

wave with $\lambda = 4L_s$ would be out-of-phase by 90°, again leading to relative displacements and strains. If $\lambda = L_s$, the ground motions would be in-phase, and there would be no contribution to relative displacements and strains due to that wavelength. Thus, the effective propagation velocity, C_{eff}, would appear to be the R-wave phase velocity, C_{ph}, for a wavelength equal to about 2-4 separation distances.to Figure 2.15 presents back calculated values for the effective propagation velocity during the 1971 San Fernando event for a number of stations at the northern end of the Los Angeles Basin, as well as the phase velocity for the fundamental R-waves, calculated for $\lambda = 2L_s$ and $\lambda = 4L_s$. The R-wave model with $\lambda = 4L_s$ seems to provide a better overall match to the observed effective propagation velocity data than the R-wave model with $\lambda = 2L_s$. As shown in Figure 3.7, for separation distances less than about 500 m (1640 ft.), the R-wave model with $\lambda = 4L_s$ matches fairly well the observed effective propagation velocity data. For separation distances greater than 500 m the R-wave model with $\lambda = 4L_s$ is conservative, i.e., an underestimation of the effective propagation velocity. However, these large separation distances are fast approaching the upper limit for engineering applications.
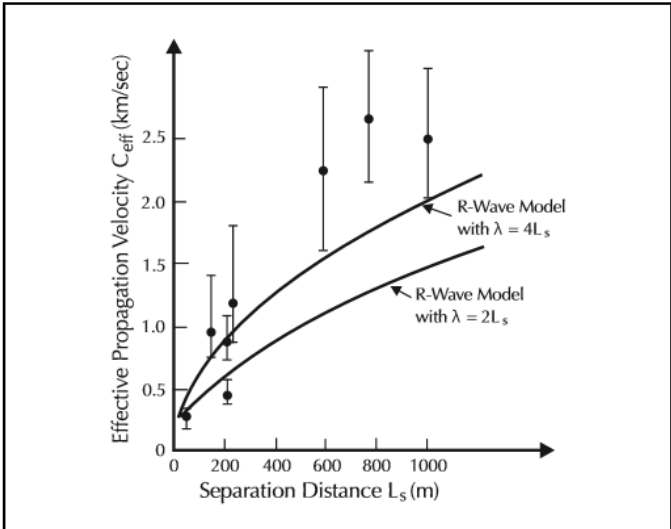
After M. O'Rourke et al., 1984

Figure 2.15: Effective propagation velocity vs. separation distance.

2.2.4 Ground Strain and Curvature Due to Wave Propagation

For the analysis and design of buried pipelines, the effects of seismic wave propagation are typically characterized by the induced ground strain and curvature. Newmark and Hall (1975) developed a simplified procedure to estimate the ground strain. He considers a simple traveling wave with a constant wave shape. That is, on

an absolute time scale, the acceleration, velocity and displacement time histories of two points along the propagation path are assumed to differ only by a time lag, which is a function of the separation distance between the two points and the speed of the seismic wave. For such a case, he shows that the maximum ground strain ε_g (tension and compression) in the direction of wave propagation is given by:

$$\varepsilon_g = \frac{V_m}{C}$$ (2.13)

Where V_m is the maximum horizontal ground velocity in the direction of wave propagation and C is the propagation velocity of the seismic wave.

Similarly, the maximum ground curvature, k_g that is the second derivative of the transverse displacement with respect to distance, is given by:

$$k_g = \frac{A_m}{C^2}$$ (2.14)

Where A_m is the maximum ground acceleration perpendicular to the direction of wave propagation.

These two relations for ground strain and curvature along the direction of wave propagation are relatively straightforward. The ground motion parameters V_m and A_m, the maximum particle velocity and acceleration can be obtained from earthquake records or from attenuation relations, discussed previously. For R-wave propagation, Equation 2.26 gives the ground strain parallel to the ground surface where C, as shown above, can be taken as the phase velocity corresponding to a wavelength equal to four times the separation distance. However, these relations for ground strain and curvature need to be modified if the direction of interest is not parallel to the direction of wave propagation.

Consider the case of S-waves. If the pipeline were orientated parallel to the direction of propagation, S-waves would induce bending in the pipeline. The corresponding ground curvature is given by Equation 2.27 where C is the apparent propagation velocity with respect to the ground surface given in Equation 2.23. If there is an angle in the horizontal plane between the pipe axis and the direction of propagation, there is a component of ground motion parallel to the pipe axis. The resulting ground strain along the pipe axis is a function of this angle in the horizontal plane. Wang and

Yeh (1985) have shown that the ground strain is a maximum for an angle of 45° in the horizontal plane where

$$\varepsilon_g = \frac{V_m}{2C} \qquad (2.15)$$

Where C is the apparent propagation velocity with respect to the ground surface given in Equation 2.15. For R-waves propagation, Equation 2.16 gives the horizontal ground strain along the direction of propagation where C is the phase velocity for a wavelength equal to roughly four times the separation distance.

When looking at a horizontally oriented pipeline, the ground curvature is only of importance when shear waves travel parallel to the pipeline. As in this report upward propagating SH waves are considered, it is not very likely that this situation will occur. Moreover, O'Rourke & Liu (1994) note that the pipeline bending strains caused by the ground curvature is typically an order of magnitude smaller than the induced axial strains from a shear wave.
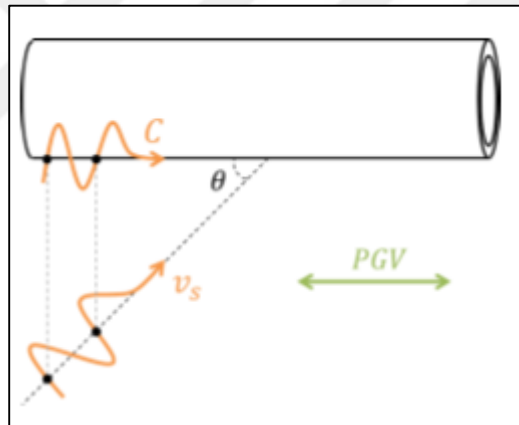
Figure 2.16: Shear wave propagation towards a continuous pipeline.

When the relative angle between the shear wave propagation path and the pipeline is, the induced axial strains from shear wave propagation are maximal. This can be shown by recalling from equation (2.16) that $\varepsilon_g = V_m/C$ where V_m is the maximum particle velocity in the direction parallel to the wave propagation path, C the apparent shear wave velocity and ε_g the ground strain parallel to wave propagation path.

If a shear wave with propagation velocity V_s travels towards a pipeline under an arbitrary angle θ as presented in Figure 2.16, the apparent shear wave velocity C in axial pipeline direction is given by $C = V_s/\cos \theta$. The maximum particle velocity in the direction of the propagation path V_m can be determined by using the horizontal

24

peak ground velocity PGV and using its component in the direction of the wave propagation path. In this way, it is obtained that

$$\varepsilon_g = \frac{PGV}{V_s} \, \sin\theta \cos\theta \tag{2.16}$$

This gives a maximum for ε_g at $\theta = 45^o$. For a constant sinusoidal wave shape, the PGV is related to the peak ground acceleration by $PGA = 2\pi f \, PGV$. Since in this report the peak ground acceleration is used, this will be done here as well.

The question that remains is how the ground strains in axial direction are transferred to the pipeline. Newmark and Hall (1975) simply assumed the pipeline strain to be equal to the ground strain, but as noted that there is a limit to the friction that can be transferred from the soil to the pipeline at the interface, in longitudinal direction given by t_u.

By assuming that this friction force t_u is reached everywhere along the pipeline, O'Rourke and Tawfik (1983) reason that the maximum pipeline strain can be found by taking into account that t_u works over a distance of $\lambda/4$ as presented in Figure 2.17.
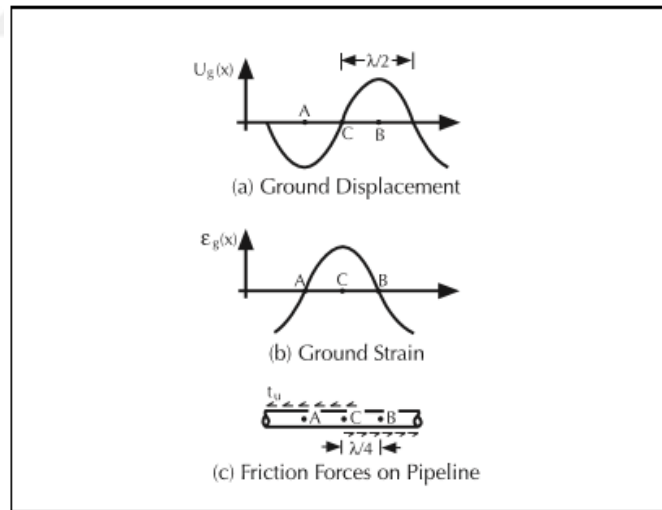
M. O'Rourke and El Hmadi, 1988

Figure2.17: Friction strain model for wave propagation effects on buried pipelines.

Given this maximum and working out equation (2.17) it can be found that the maximum pipeline strain ε_x, given that a shear wave that approaches the pipeline at an angle of 45°, is:

$$\varepsilon_x = \frac{t_u v_s}{4 E A_s f} \tag{2.17}$$

Where :

ε_x = Pipe strain

t_u = Friction force between pipe and ground

v_s = Shear wave velocity

E = Elastisite modulus of pipe

A_s = Pipe section area

f = Ground frequency

2.3 Soil –Pipe Interaction

Buried pipelines are interaction with soil surrounding them. Earthquakes cause that the buried pipelines are damaged because of deformation and forces loaded on them along interactions at the pipe soil interface. When the earthquake occurs, the pipe and the soil-surrounding pipe move relatively different from each other. This relative movement induces pipe to become deformed (O'Rourke and Liu, 1999). According to O'Rourke and Liu (1999), the interaction between soil and pipe can be divided into two groups as longitudinal and transverse. In the transverse direction, the interaction between soil and pipe includes horizontal and vertical movement. Furthermore, the vertical component of the interaction between soil and pipe involves upward and downward pipe movement. The interaction between soil and pipe should be divided into two groups with regards to the soil surrounding pipe as the pipelines surrounded by non-liquefied soil, and pipelines located in a liquefied layer (O'Rourke and Liu, 1999). As mentioned before, in this research the case of non-liquefied soil is considered.

Despite laboratory tests have demonstrated that at large relative displacement the maximum soil force on pipeline decreases, ALA (2001) proposes an assumption based on that the soil force is constant once it reaches the maximum value.

The Pipeline Located in Non-liquefied Soil

Trautmann and O'Rourke (1985) found a force-deformation relation for horizontal lateral movement as a result of laboratory tests, which were performed to determine soil interaction forces for a pipeline surrounded by non-liquefied soil. The ASCE Technical Council on Lifeline Earthquake Engineering (TCLEE) Committee on Gas and Liquid Fuel Lifelines (ASCE, 2001) proposed idealized elasto-plastic models in

order to model the interaction between soil and pipe. The elasto-plastic model consists of two parameters. These parameters are the maximum resistance Pu, Tu, Qu, Qd in transverse horizontal, axial and transverse vertical directions respectively and the maximum elastic deformation Δp, Δt, Δqd, Δqu respectively (Figure 2.18 to 2.20).

2.3.1 Axial soil springs

Regarding to the soil embankment material used for trench of pipeline, soil axial spring features are estimated. Though this is appropriate only when pipeline movement response relative to neighboring embankment is not significantly affected by trench outside soil, in the Figure 2.18 ideal behavioral curve of axial soil spring is shown.
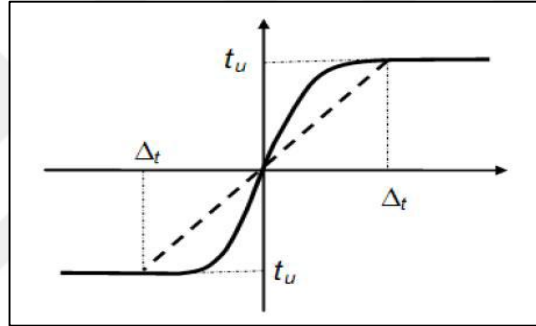
Figure 2.18: Bi-linear axial soil springs used to represent soil force on pipe (ALA, 2001).

The maximum axial soil force per unit length of pipe can be calculated by using equation 2.18.

$$T_u = \pi D \alpha c + \pi D H \gamma \left(\frac{1+K_0}{2}\right) \tan \delta \qquad (2.18)$$

$$\alpha = 0.608 - 0.123c - \frac{0.274}{c^2+1} + \frac{0.695}{c^3+1} \qquad (2.19)$$

In the above equations, parameters are as follows:

D = Pipe external diameter

C = Soil coherence inside channel (c is in kPa/100)

H = Pipe axis depth from ground surface

γ = Specific weight of soil

K_0 = Coefficient of soil pressure at rest

α = Coherence ratio

δ = Friction angle between pipe and soil ($\delta = f\emptyset$)

$\emptyset$ = Soil internal friction angle

f = Coating dependent factor resulting from Soil internal friction angle and friction angle between pipe and soil

The following table (Table 2.1) is used to determine the coating dependent factor for different materials.

Table 2.1: Coating dependent factor of soil.

Material	f
Concrete	1
Coal tar	0.9
Hardened steel	0.80
Mild steel	0.7
Epoxy	0.6
Polyethylene	0.6

The maximum elastic deformation (Δ_t) values change depending on types of soil surrounding pipe. The maximum elastic deformation for various soil types are given below.

Δ_t = displacement at T_u

    = 0.1 inches (3 mm) for dense sand

    = 0.2 inches (5 mm) for loose sand

    = 0.3 inches (8 mm) for stiff clay

    = 0.4 inches (10 mm) for soft clay

2.3.2 Lateral soil springs

Lateral soil springs simulate the resistance of surrounding soils to any horizontal translation of pipeline. Therefore, the mechanisms of soil pipeline interaction are similar with vertical anchor plates or footings moving horizontally relative to the surrounding soils, and thus passive type of earth pressure (Figure 2.19). The maximum lateral soil force per unit length of pipe can be calculated by using equation 2.20.

Figure 2.19: Bi-linear lateral soil springs used to represent soil force on pipe (ALA, 2001).

$$P_u = N_{ch}cD + N_{qh}\gamma HD \tag{2.20}$$

Where:

N_{ch} = horizontal bearing capacity factor for clay (0 for c= 0)

$N_{ch} = a + b(x) + \dfrac{c}{(x+1)^2} + \dfrac{d}{(x+1)^3} \leq 9$

N_{qh}= horizontal bearing capacity factor (0 for $\varphi = 0°$)

$N_{qh} = a + b(x) + c(x^2) + d(x^3) + e(x^4)$

D= pipe outside diameter

c= soil cohesion representative of the soil backfill

H= depth to pipe centerline

γ= effective unit weight of soil

N_{ch} and N_{qh} values can be derived from Table 2.2.

In addition, displacement in lateral force point transferred to pipe Pu is obtained by the equation 2.21:

$$\Delta_p = 0.04\left(H + \frac{D}{2}\right) \leq 0.1D - 0.15D \tag{2.21}$$

or;

Δ_p = displacement at P_u

 = (0.07 ~ 0.10)(H + D/2) for loose sand

 = (0.03 ~ 0.05)(H + D/2) for medium sand

 = (0.02 ~ 0.03)(H + D/2) for dense clay

Table 2.2: Nch and Nqh value determination for lateral soil springs.

Factor	$\emptyset$	X	a	b	c	d	e
N_{ch}	0°	H/D	6.752	0.065	-11.063	7.119	-
N_{qh}	20°	H/D	2.399	0.439	-0.03	1.059 E-3	-1.1754 E-5
N_{qh}	25°	H/D	3.332	0.839	-0.090	5.606 E-3	-1.319E-4
N_{qh}	30°	H/D	4.565	1.234	-0.089	4.275 E-3	-9.159E-5
N_{qh}	35°	H/D	6.816	2.019	-0.146	7.651 E-3	-1.683E-4
N_{qh}	40°	H/D	10.959	1.783	0.045	-5.425 E-3	-1.153E-4
N_{qh}	45°	H/D	17.568	3.309	0.048	-6.443 E-3	-1.299E-4

2.3.3 Vertical soil springs

2.3.3.1 Vertical uplift soil springs

The maximum vertical uplift soil force per unit length of pipe can be calculated by using equation 2.22. Figure 2.20 shows the vertical bearing and uplift soil force on pipe.
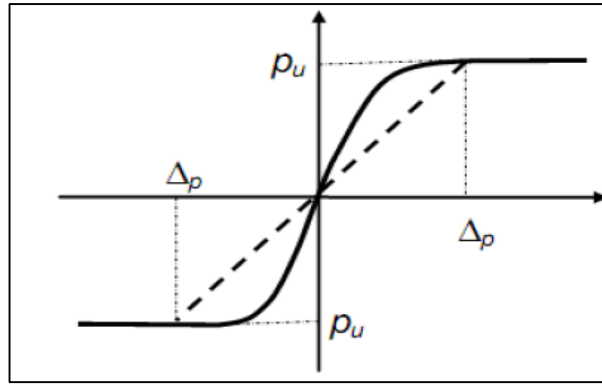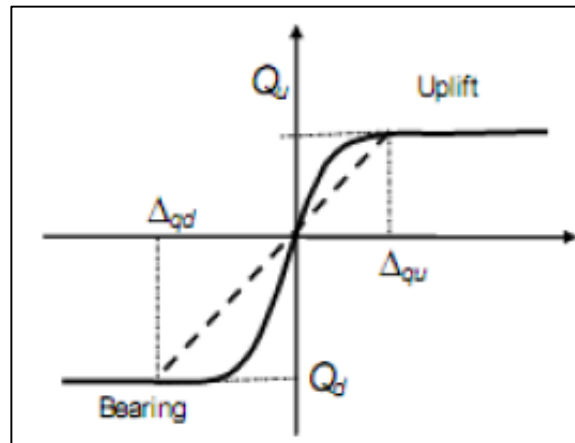

Figure 2.20: Bi-linear vertical soil springs used to represent soil force on pipe (ALA, 2001).

$$Q_u = N_{cv} \, c \, D + N_{qv} \, \gamma HD \qquad (2.22)$$

Where:

N_{cv}= vertical uplift factor for clay (0 for c= 0)

N_{qv}= vertical uplift factor for sand (0 for φ= 0)

$N_{cv}= 2*(\frac{H}{D}) \leq 10$ applicable for sand $(\frac{H}{D}) \leq 10$

$N_{qv}= (\frac{\varnothing H}{44D}) \leq N_q$

$N_q= \exp(\pi \tan \varnothing) tan^2(45+\frac{\varnothing}{2})$

$\Delta_{qu} = $ displacement at Q_u

    $= 0.01$ to 0.02 for dense to loose sands < 0.1 D

    $=0.1$ to 0.2 for stiff to soft clays < 0.2 D

2.3.3.2 Vertical bearing soil springs

The maximum vertical bearing soil force per unit length of pipe can be calculated by using equation below.

$$Q_d = N_c cD + N_q \gamma HD + N_\gamma \gamma \frac{D^2}{2} \tag{2.23}$$

Where:

$N_c, N_q N_\gamma = $ bearing capacity factors

$N_c= [\cot(\varnothing + 0.001)] \left(exp[\pi \tan \varnothing + 0.001] tan^2 \left(45 + \frac{\varnothing+0.001}{2}\right) - 1 \right)$

$N_q= \exp(\pi \tan \varnothing) \, tan^2(45 + \frac{\varnothing}{2})$

$N_\gamma= e^{(0.18\varnothing - 2.5)}$

$N_c, N_q N_\gamma$ can also be determined by using Figure 2.21

$\gamma=$ total unit weight of soil

$\Delta_{qd} = $ displacement at Q_d

    $=0.1$D   for granular soils

    $=0.2$D   for cohesive soils

2.4 Pipe Failure Modes and Failure Criterion

When earthquake occurs, buried pipelines can be damaged because the buried pipelines are exposed to seismic loading. The principal failure modes for corrosion-free continuous pipelines are rupture due to axial tension, local buckling due to axial compression and flexural failure. Tensile failure occurs due to excessive axial tension along the buried pipeline and local buckling occurs because of excess axial compression and flexural failure. Beam buckling is a failure mode that occurs if the burial depth is shallow and if continuous pipelines are exposed to axial compression.

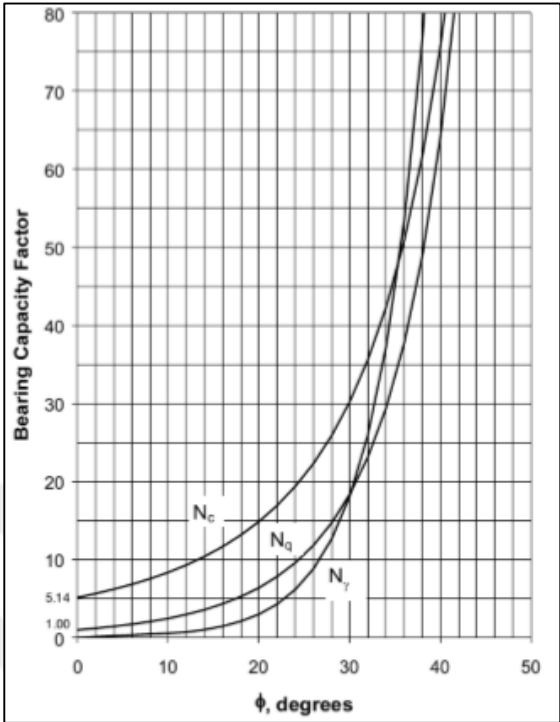These failure modes will be summarized and failure criterion for these failure modes will be presented.

Figure 2.21: Bearing capacity factors (N_c, N_q and N_γ) (ALA, 2001).

According to O'Rourke and Liu (1999), the principal failure modes for continuous pipeline with burial depth of about one meter or more are tensile failure and local Buckling. If the burial depth of continuous pipeline is less than about one meter, continuous pipeline may be experienced to beam buckling behavior

2.4.1 Tensile failure criterion

The strain associated with tensile failure is generally well above about 4% (Newmark and Hall, 1975). Beyond the tensile value of 4%, the pipeline is considered to have failed in tension so ultimate tensile value can be considered as 4%.

Tensile failure can be divided into four categories as ductile tensile failure, brittle tensile failure, fatigue failure and bending failure. According to material behavior and loading conditions, tensile failure can occur in various forms. If pipe material has a good degree of ductility, the pipe will stretch until ultimate strength of pipe is reached. The brittle tensile failure is opposite of the ductile tensile failure. The pipe material is working properly one moment and the next it has failed. Fatigue failure occurs due to the application of cyclic tensile load.

To understand failures we must understand the behavior of the pipe material. Ramberg and Osgood (1943) proposed a model for description of the post yield stress-strain behavior. The Ramberg and Osgood (1943) model is given by:

$$\varepsilon = \frac{\sigma}{E}\left[1 + \frac{n}{1+r}\left(\frac{\sigma}{\sigma_y}\right)^r\right] \tag{2.24}$$

Where E is the initial Young's modulus, σ is the uniaxial tensile stress, ε is the engineering strain, σ_y is the apparent yield stress, n and r are Ramberg and Osgood (1943) parameters.

Table 2.3: Ramberg and Osgood (1943) for mild steel and X-grade steel.

	Grade-B	X-42	X-52	X-60	X-70
Yield Stress (Mpa)	227	310	358	413	517
n	10	15	9	10	5.5
r	100	32	10	12	16.6

2.4.2 Local buckling

Local buckling occurs due to axial compression. The axial compression in the pipe causes structural stability broken down. In consequence of a sudden change from a stable to unstable condition, local instability of pipe wall can occur. Hall and Newmark (1977) performed laboratory tests on thin wall cylinders and they observed that local buckling in a pipe starts at a strain of 1/3 to 1/4 of the theoretical value of:

$$\varepsilon_{theory} = 0.6 * t/R \tag{2.25}$$

2.4.3 Beam buckling

Beam buckling generally occurs when the pipelines are buried in shallow trenches and /or backfilled with loose material (O'Rourke and Liu, 1999). Meyersohn (1991) made a study about critical cover depth when the beam buckling of pipelines occurs. Meyersohn (1991) obtained the relationship between critical cover depth and t/D ratio for sands having different relative density.

3. FINITE ELEMENT ANALYSIS

3.1 Finite Element Method Definition

PLAXIS is software used for analyzing deformations and stability in geotechnical engineering projects. Usually, in major geotechnical issues, there is a need for an advanced behavioral model for modeling non-linear and time-dependent behavior of soils relative to desired purpose. By this software, one can model excavation and embankment with various loading and boundary conditions using 6 and 15 nodal triangle elements. First edition of this software was commissioned by water resource management of Netherlands in Delft Industrial University in 1987 to analysis earth dams constructed on soft soil in low-level areas of this country. Then in 1993, it was extended and confirmed and supported by Center for Civil Engineering Research and Codes institution. In this software, behavioral models of Mohr-Coulomb, hardening hyperbolic model, softening model (Cam-Clay) and soft soil creep model are applicable. As it became apparent in the previous chapters, there are many restrictions when applying and combining relatively simple methods to estimate ground deformations and the corresponding pipeline responses. An alternative approach altogether is using finite element software such as PLAXIS. The basic idea behind a finite element approach is cutting up the construction (or in this case cross-sectional plane) into a finite number of smaller elements that are connected to each other at their nodes. Continuous field parameters, such as displacements, are described by the values at these nodes and the values between the nodes are determined by interpolation. Because the relations that describe the behavior of the nodes are dependent on the other nodes as well, the governing equations have to be solved simultaneously by using a numerical, often iterative procedure. As the size of the used elements approaches zero (number of nodes goes to infinity), the outcome of the model is expected to be an exact solution of the governing equations.

Although the description above sounds very promising, various aspects may cause problems, the most important being calculation time and/or computing power. For

this reason the choice is made to use PLAXIS 2D, considering the limited amount of time available for the research described in this report. Because the nature of the physical behavior in some cases is clearly three-dimensional, smart workarounds may be required. Furthermore, although in theory the outcome of the model could be exact, the question is whether the selected governing equations are indeed capable of describing the actual physical behavior.

In line with this approach, also for the finite element analysis it is chosen to first consider the ground deformations and later add the pipeline to the cross-section. By doing this it is will be easier to address the cause of deviating results.

3.2 Soil Models

This section will treat the constitutive soil model that will be used for the finite element calculations. A constitutive soil model can be seen as a specific set of governing equations that describe a certain type of soil behavior. In the following paragraphs, the pros and cons of the used model will be discussed. As some basic terminology is required to explain this model.

3.2.1 Calibration of the HS small model

In dynamic conditions, the soil is subjected to cyclic shear loading, showing not only a non linear but also a dissipative behavior. The hysteretic loop genenrated during cyclic shear loading consist of a sequence of loading and unloading paths,because of the irrevesibale behavior of the soil. In general, it has been observed that earthquakes induce a small strain level in the soil, that exhibits a high shear stiffness G_0 ,and that G decreases while the amount of dissipated energy increased by increasing the magnitude of the shear strain γ (Brinkgreve, 2015).

The account for these aspects of maerial behavior, the Hardening Soil model with small-strain stiffness (HS small model), based on the Hardening Soil model, is used in this study. The Hardening Soil model already accounts for the stress dependency of the stiffness according to a power law expressed by the **m** parameter. Compared to the Hardening Soil model, the HS small is extended by introducing two additional parameters: the high stiffness at small strain level (G_0) and the shear strain at which G has reduced to 70% of the initial G_0 ($\gamma_{0.7}$) (PLAXIS-2D, 2014).

The stress dependency is expressed by the following formula:

$$G_0 = G_0^{ref} \left(\frac{c.\cos\varphi - \sigma_3'.\sin\varphi}{c.\cos\varphi + p^{ref}.\sin\varphi} \right)^m \tag{3.1}$$

Where the initial shear stiffness G_0 is a function of the effective stress, the strengh parameter (c and ø) and the m parameter which depends on the soil type (it generally varies between 0.5 and 1, according the soil type).

The typical hysteretic behavior is shown in Figure 3.1. The initial tangent and secant stiffness of the initial loading curve coincide with the maximum shear stiffness G_0. By increasing the shear strain, the stiffness decays. When the load direction is inverted, the stiffness starts from the same G_0 and decreases until the next laod reversal. The stress-strain relationship is given by:

$$\tau = G_s.\gamma \tag{3.2}$$

Where G_s represents the secant shear stiffness.

The local hysteretic damping ratio is described by the following formula:

$$\xi = \frac{E_D}{4\pi E_s} \tag{3.3}$$

Where E_D repressnts the dissipated energy, given by the area of the closed loop (yellow and green areas), and E_s is the energy accumulated at the maximum shear strain γ_c (green and blue areas). The damping ratio ξ applies until the material behavior remains elastic and the shear modulus decreases with the strian.

To calibrate the parameters that need to be entered in PLAXIS it is suggested to refer to experimental data from site and laboratoary tests performed in the chosen area.

Considering the Eq.(3.1), it is possible to calibrate G^{ref} and m in order to have the best fitting. The decay of the shear modulus with strain is displayed Figure 3.1. The green curve shows the ratio of the secant shear modulus over the initial shear stiffness G_s/G_0 and the orange curve shows the ratio of tangent shear modulus over the initial shear stiffness G_t/G_0, which can be calculated from Eq.(3.2) by taking the derivative with respect to thee shear strain.

In the HS small model, the tangent shear modulus is bound by a lower limit, G_{ur}, to scale back to the original Hardening Soil model at higher strain levels. G_{ur} is related to E_{ur}, and v_{ur} according to the following expression:

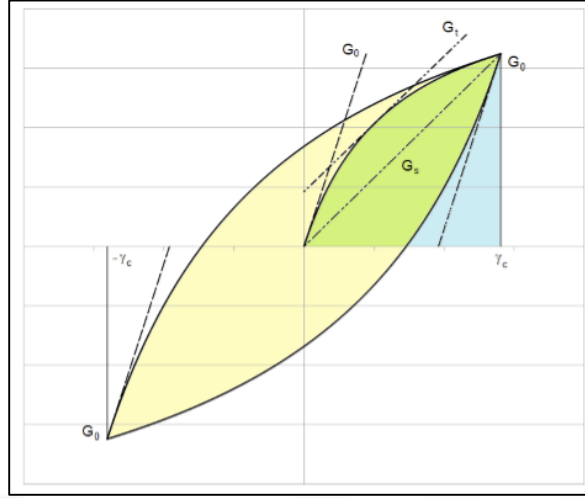$$G_{ur} = \frac{E_{ur}}{2(1+v_{ur})} \qquad (3.4)$$

Figure 3.1 : Hysteretic behavior in the HS saml model

Here the most important properties of the model will be explained without going into too much detail on the equations that are used (see Benz, 2007 and Brinkgreve, 2015).

Consider the case that some element of soil is loaded by the combination of a shear and compressional force. Before loading the stress, state was p_1' ,q_1 and afterwards the stress state becomes p_2', q_2. If both stress states lie within the elastic region of Figure 3.2, the stiffness of the soil is constant and has a magnitude E_{ur}, where the subscript stand for unloading/reloading.

If the stress-path from p_1' ,q_1 to p_2' ,q_2 reaches the shear yield surface f^s the edge of the elastic region is reached, where plastic (irreversible) strains will develop due to the amount of induced shear stress.

The amount of plastic strains depends on the mobilized dilatancy angle Ψ_m . This is a function of both the mobilized friction angle φ_m, which represent the stress state of the soil, and the critical friction angle φ_{cv}, which is a material constant that determines whether the soil shows dilative or contractive behavior. In the HS small model only positive values of Ψ_m are considered, which means that only dilative behavior is accounted for, contractive behavior is not. The parameter that largely controls the behavior of the shear yield surface is E_{50}.
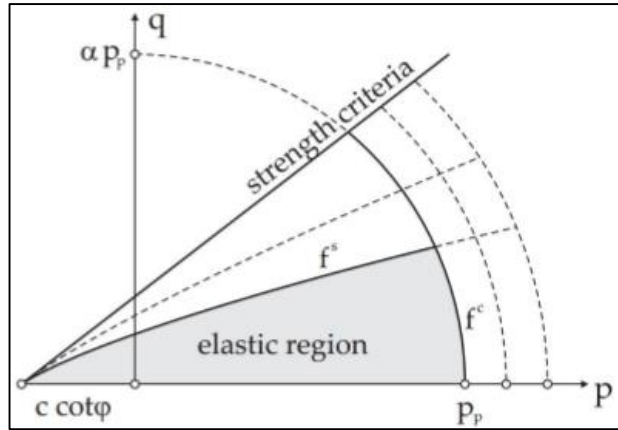
Figure 3.2: Yield surfaces for the HS small model (Benz, 2007).

If the stress-path from p_1' ,q_1 to p_2' ,q_2 reaches the cap yield surface f^c the edge of the elastic region is also reached, where in this case plastic strains will develop due to the amount of induced compressive stress. The parameter that largely controls the behavior of the cap yield surface is $E_{oed.}$

As the soil, stiffness is very dependent on the magnitude of the shear strains. The shear strains induced by earthquakes are very small and therefore the unloading/reloading stiffness of the soil E_{ur} may underestimate this stiffness significantly.
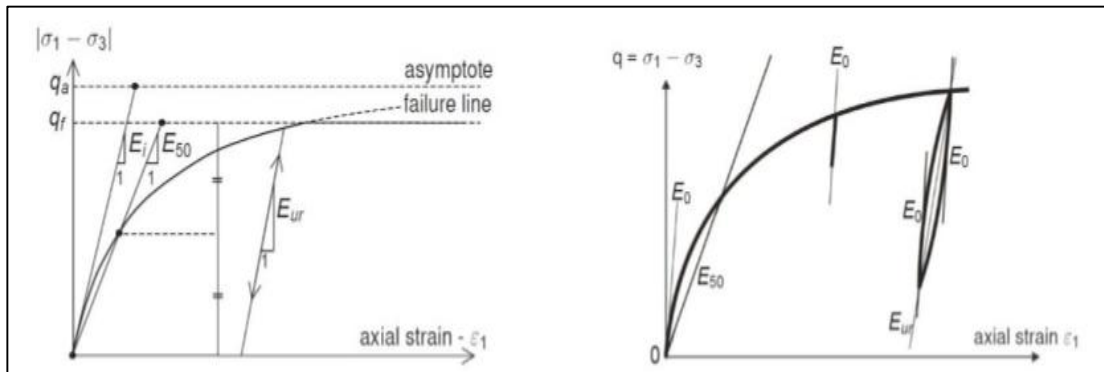

Figure 3.3: Hyperbolic relation between vertical strain (ε_1) and deviatoric stress in a triaxial test. On the left for the standard Hardening Soil model, on the right by also accounting for the small strain stiffness.

For shear strains that are below a certain threshold value (dependent on the parameter $\gamma_{0.7}$) of the shear strain γ_s , the soil stiffness is thus dependent on the level of itself. Above this threshold, value E_{ur} is still applied for unloading/reloading situations Figure (3.3).

3.2.2 Soil parameters

To determine the initial stress distribution in the cross-section for sandy soil layers also parameters are defined for the HS small model. Brinkgreve (2010) present several correlation equations based on the relative density D_R that can be used to estimate these parameters. The correlations are obtained by performing a regression analysis on a collection of soil test data. It is noted that although not all derived equations and parameters have been validated in sufficient detail, the equations may give a reasonable approximation and are useful when only limited soil data is available. They are presented at the end of this paragraph in Table 3.3.

3.3 Damping (Site Response Analysis)

The governing equations in a finite element model do not always take into account damping, which means it has to be added manually. PLAXIS allows two ways to do this: Newmark time integration damping and Rayleigh damping. The parameters for the Newmark time integration damping are by default set to a minimum to allow for a stable calculation process. These parameters will not be adjusted here and only Rayleigh damping will be considered.

Rayleigh damping is a frequency dependent type of damping and the curve that determines the damping ξ per frequency f ($=\omega/2\pi$) is given by equation (3.6) in which α_R and β_R are the Rayleigh damping parameters. By assigning two different damping percentages at two different frequencies these parameters can be calculated

$$\xi(\omega) = \frac{\alpha_R}{2\omega} + \frac{\beta_R}{2} \tag{3.5}$$

Rayleigh damping is in engineering practice mostly between 0.5% and 2% for both the first and second target frequencies. In this study, the first calculations were performed based on the method target frequencies. In this study the first calculations were performed based on the method mentioned by Hudson, et al. (1994) where the first target frequency is set equal to fundamental frequency of the soil profile and the second frequency is the first odd number of the ratio: fundamental frequency of the input signal/ fundamental frequency of soil profile. According to this procedure, the frequency of Target 1 is given by:

$$f = \frac{V_s}{4H} \tag{3.6}$$

Where V_s represents the shear wave velocity and H is the thickness of the soil layer. The value of V_s has been chosen as an average value over the whole depth. Based on the shear stiffness profile G and the unit weight of soil, it is possible to calculate the shear wave velocity profile with depth:

$$V_s = \sqrt{\frac{G}{\rho}} \tag{3.7}$$

Where ρ is equal to the ratio over the gravity acceleration g.

3.4 Calibration of the Finite Element Model (FEM)

For the site response analysis of the FEM model, DEEPSOIL program was used to compare the soil behavior during a harmonic load applied at 30 m depth. This comparison was mainly executed to examine the influence of the boundaries disturbances at the bottom and sides, kind of boundaries chosen in DEEPSOIL and PLAXIS, mesh size and performance of the chosen soil model.

3.4.1 PLAXIS model

In this problem, analysis of a nonlinear, drained soil subjected to a specific seismic ground motion has been performed using Hs small Strain model in PLAXIS Dynamic module. The applied ground motion corresponds to the harmonic load with certain values of Amplitude and Frequency (Figure3.4).
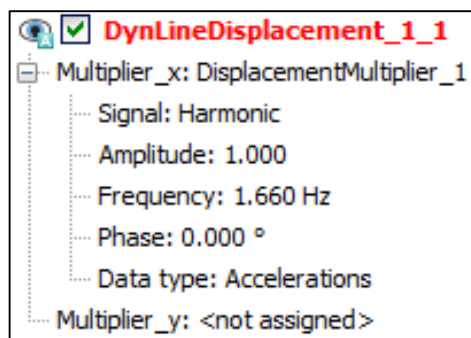

Figure3.4: The values of amplitude and frequency.

Table 3.1: Parameters of the HS small model for sandy soil layers (D_R in %).

Symbol	Unit	Explanation	Used from Brinkgreve Eq.	Loose Sand (Dr=%25)	Dense Sand (Dr=%100)	Soft Backfill	Stiff Backfill
γ_{unsat}	kN/m^3	Unit Weight	15 + 4.0 Dr/100	16	19	14	16
γ_{sat}	kN/m^3	Saturated Unit Weight	19 +1.6 Dr/100	19.4	20.6	18	19.4
E_{50}^{ref}	kN/m^2	Secant stiffness in standard drained triaxial	60000 Dr /100	15000	60000	10000	15000
E_{oed}^{ref}	kN/m^2	Tangent stiffness for primary odometer loading	60000 Dr /100	15000	60000	10000	15000
E_{ur}^{ref}	kN/m^2	Unloading / reloading stiffness	180000RD /100	45000	180000	30000	45000
m	-	Power for stress-level dependency of stiffness	0.7 –Dr/320	0.622	0.387	0.65	0.622
C_{ref}'	kN/m^2	Cohesion	--	1.0	1.0	1.0	1.0
φ	o	Friction angle	28+12.5 Dr/100	31	40.5	25	31
Ψ	o	Dilatancy angle	-2 + 12.5 DR/100	1	10.5	0	1
R_f	-	Failure ratio	1-Dr /800	0.969	0.875	.99	0.969
$\gamma_{0.7}$	-	Shear strain at which (G_s=0.722G_o)	(2 –Dr/100)x10^{-4}	1.8E-4	1E-4	1.8E-4	1.8E-4
G_o	kN/m^2	Shear modulus at very small strains	60000 +68000Dr/100	77000	128000	40000	77000
ν_{ur}	-	Poisson's ratio	0.2	0.2	0.2	0.2	0.2

3.4.2 DEEPSOIL model

DEEPSOIL is a one-dimensional site response analysis program that can perform: a) 1-D nonlinear time domain analyses with and without pore water pressure generation, and b) 1-D equivalent linear frequency domain analyses including convolution and deconvolution. The program is provided as-is and the user assumes full responsibility for all results. The use of the DEEPSOIL program requires knowledge in the theory and procedures for seismic site response analysis and geotechnical earthquake engineering. It is suggested that the user reviews relevant literature and seek appropriate expertise in developing input of the analysis and interpretation of the results.

In PLAXIS 2D the plane strain mesh is 50 m wide and 30 m deep and consists of 6-node elements. In PLAXIS 3D the model is extended by 1m in the y-direction. The input motion is applied horizontally at the base of model; the model is shown in Figure 3.5. A nonlinear material is used with Vs=200 m/s and ϒ=16.5 kN/m^2(Loose Sand).The first natural frequency of this deep deposit may be calculated to be:

$$\text{f} = \frac{V_S}{4H} = \frac{200}{4*30} = 1.66 \text{ Hz} \tag{3.8}$$

The soil damping is taking into account using Rayleigh damping with α_R =0.0928 and β_R =138E-3 (this values correspond to 1.0 % damping according to DEEPSOIL results with natural frequencies of the deposit being considered as 1.03 Hz and 5.15 Hz). Figure 3.6 shows the geometry 1-D modeling and soil profile definition of DEEPSOIL.

3.4.3 Boundary conditions

For the vertical model boundaries, the proper options can be applied: free field or tied degrees of freedom. The free-field option implies that waves from the model travel outward with minimum reflection at the boundaries. Energy is thus absorbed at the boundaries, but it can be reasoned that in reality also energy enters the model from outside the boundaries.
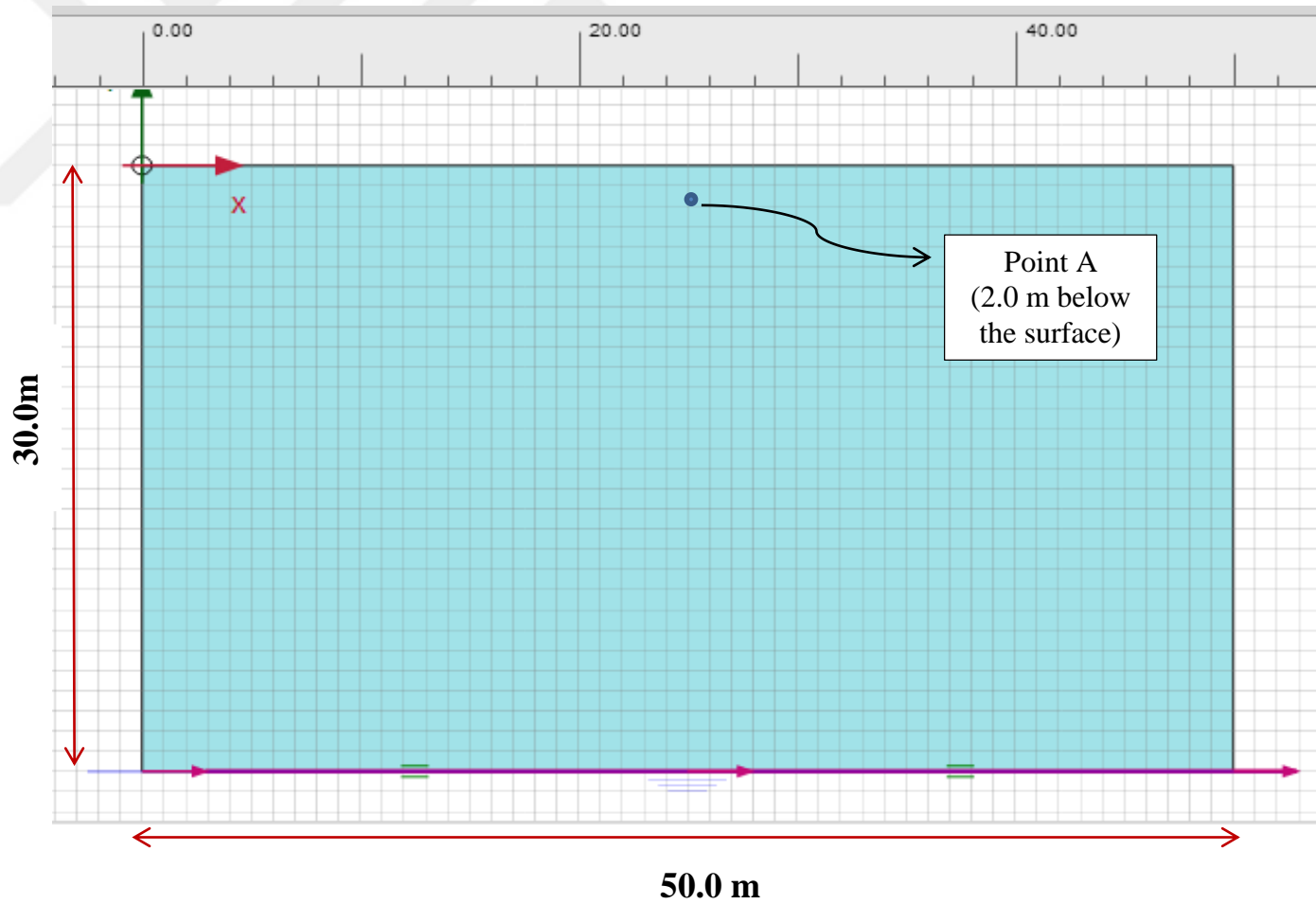
Figure 3.5: Geometry (50 × 30 m) and boundary conditions of PLAXIS modeling with seismic acceleration applied at the base.
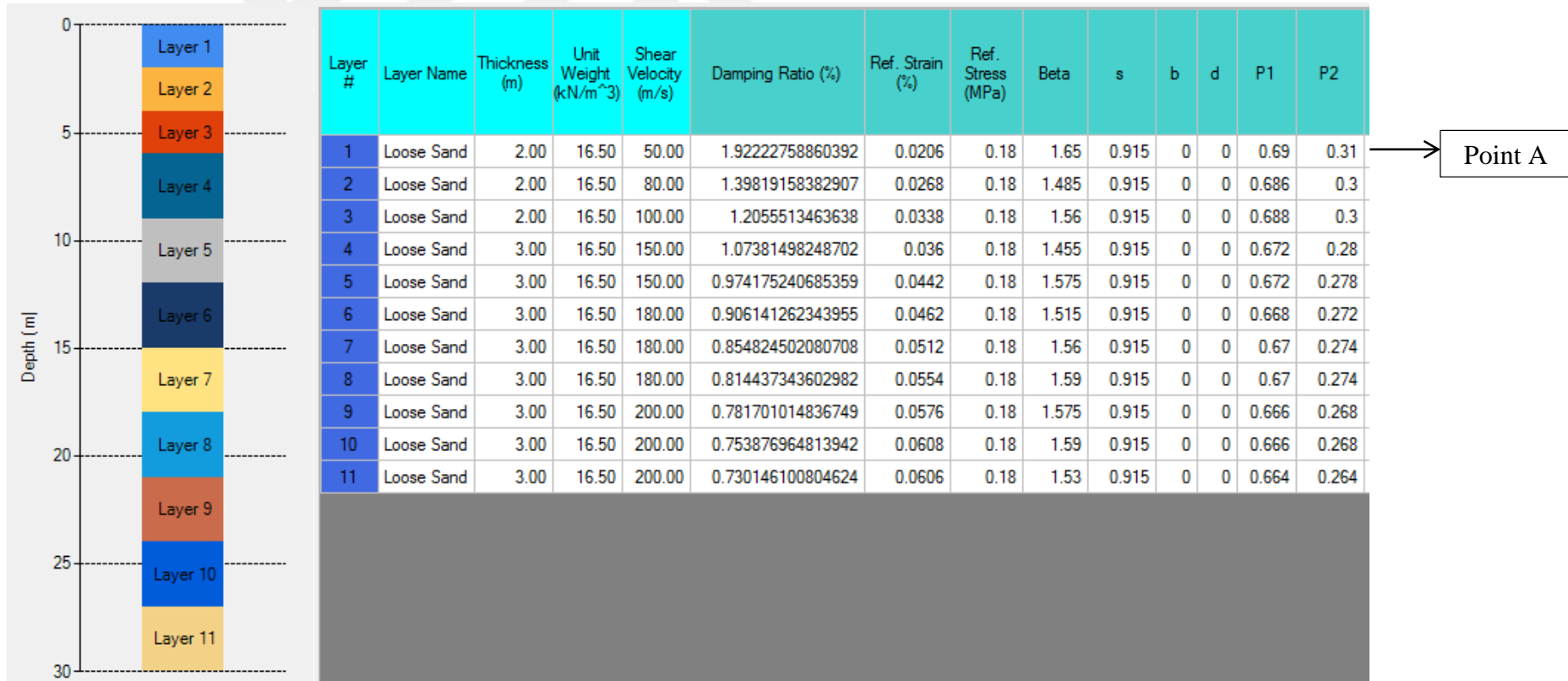
Layer #	Layer Name	Thickness (m)	Unit Weight (kN/m^3)	Shear Velocity (m/s)	Damping Ratio (%)	Ref. Strain (%)	Ref. Stress (MPa)	Beta	s	b	d	P1	P2
1	Loose Sand	2.00	16.50	50.00	1.92222758860392	0.0206	0.18	1.65	0.915	0	0	0.69	0.31
2	Loose Sand	2.00	16.50	80.00	1.39819158382907	0.0268	0.18	1.485	0.915	0	0	0.686	0.3
3	Loose Sand	2.00	16.50	100.00	1.2055513463638	0.0338	0.18	1.56	0.915	0	0	0.688	0.3
4	Loose Sand	3.00	16.50	150.00	1.07381498248702	0.036	0.18	1.455	0.915	0	0	0.672	0.28
5	Loose Sand	3.00	16.50	150.00	0.974175240685359	0.0442	0.18	1.575	0.915	0	0	0.672	0.278
6	Loose Sand	3.00	16.50	180.00	0.906141262343955	0.0462	0.18	1.515	0.915	0	0	0.668	0.272
7	Loose Sand	3.00	16.50	180.00	0.854824502080708	0.0512	0.18	1.56	0.915	0	0	0.67	0.274
8	Loose Sand	3.00	16.50	180.00	0.814437343602982	0.0554	0.18	1.59	0.915	0	0	0.67	0.274
9	Loose Sand	3.00	16.50	200.00	0.781701014836749	0.0576	0.18	1.575	0.915	0	0	0.666	0.268
10	Loose Sand	3.00	16.50	200.00	0.753876964813942	0.0608	0.18	1.59	0.915	0	0	0.666	0.268
11	Loose Sand	3.00	16.50	200.00	0.730146100804624	0.0606	0.18	1.53	0.915	0	0	0.664	0.264

Point A

Figure 3.6: Geometry 1-D modeling and soil profile definition of DEEPSOIL.

By using the tied degrees of freedom option, the nodes on the left side of the model undergo the same displacements as the nodes on the right side of the model. Due to the fact that, the used PLAXIS program in this study (2D, AE) done have no Free Field option, therefore to adapt to free filed case, the wide of model consider 50.0 meter by trial and error, but the coefficient of boundary conditions assumed by default ($C_1 = C_2 = 1.0$).

3.4.4 Mesh size

The mesh generation is fully automatic and base on a robust triangulation procedure. The dimension of the triangular elements needs tube controlled and the mesh refinement allows to get specific value for the average length of the element side. Kuhmeyer & Lysmer (1973) suggest to assume a size less than or equal to one-eighth of the wavelength associated with the maximum frequency component f_{max} of the input wave (i.e. the highest frequency component that contains appreciable energy):

$$\text{Average Element Size} \leq \frac{\lambda}{8} = \frac{V_{s,min}}{8 f_{max}} \tag{3.9}$$

Where $V_{s,min}$ is the lowest wave velocity. Based on the shear stiffness profile and the unit weight of soil, it is possible to calculate the shear wave velocity profile with depth. The lowest $V_{s,min}$ is equal to 70 m/s in sandy soils. From the Fourier spectrum, it can be found that the maximum frequency component is about 5 Hz, which leads to an average length of 1.75 m.

3.4.5 Comparison of results

The results of the analysis have been obtained in form of Acceleration and Relative displacement of certain point close to surface. These results are compared with the results obtained from the analysis of the same problem in DEEPSOIL.

Figure 3.7 shows the horizontal Displacement Ux of the point (25,-2) versus time located at the depth of 2 m below the surface, as obtained from PLAXIS. In addition, Figure 3.8 indicates the Acceleration (g) obtained from PLAXIS versus time. The Acceleration (g) and Relative Displacement obtained from DEEPSOIL versus time it can be seen in figure 3.9.
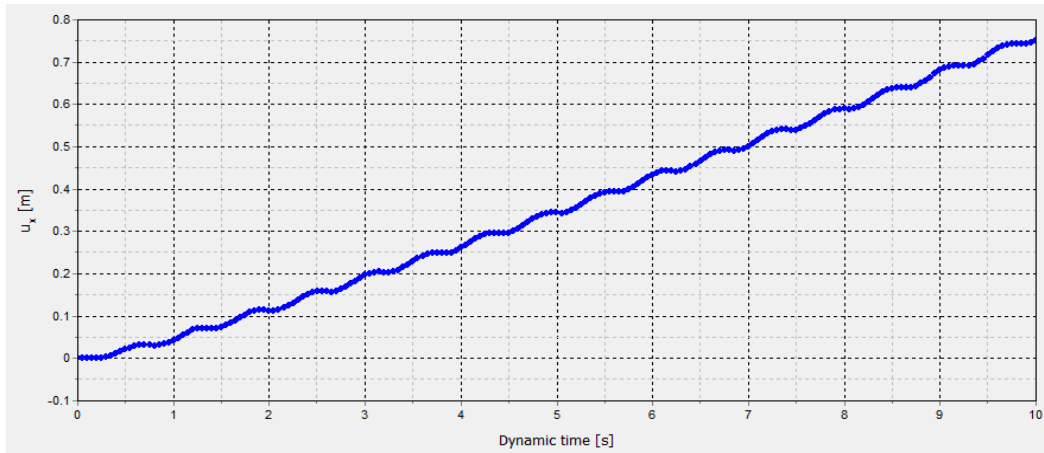
Figure 3.7: The relative displacement (Ux) of the point (25,-2) versus time
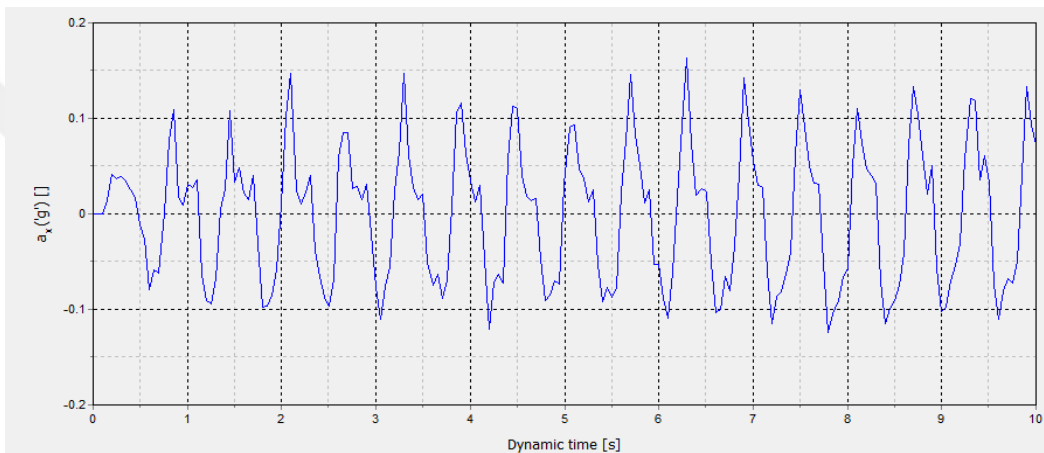
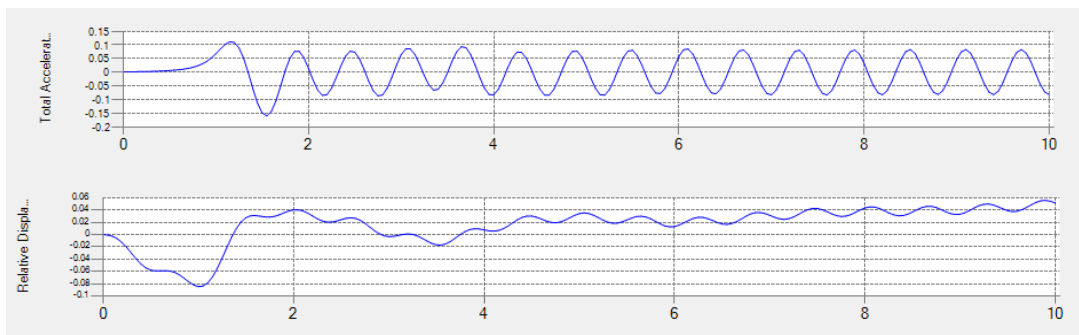**Figure 3.8:** The Acceleration (g) obtained from PLAXIS versus time.

Figure 3.9: The acceleration (g) and relative displacement obtained from DEEPSOIL vs. time.

The results at a depth of 2.0 m from the surface level are compared in terms of time history horizontal acceleration and horizontal relative displacement. The results obtained in PLAXIS are in good agreement with the output of DEEPSOIL. Small differences may be due to the different hypothesis at the origin of the calculations: while DEEPSOIL considers a viscoelastic nonlinear soil, PLAXIS accounts for plasticity in the HS small model. One additional reason may be to boundary

condition that has been set at the bottom of the model: when a fully reflective boundary is modeled, the downward propagating waves are reflected back into model leading to large amplitude periodic vibration and smaller displacement. Figures 3.10 and 3.11 show the comparison acceleration and relative displacement, respectively in EXCEL charts.
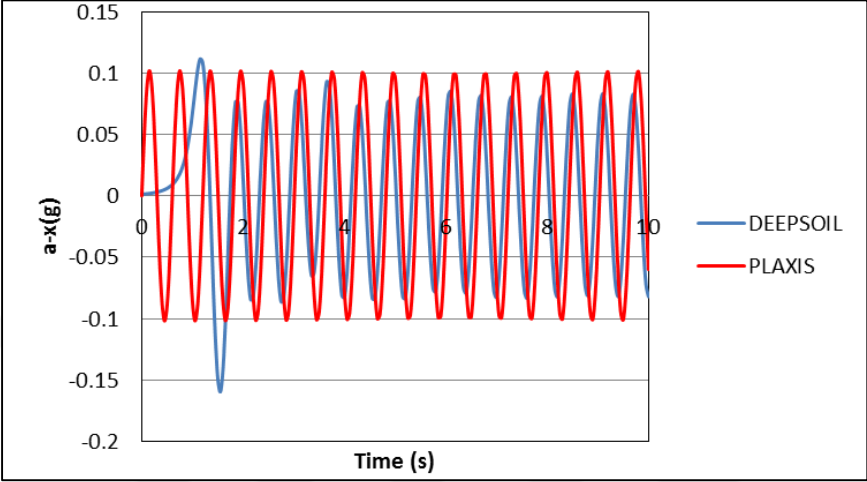
Figure 3.10: Comparison acceleration (g) obtained from DEEPSOIL and PLAXIS.
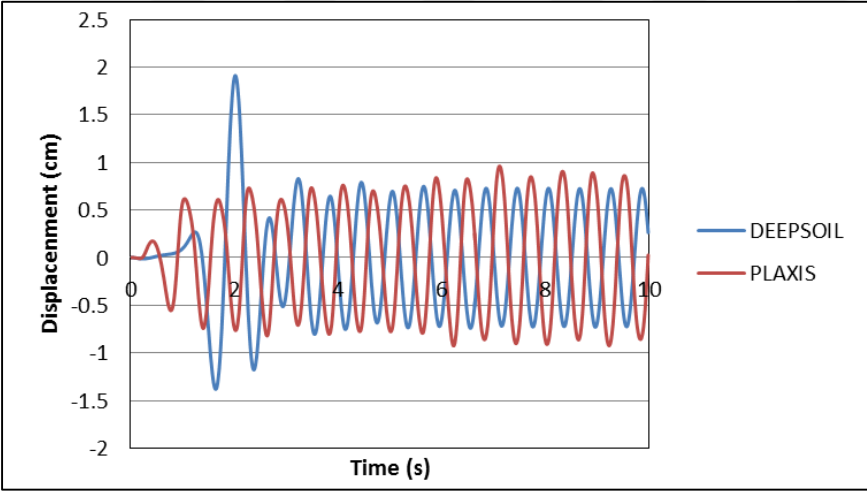
Figure 3.11: Comparison relative displacement obtained from DEEPSOIL and PLAXIS.

4. NUMERICAL ANALYSIS OF BURIED PVC PIPELINES

To evaluate the behvior of bureid plastic pipeline and soil-pipe interaction under seismic loads, a certain type of flexible continuous pipe is modeled in four different cases of soil conditions. The details are presented below.

4.1 The Geometry of the Model

The soil was zoned into two sections as bedding and backfill in order to represent normal method of installation. Appropriate properties have been assigned where the model consists of a square with 10.0 m depth and 10.0 m wide. Also a trapezius as backfill of surrounding the pipe, with 2.0 m wide at surface and 1.0 m in bottom under 2.0 m of surface have been considered as can be seen in Figure 4.1. Soil layer as bedding is considered sandy soils (Loose Sand, Dense Sand) and backfill materials with two types of soft and stiff soil properties covered the pipe around. The properties of four soils (loose sand, dense sand, soft backfill, stiff backfill) are given in Table 3.3 in the previous chapter. The axial center of pipe is located 1.80 meter under the surface level.
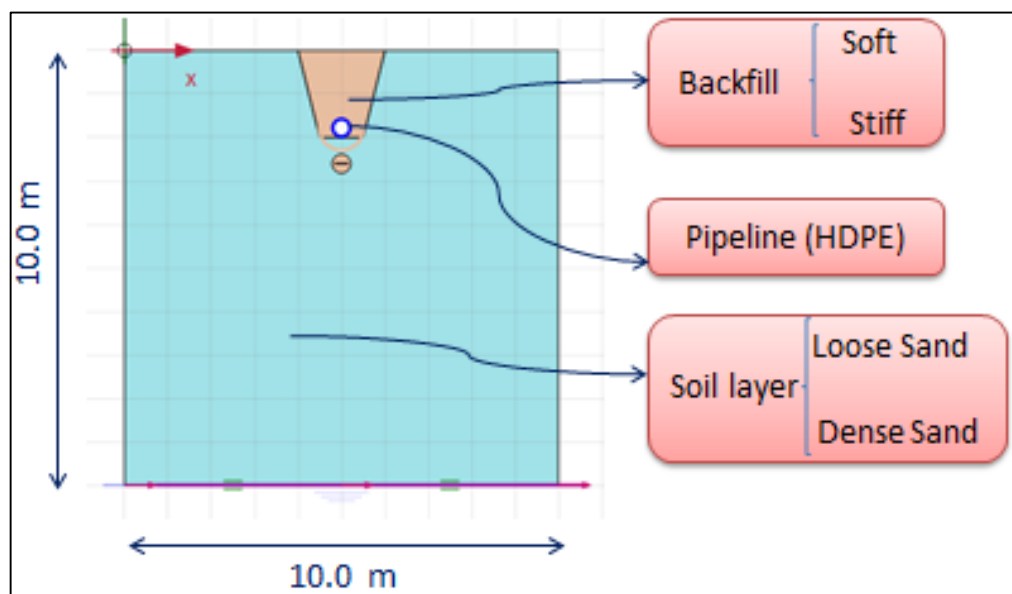
Figure 4.1: A sketch of buried pipeline modeled in PLAXIS 2D.

4.2 Pipeline Properties

In order to accomplish the specific study for failure aspects of buried pipelines caused by earthquake, the relative large diameter HDPE pipeline that is used for water supply has been chosen, and an elastic, perfectly plastic and isotropic analysis for pipeline has been conducted on this study as mentioned in Table 4.1. The position of points A, B, C, D, E, F and G are shown in Figure 4.2. Coordinates of the points A to G in Figure 4.2 are given in Table 4.2.

Table4.1: Properties of HDPE pipe

Material	PIPE (ASTM D638)
Diameter (m)	0.4
Thickness (mm)	12
Elasticity modulus (psi)	130000
Tensile Strength (psi)	3200
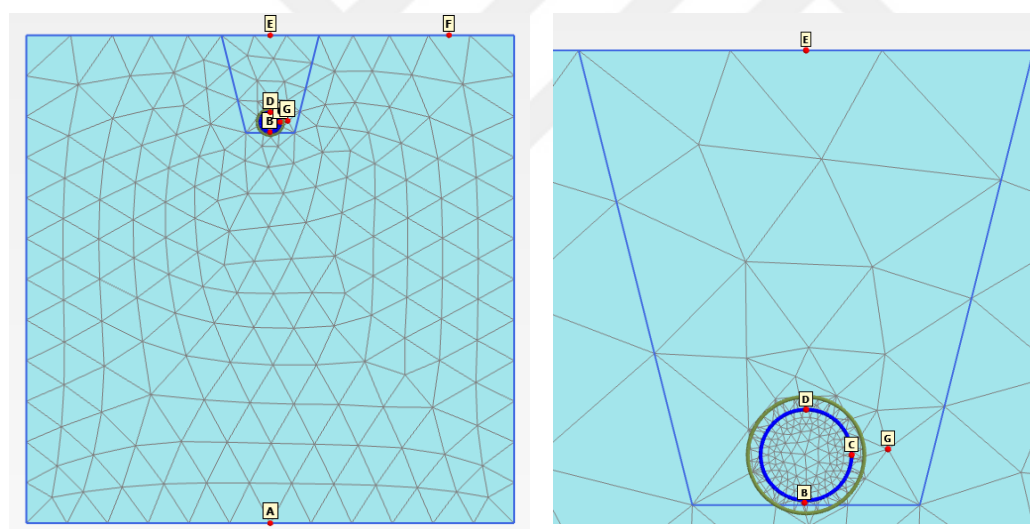
Figure 4.2: Positions of the points A to G in the model.

Table 4.2: Coordinates of the points A to G in PLAXIS model.

Points	Coordinates	Location
A	(5.0,-10.0)	bottom
B	(5.0,-2.0)	pipe
C	(5.20,-1.80)	pipe
D	(5.0,-1.60)	pipe
E	(5.0,0.0)	surface
F	(8.50,0.0)	free field
G	(5.30,-1.80)	Adjacent to the pipe

4.3 Finite Element Analysis Results

4.3.1 Numerical analysis under harmonic loading

At the first step of pipeline analysis under seismic loads, the case of model including dense sand as soil layer with stiff backfill is presnted.

Table4.3: Harmonic load properties

Amplitude	Fequency	Time interval
1 m/s^2	5 Hz	10 sec

Figure 4.3 shows the acceleration versus time for points A, B, C, D, E and F. As can be seen in all graphs, since the material properties are changed at point B, a significant change in acceleration is observed while transferring from soil to the backfill. However, this difference is not such significant at point F.
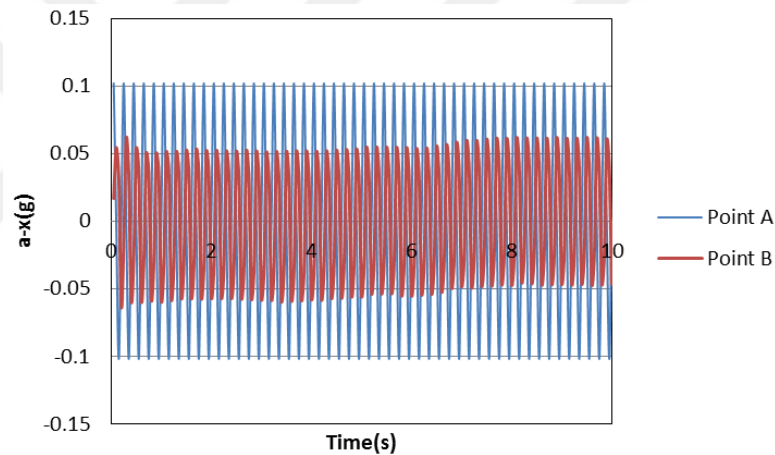
(a) Point B versus Point A
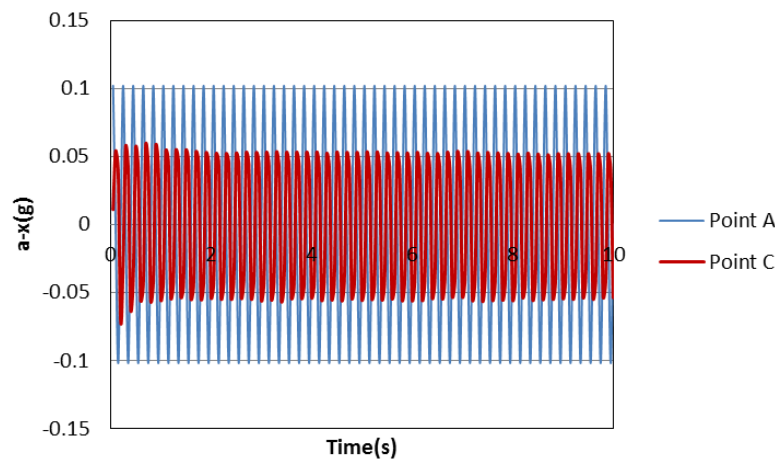
(b) Point C versus Point A

Figure 4.3: Acceleration in points A,B,D,E and F under harmonic load in dense sand with stiff backfill.
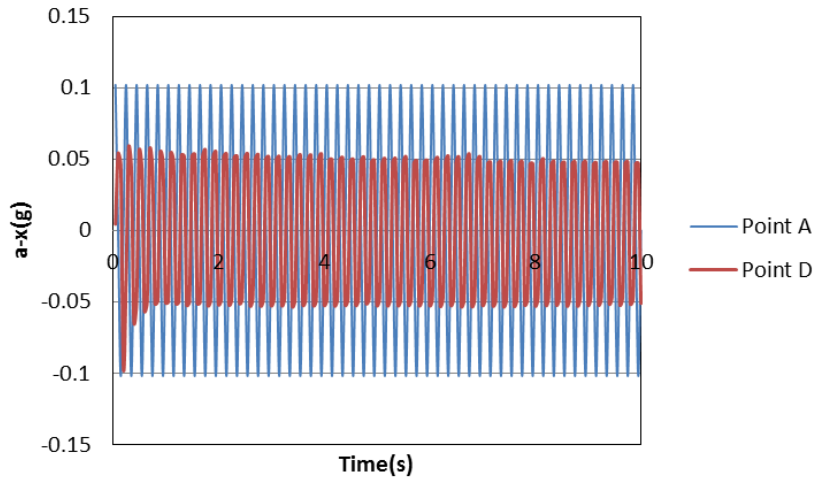
(c) Point D versus Point D
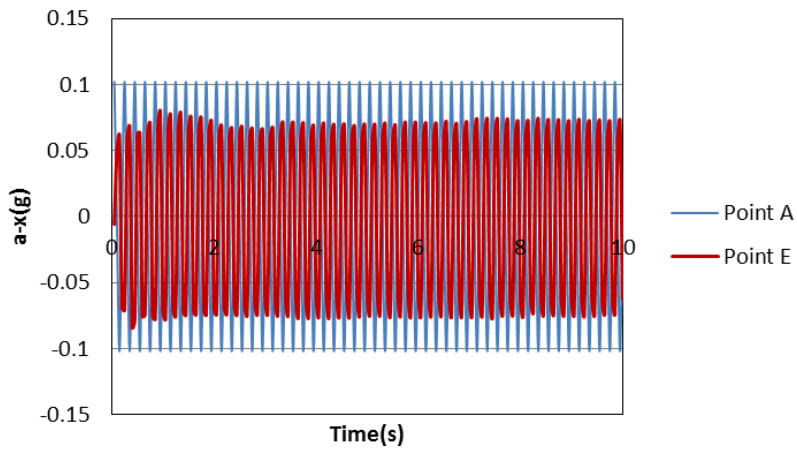
(d) Point E versus Point A
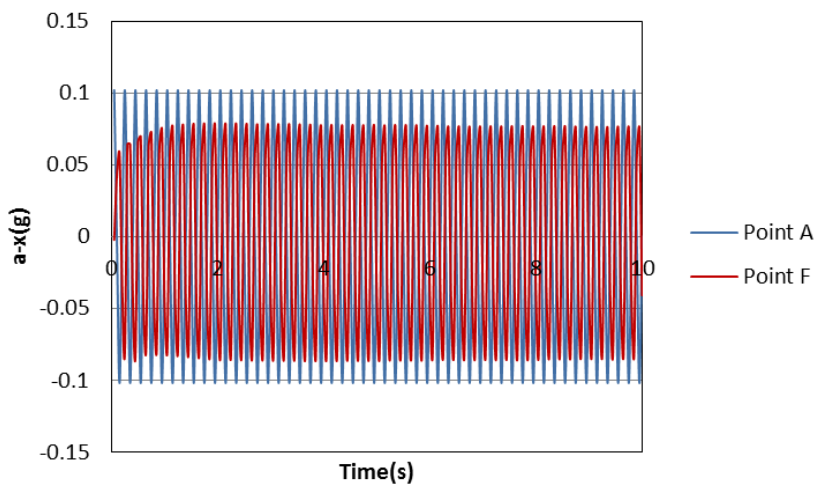
(e) Point F versus Point A

Figure 4.3 (continued): Acceleration in points A,B,D,E and F under harmonic load in dense sand with stiff backfill

When acceleration records are double integrated to get displacement records, the data may be shifted up due to integration constants added. In order to overcome this issue
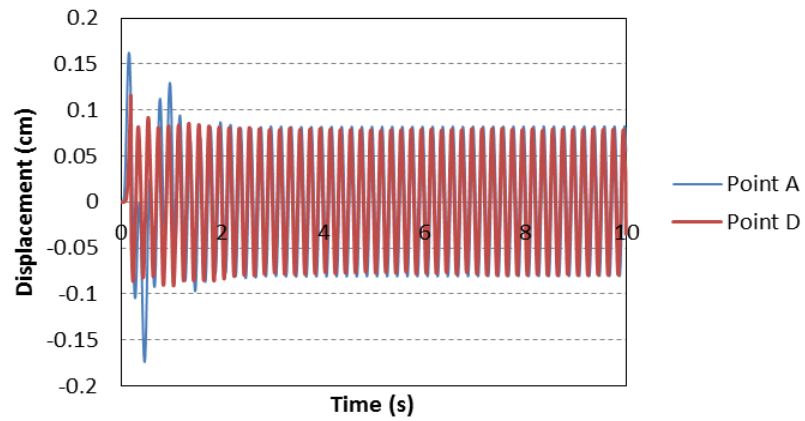
Baseline Correction was applied for obtaining harmonic displacements. Figure 4.4 shows horizontal displacement of the points after baseline correction process.
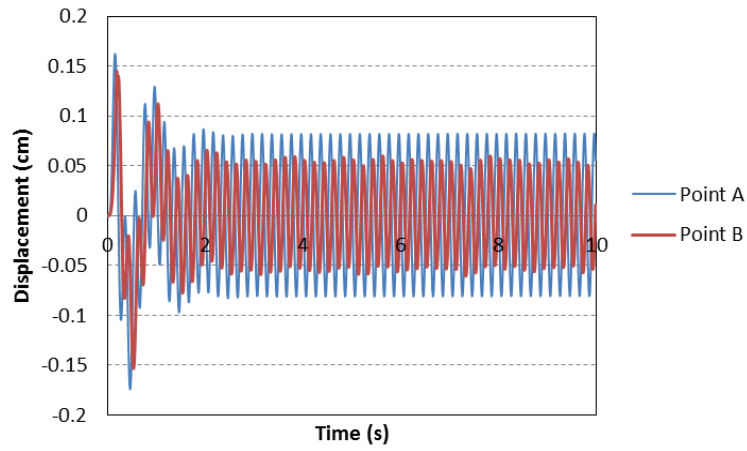
(a) Point B versus Point A
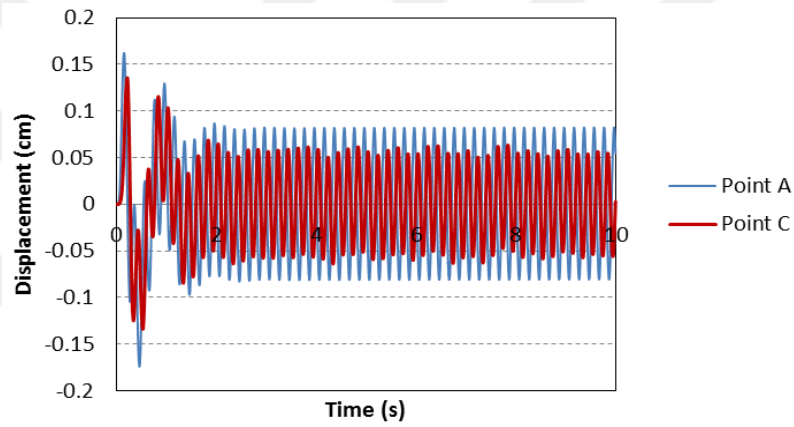
(b) Point C versus Point A

(c) Point D versus Point A

Figure 4.4: Baseline corrected relative horizontal displacement of points B to F to point A.
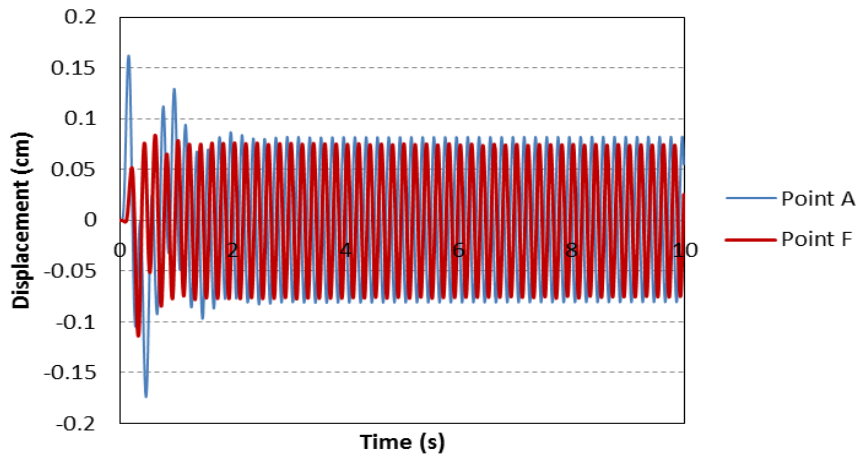
(d) Point F versus Point A
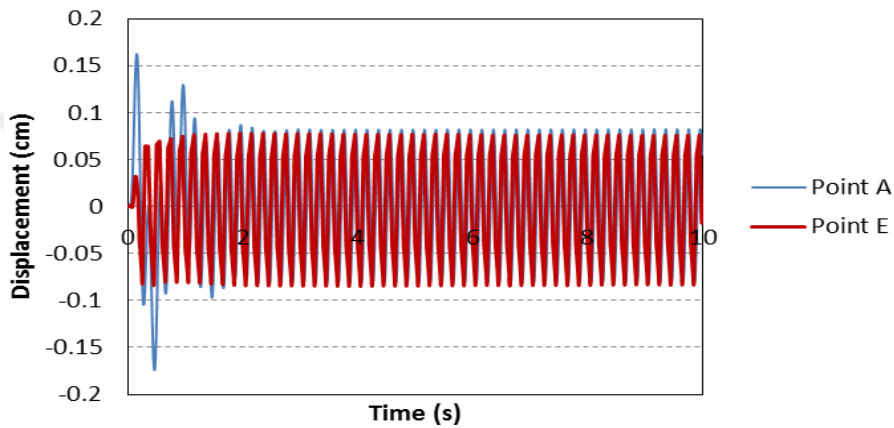
(e) Point E versus Point A

Figure 4.4 (continued): Baseline corrected relative horizontal displacement of points B to F to point A.

According to figure 4.4, considering that the amount of damping at backfill material surroundnig the pipe is higher than the bedding material, the energy loss around the pipe is high in comparison to the other points (A, E, F).

In figure 4.5 Pesedo Spectral response of Acceleration (PSA) for all points illustrated versus period. From these plots, it can be derived that, acceleration responses at points E, F are closed to the acceleration applied at the base at point A, while the PSA values drop at points B, C, D.

4.3.2 Numerical analysis under earthquake loading

For better evaluation of the soil- pipe interaction and the effect of backfill role, analysis continued under Earthquake loading under four different bedding and backfill conditions seperately.
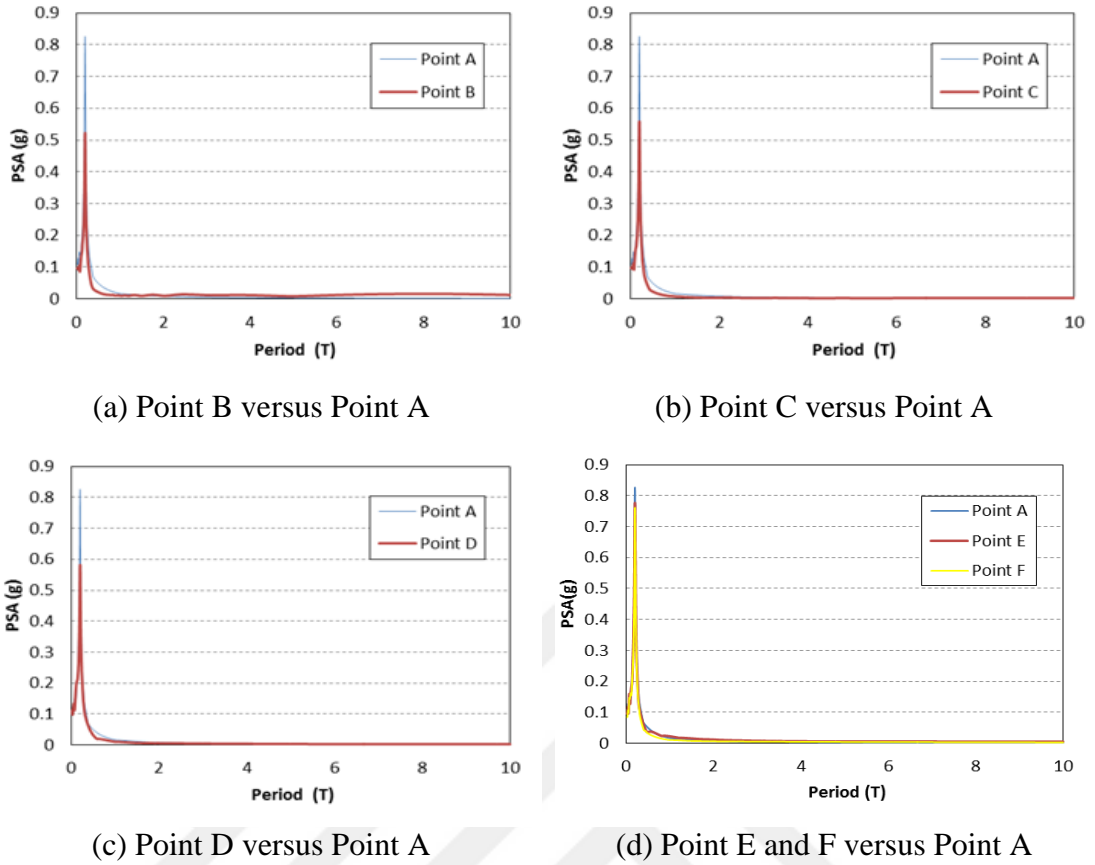
(a) Point B versus Point A   (b) Point C versus Point A

(c) Point D versus Point A   (d) Point E and F versus Point A

Figure 4.5: PSA for points A, B,C,D,E and F.

Table4.4: Earthquake load properties

Earthqake	PGA	Time interval
Kobe	0.76g	48 sec

4.3.2.1 Acceleration-time histories

In Figure 4.6, acceleration response of each local points is shown in four different soil conditions (dense and loose bedding with soft and stiff backfill). It can be seen that the maximum acceleration response is observed in dense sand with stiff backfill and vice versa the minimum acceleration response is illustrated in loose sand with soft backfill.
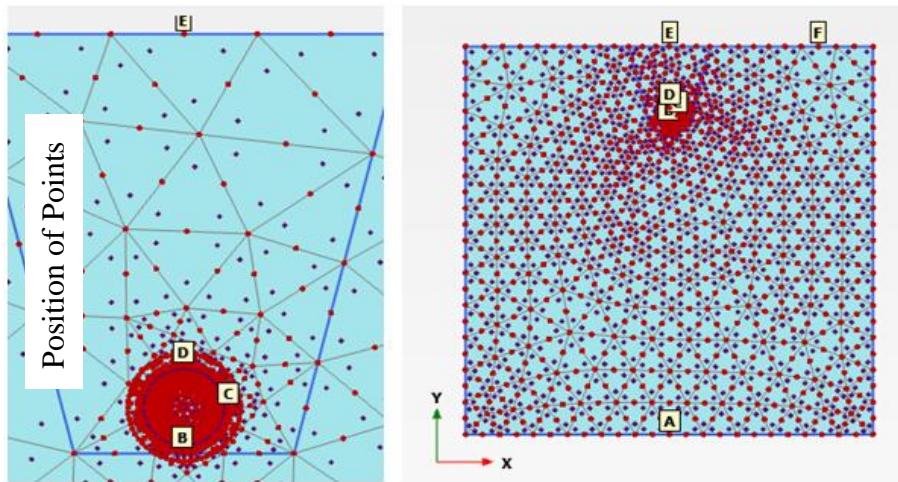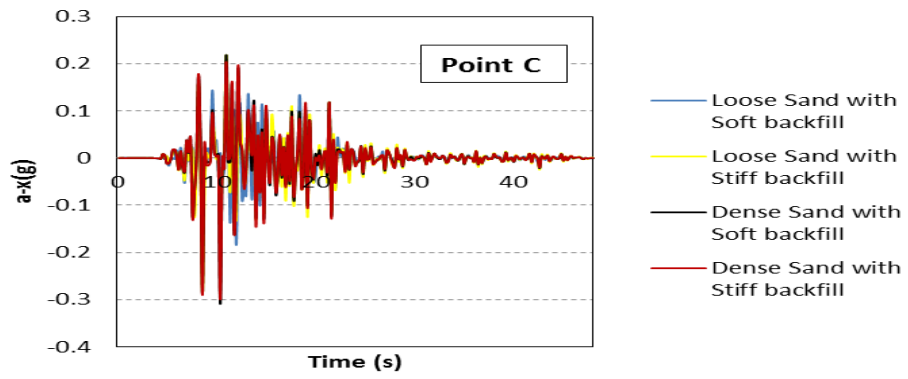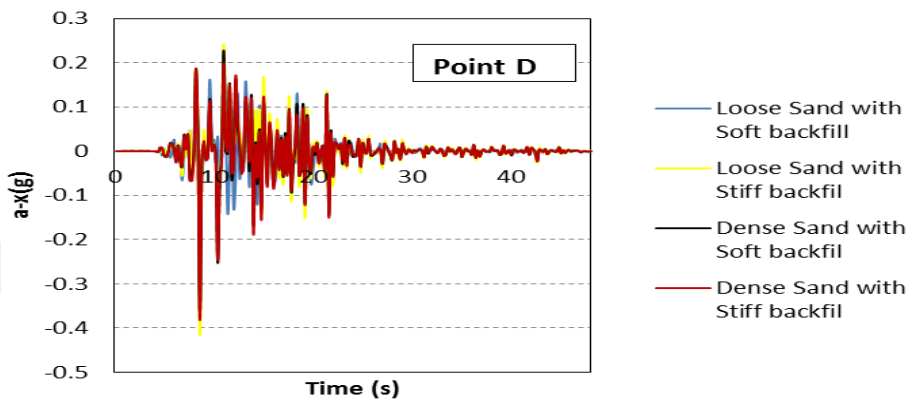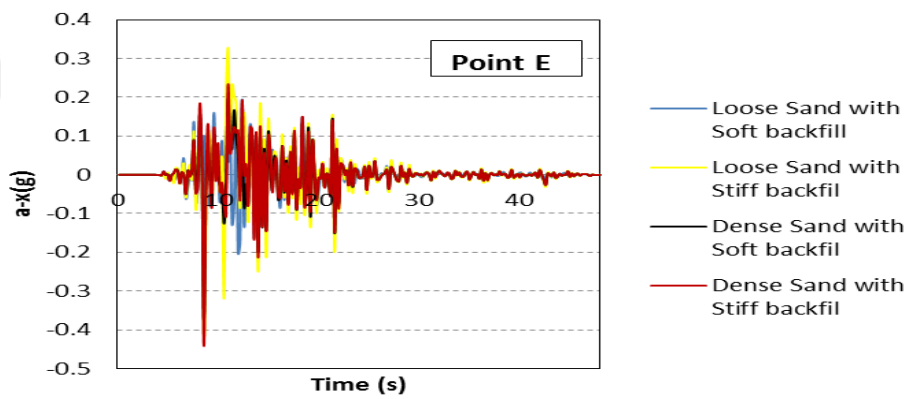
(a) Cross Section
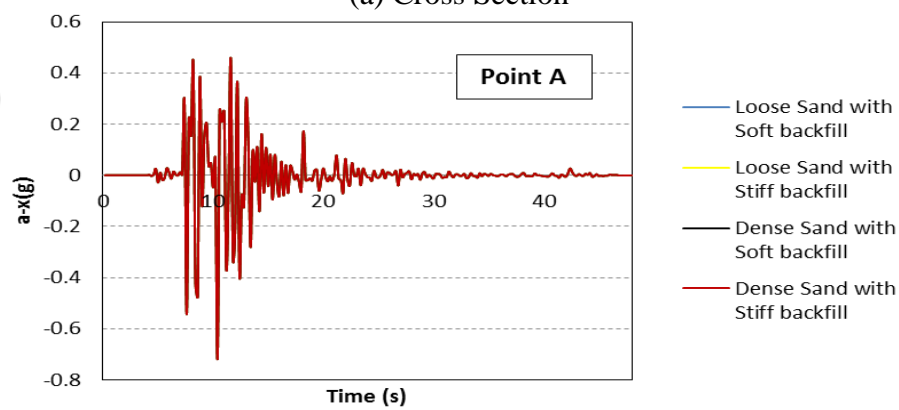
(b) Point A
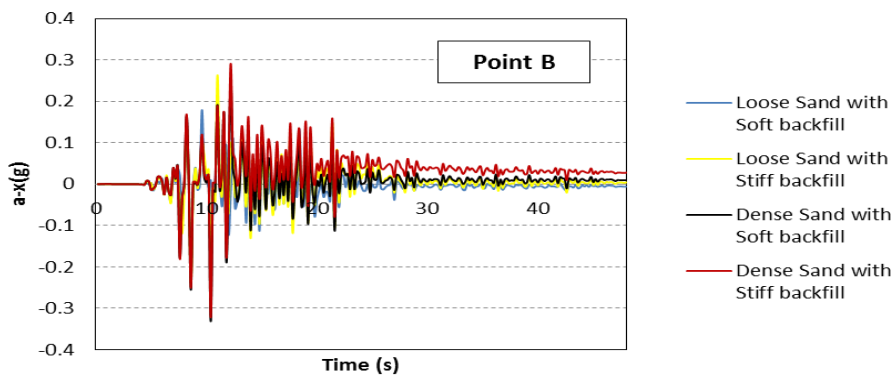
(c) Point B

Figure 4.6: Acceleration in points A,B,C,D,E and F under earthquake in four different soil and backfill.
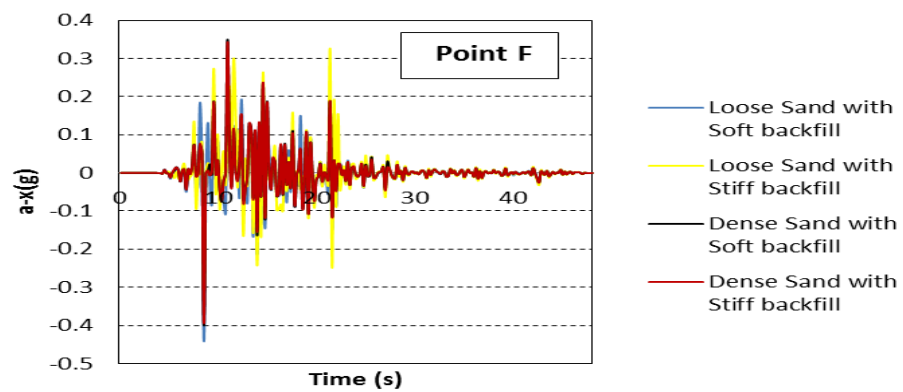
56

(d) Point C

(e) Point D

(f) Point E

(g) Point F

Figure 4.6 (continued) : Acceleration in points A,B,C,D,E and F under earthquake in four different soil and backfill.

57

**4.3.2.2 Horizontal displacement - time histories**

In Figure 4.7 (a to e), horizontal displacement versus time are plotted for each point in all cases of soil conditions. It can be seen that the maximum horizontal displacement values for all soil cases are approximately the same. However, comparing the points located on pipe, point B that located just on bedding, shows more displacement in comparison to the points C and D in all four cases.
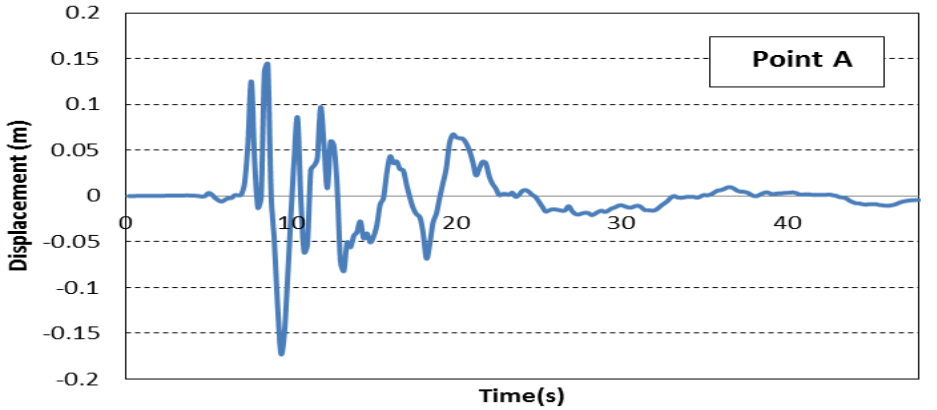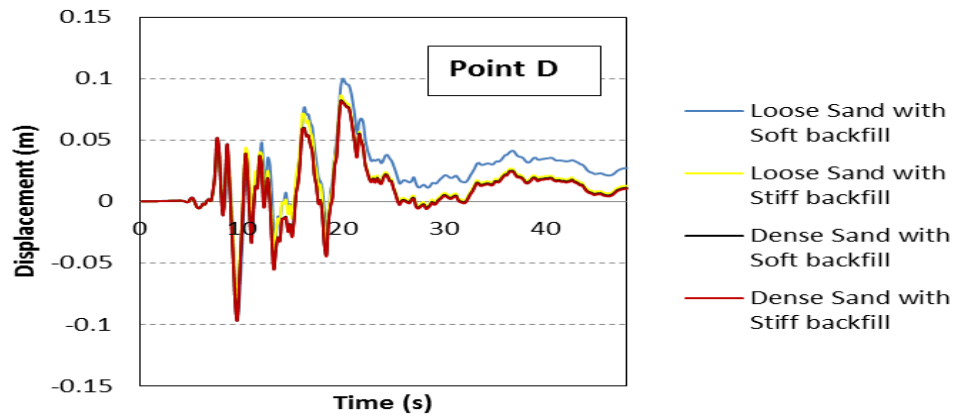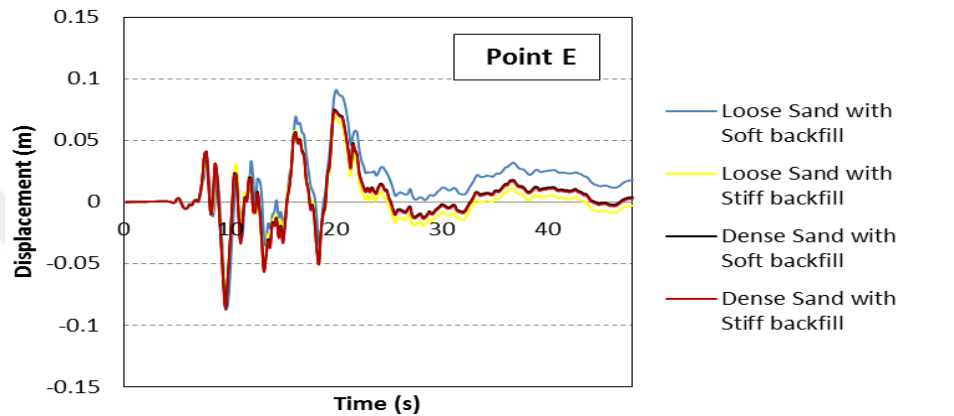

(a) Point A
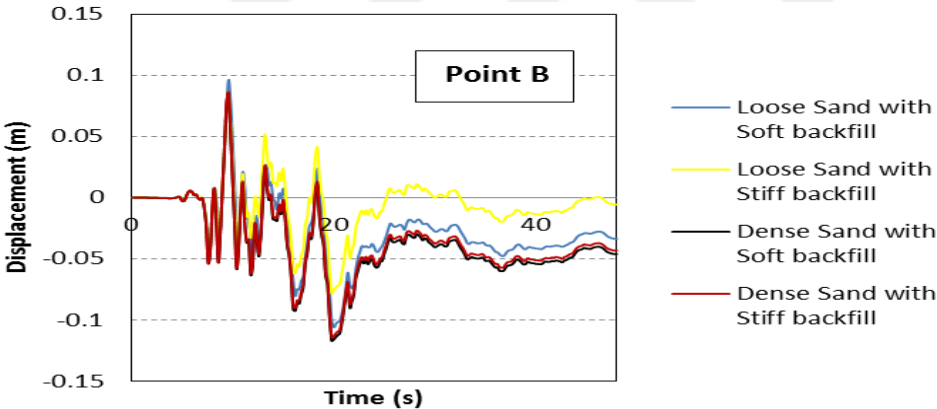
(b) Point B
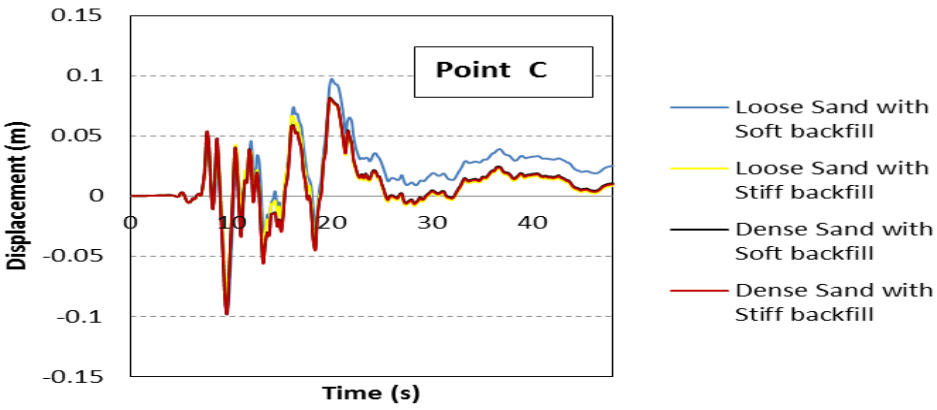
(c) Point C

Figure 4.7: Horizontal displacement in points A,B,C,D,E and F under earthquake loading in four different soil and backfill.

(d) Point D

(e) Point E
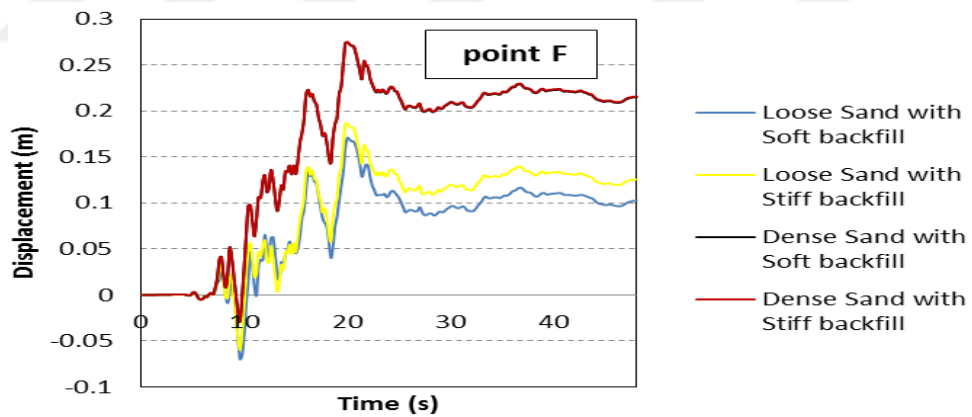
(f) Point F

Figure 4.7 (continued): Horizontal displacement in points A,B,C,D,E and F under earthquake loading in four different soil and backfill.

To evaluate the relative displacement between pipe and backfill, a certain point G (adjacent to point C) was selected in the model into backfill. Figure 4.8 shows the difference horizontal displacements between two mentioned points. The relative displacement is significant in dense bedding soil in comparison to loose sand. Hence, due to more slippage between pipe and soil, it is clear that looser sands provide safer condition for the buried pipeline.

59

(a) Cross Section

(b) Points C to G
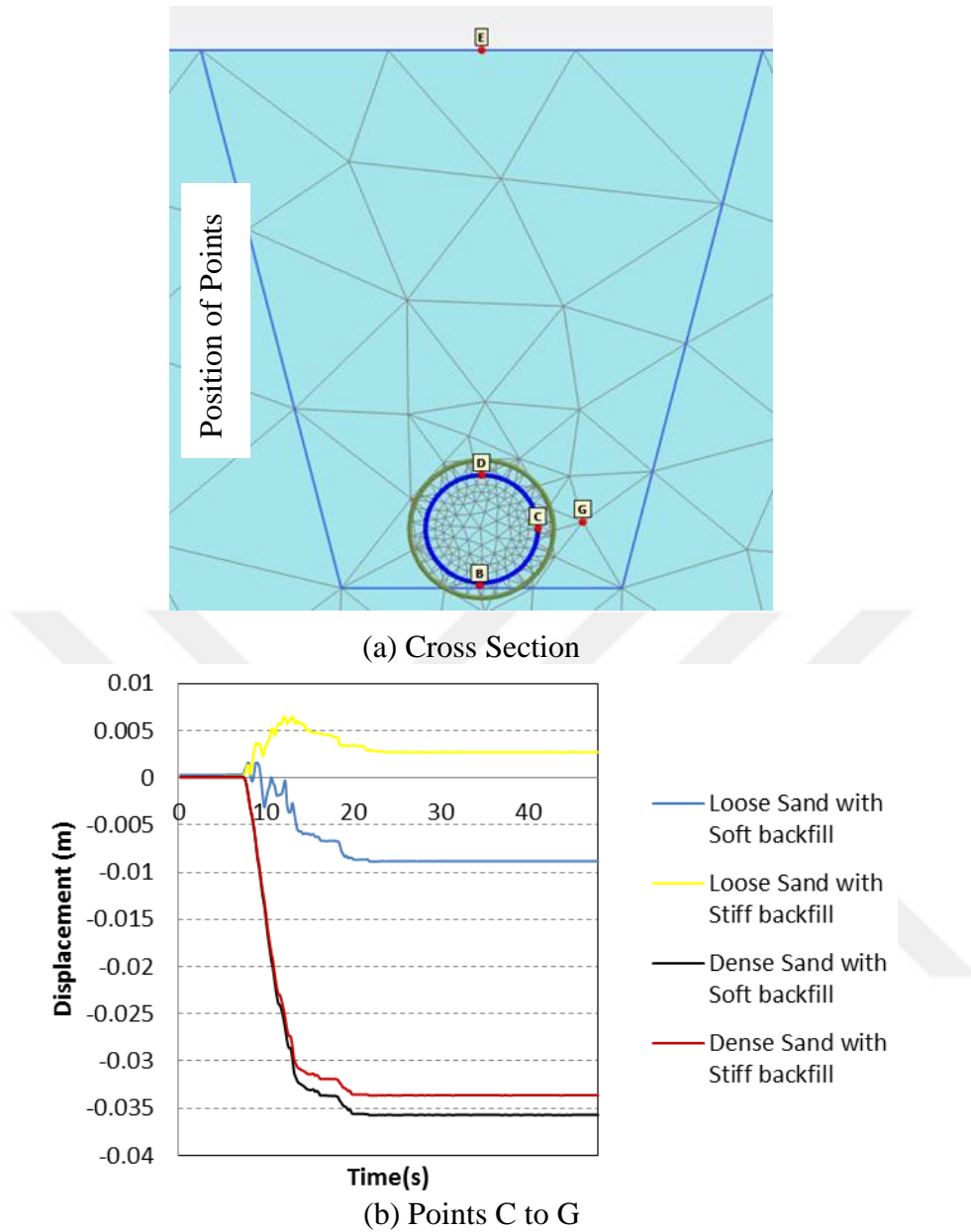
Figure 4.8: Relative horizontal displacement of point C to point G.

4.3.2.3 Vertical displacement - time histories

In Figure 4.9 vertical displacement are plotted for different soil material conditions. Unlike the horizontal displacement, the vertical displacement in loose sand without considering the backfill materials has significant amount (around four times of the value in dense sand).
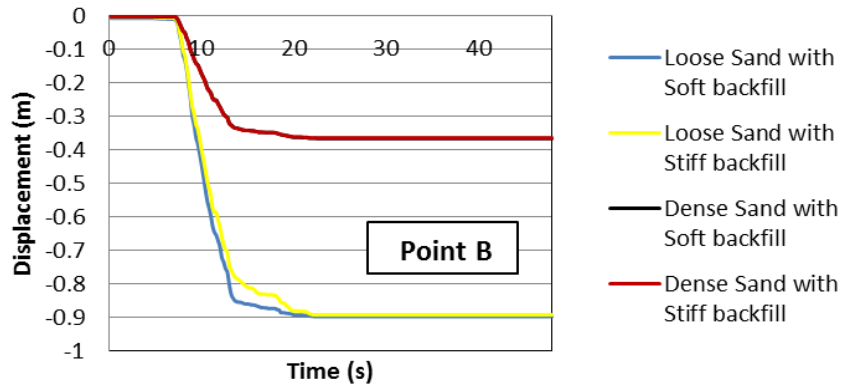
(a) Point B
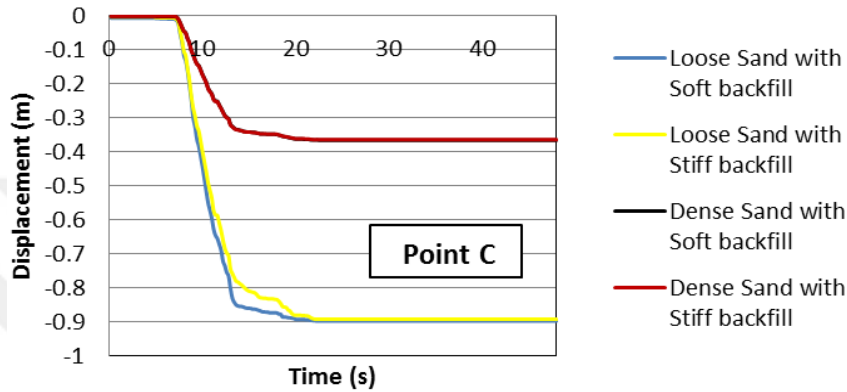
(b) Point C
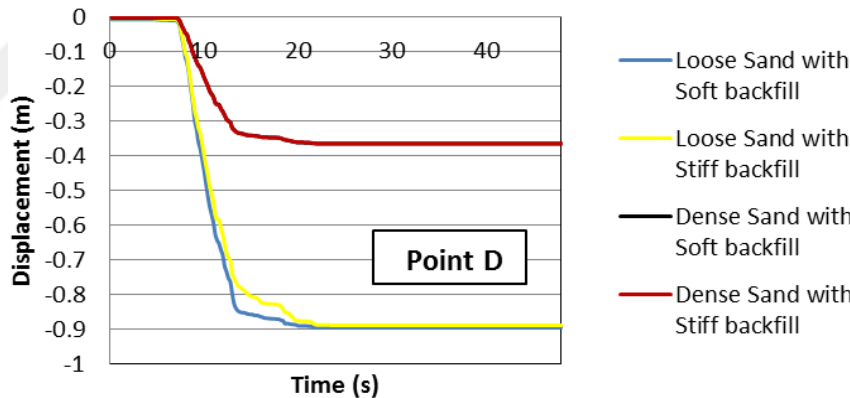
(c) Point D
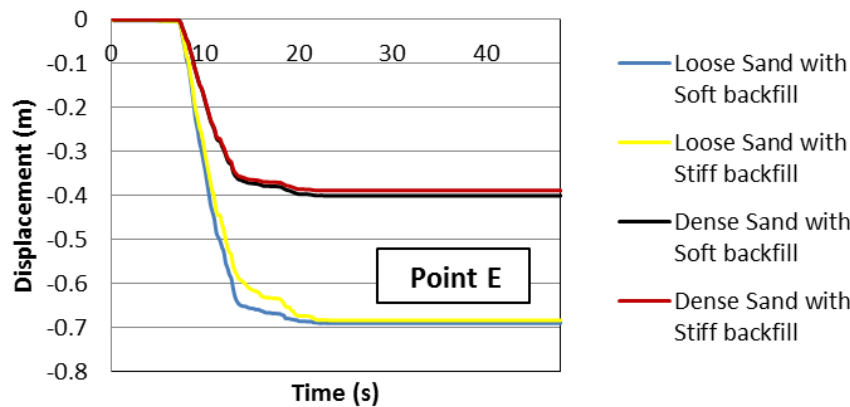
(d) Point E

Figure 4.9: Vertical displacement at points A,B,C,D,E and F under earthquake loading in four different types of soil and backfill.

(e) Point F
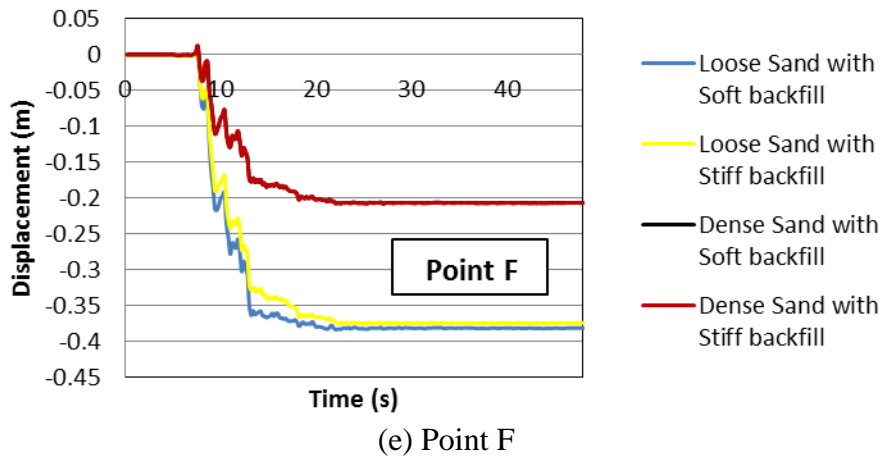
Figure 4.9 (continued): Vertical displacement at points A,B,C,D,E and F under earthquake loading in four different types of soil and backfill.

4.3.2.4 Pseudo-acceleration response spectrum (PSA)

According to figure 4.10 the peak spectral acceleration response shows that since point B is located on the bedding, it has less damping value and energy dissipation. Therefore, the acceleration response is higher than points C and D. Also points B and C in contrast to points D, E, F, in dense sand bedding have greater values of acceleration response. For points D, E and F ,the maximum response can be seen in the soils with loose materails.
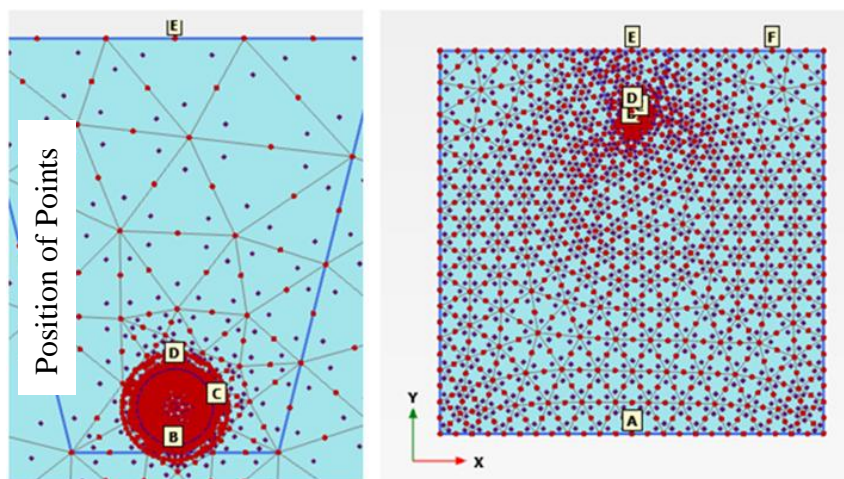
(a) Cross Section

Figure 4.10: PSA for points A, B,C,D, E and F.

62

(b) Point A (c) Point B

(d) Point C (e) Point D

(f) Point E (g) Point F
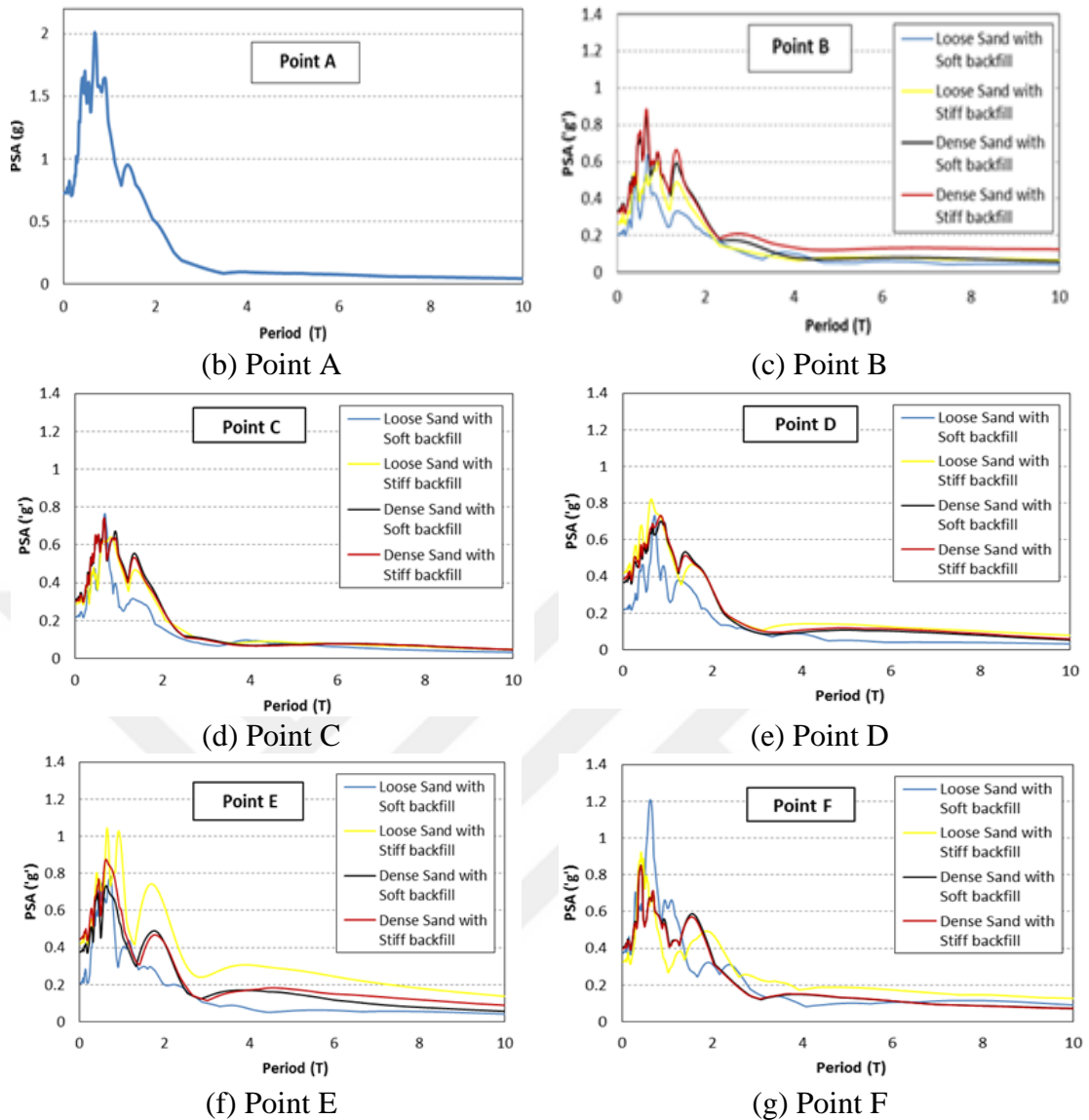
Figure 4.10 (continued): PSA for points A, B,C,D, E and F.

4.3.2.5 Strain distributions

With respect to the cited analysis results, it can be concluded that among the four different cases of bedding and backfill materials, the case of dense soil layer with stiff backfill could be considered as critical condition in terms of soil-pipe interaction and more slippage between soil and pipe. However, the vertical displacement and settlement, in loose sand is more considerable. In below figures, graphically the behavior of pipe is illustrated.

Figures 4.11 and 4.12 show the strain distributions in both horizontal and vertical directions in dense and loose sand. As can be observed, the horizontal and vertical

strains around the pipe have the same quantity in both soil conditions; however, the values in loose sand are greater than the dense sand.

Total cartesian strain ε_{xx}

Maximum value = 1.285 (Element 19 at Node 648)

Minimum value = -0.2462 (Element 48 at Node 455)

Total cartesian strain ε_{yy}

Maximum value = 0.2686 (Element 48 at Node 455)

Minimum value = -1.382 (Element 19 at Node 649)
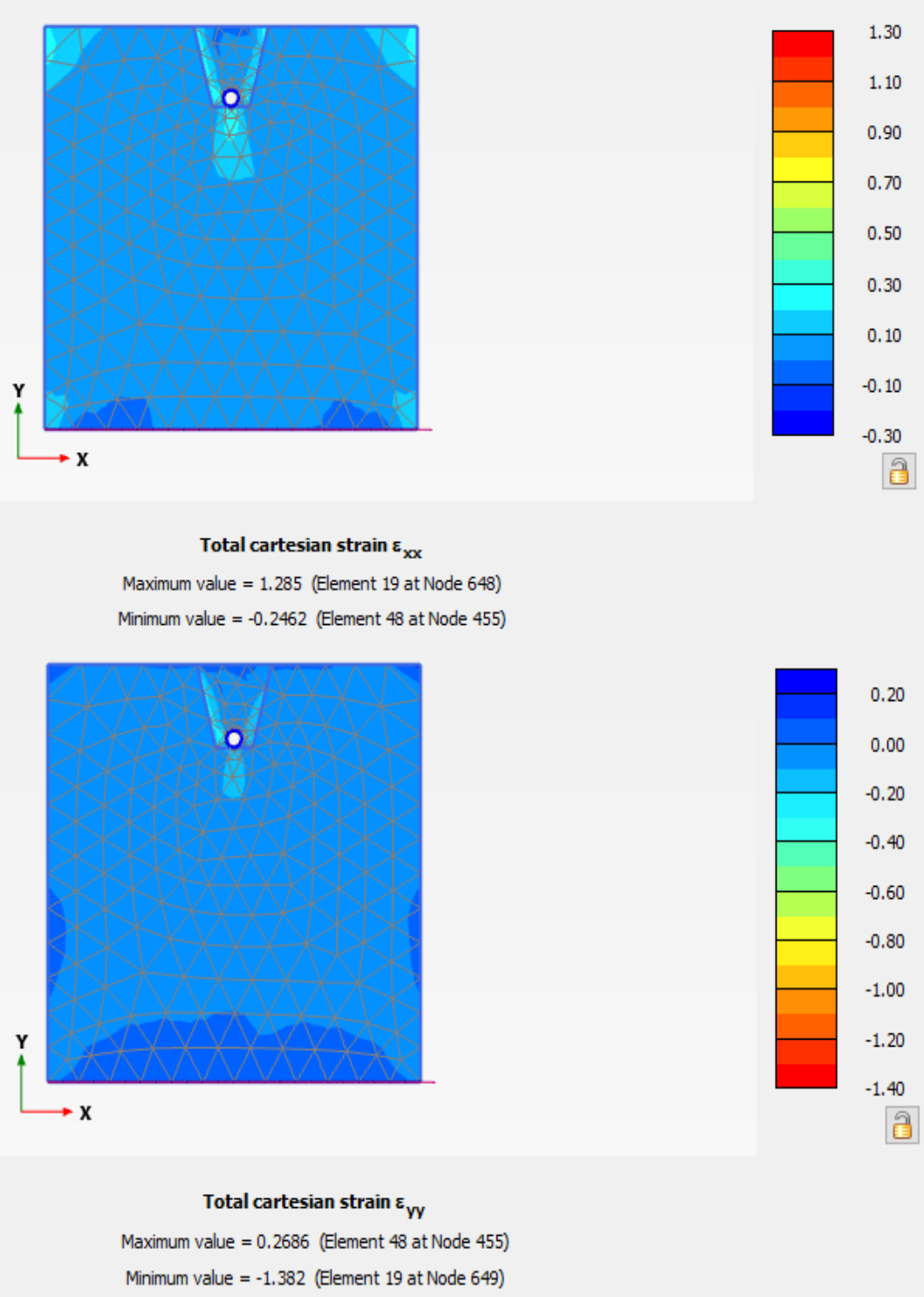
Figure 4.11: Horizontal and vertical strain distributions in dense sand.

Total cartesian strain ε_{xx}

Maximum value = 3.119 (Element 19 at Node 648)

Minimum value = -1.821 (Element 35 at Node 449)

Total cartesian strain ε_{yy}

Maximum value = 1.998 (Element 35 at Node 449)

Minimum value = -3.527 (Element 19 at Node 648)
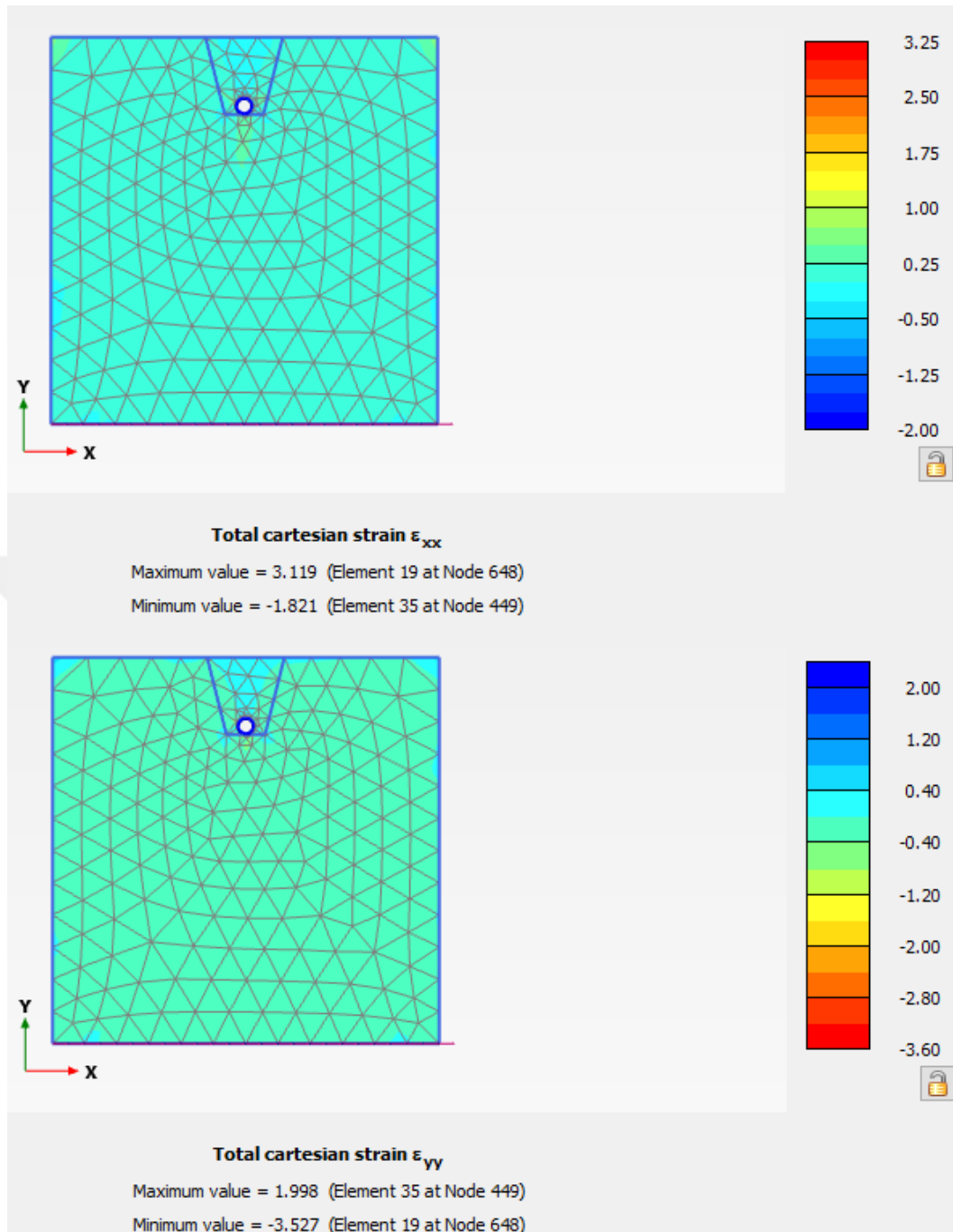
Figure 4.12: Horizontal and vertical strain distributions in loose sand.

4.3.2.6 Distribution of displacements in differnt sections.

Figures 4.13 and 4.14 illustrate the distribution of total displacement in the height of the model, inside and outside of backfill for both cases. With respect to the given maximum values, it is obvious that loose soil has more displacement in the height of the model. Hence, it would cause significant damage to the pipe in comparison to dense sand.

65

Total displacements |u| (scaled up 5.00 times)

Maximum value = 0.2190 m

Total displacements |u| (scaled up 5.00 times)

Maximum value = 0.3931 m
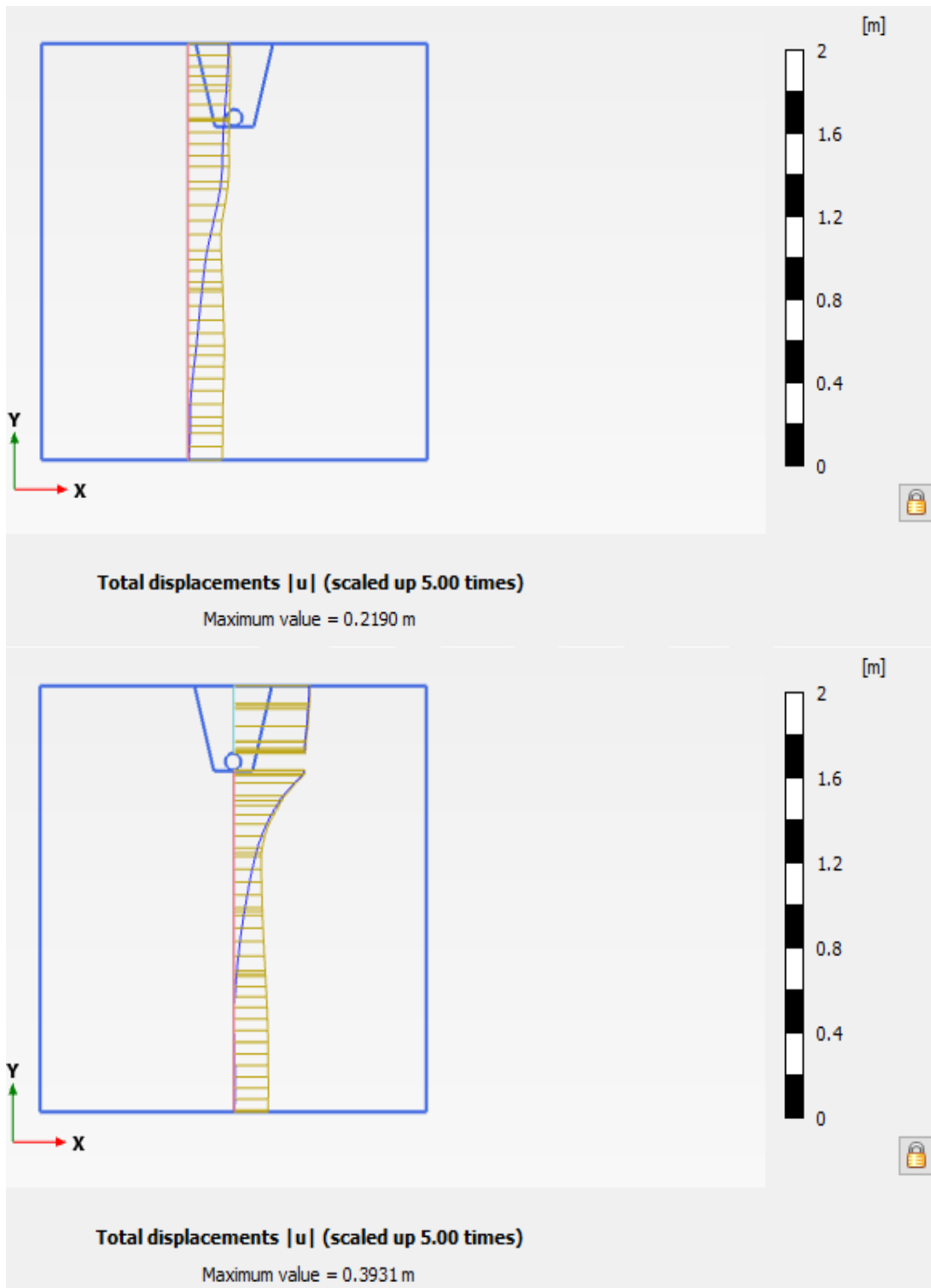
Figure 4.13: Distribution of total displacement in two vertical sections (dense sand).
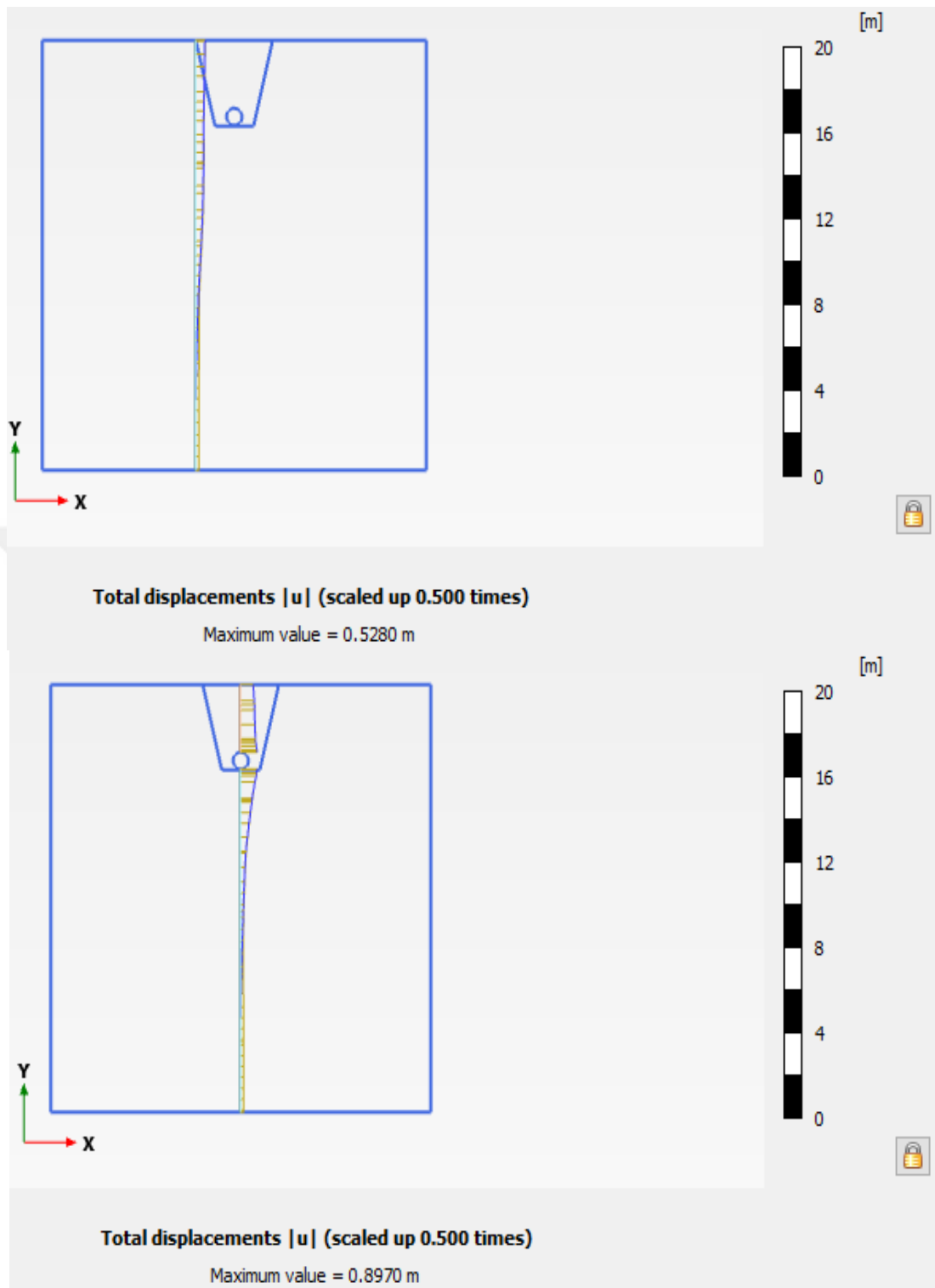
Figure 4.14: Distribution of total displacement in two vertical sections (loose sand).

Similarly, for the distribution of total displacement and settlement in the width of the model, the results repeat and represent that vertical displacement is more in soft backfill and loose sand.
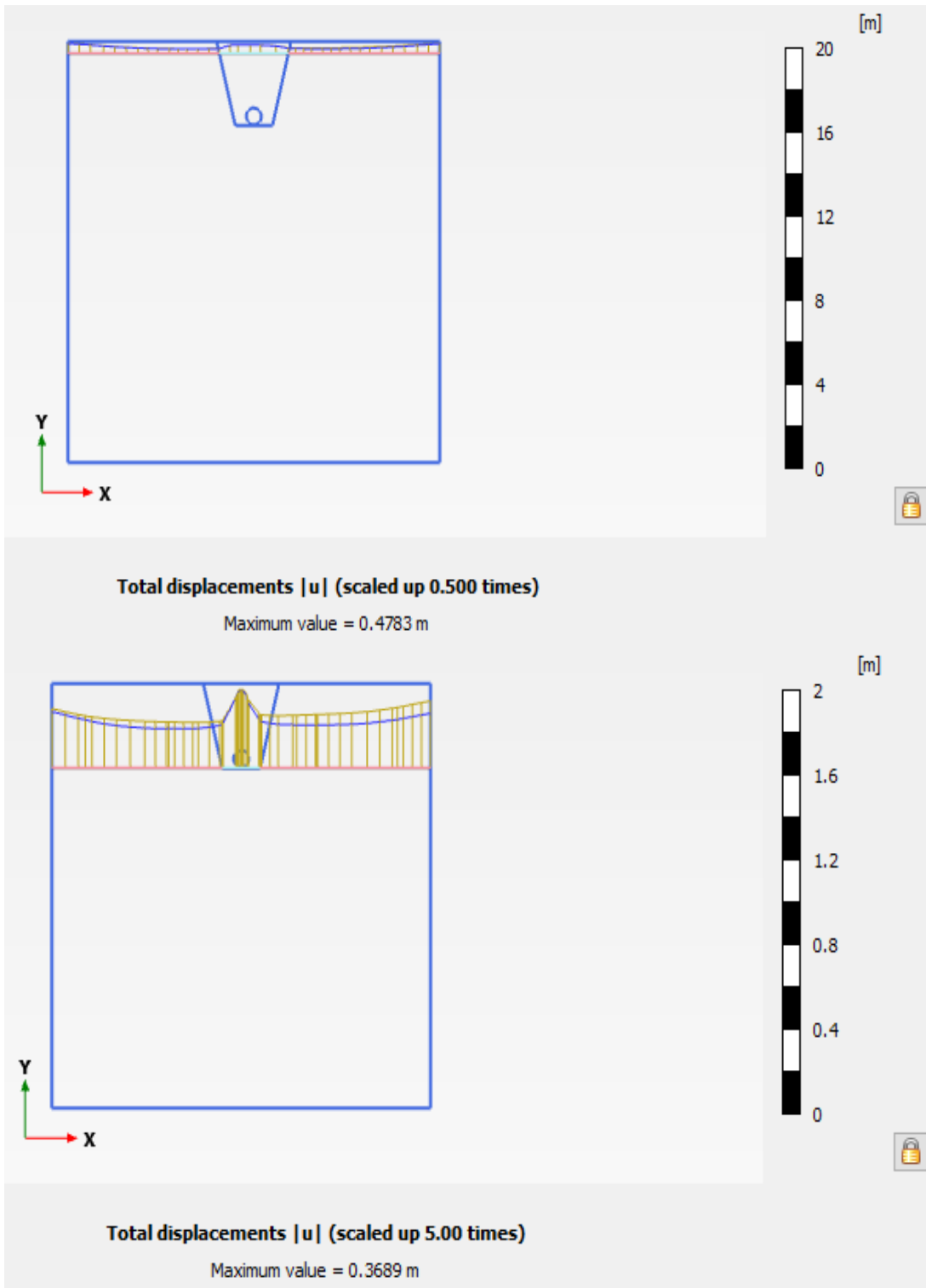
Figure 4.15: Distribution of total displacement in two horizontal sections (dense sand).

Total displacements |u| (scaled up 0.500 times)

Maximum value = 0.7505 m

Total displacements |u| (scaled up 0.500 times)

Maximum value = 0.8957 m
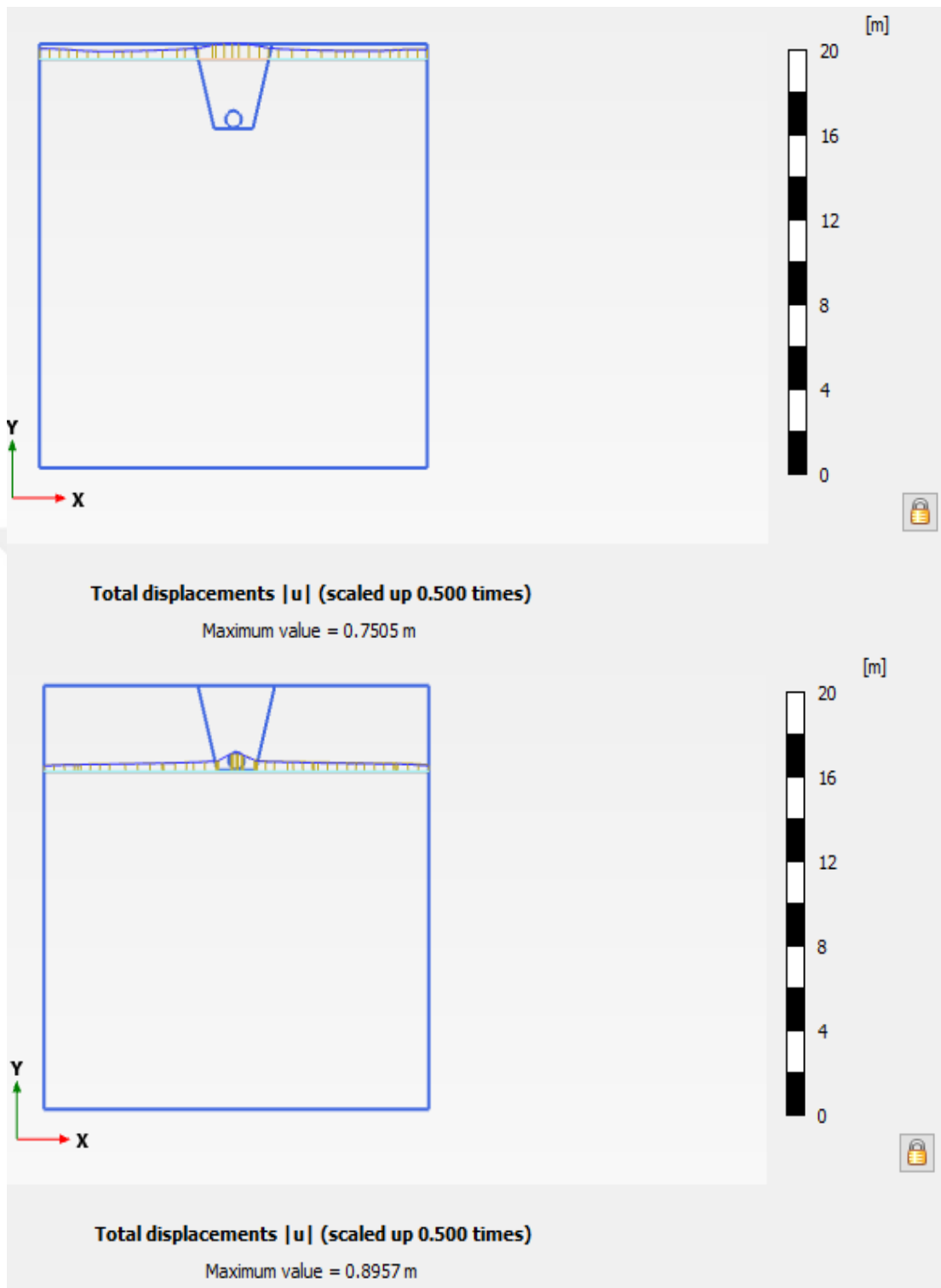
Figure 4.16: Distribution of total displacement in two horizontal sections (loose sand).

Since this analysis computed applying the earthquake load with high intensity (Kobe earthquake, PGA =0.76 g), to verify the results, the whole process was performed using another earthquake loading with low intensity (Kocaeli earthquake, PGA = 0.16g). To compare the results obtained from two analysis under different

earthquakes loading, data about acceleration, horizontal and vertical displacemnet are plotted for point C(critical point on pipe) in four soil conditions. From the figure (4.17), it can be concluded that, the beahavior of pipe under differnt earthquakes in every soil condition has the same response with different value. For instance, the acceleration at point C has high value in dense sand, vice versa the maximum vertical displacement happens in loose sand.

(a) Acceleration vs. time hostories

(b) Horizontal displacement vs. time histories

(c) Vertical displacement vs. time histories

Figure 4.17: Comparison between acceleration, horizontal displacement and vertical displacement at point C under two different earthquakes loading.

4.3.2.7 The forces and moments exerted on the pipe

Since in PLAXIS the pipe is modeled using plate option, when a plate is displayed, the options axial force N, Shear Force Q and Bending Moment are available from

70

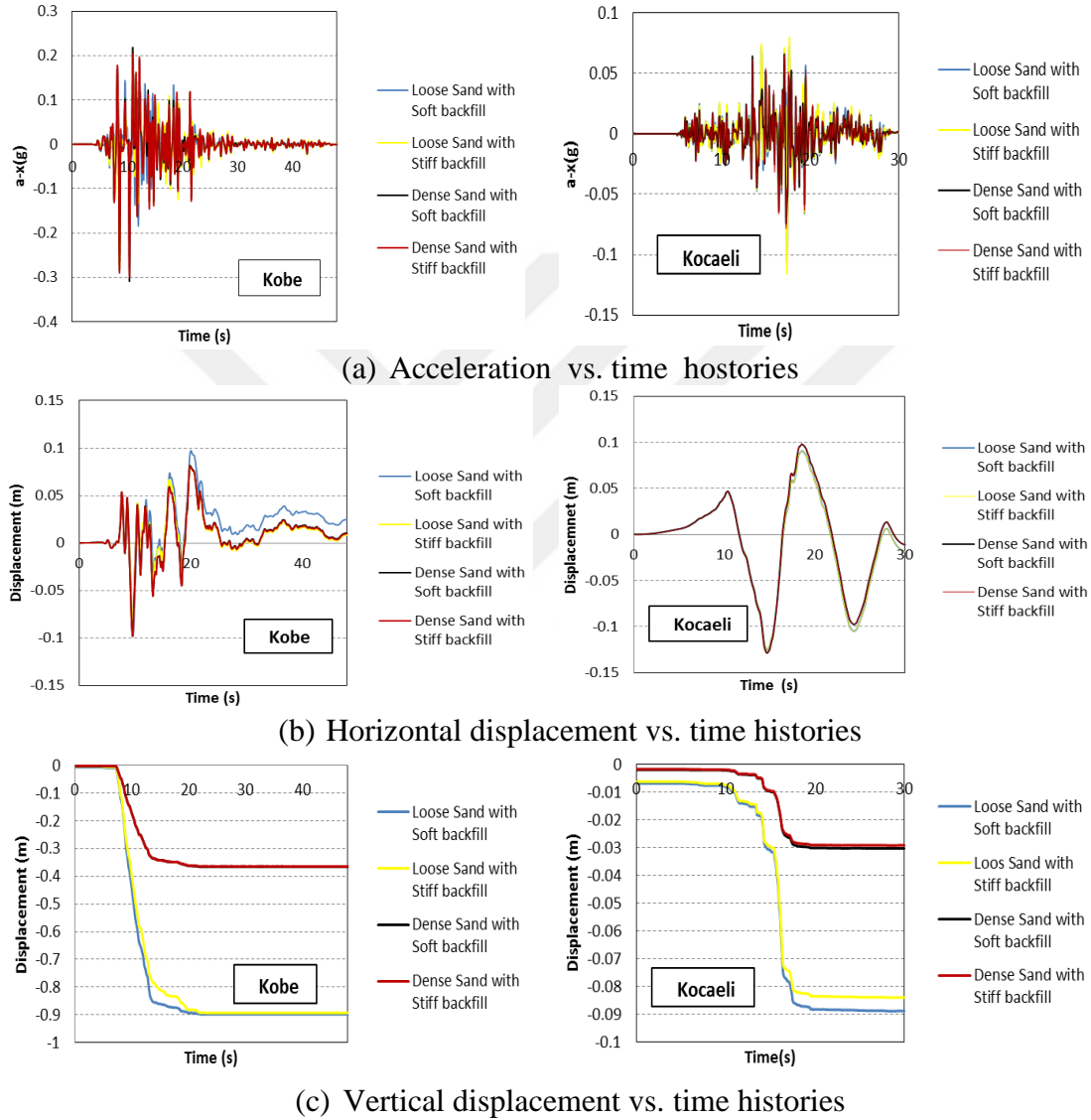the Force ment in Output of the program. All of these forces represent the actual forces at the end of the calculation step.

In addition to the actual forces, PLAXIS keeps track of the historical maximum and minimum values forces in all subsequent phases.

The Axial force N_1 is the axial force in the first direction. The Shear force Q_{13} is in the plane shear force. The bending moment M_{11} is the bending moment over the second axis. Figure 4.18 illustrates the configuration of forces applied in plate.
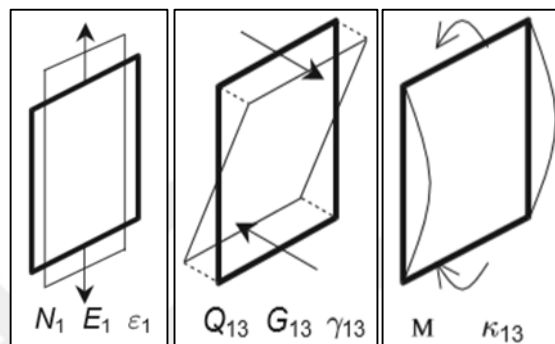
Figure 4.18 : Positive axial force N, shear force Q and bending moment M in plates.

As mentioned above, since the pipe is modelled by plate, so for pipe this force can be shown in figure 4.19.
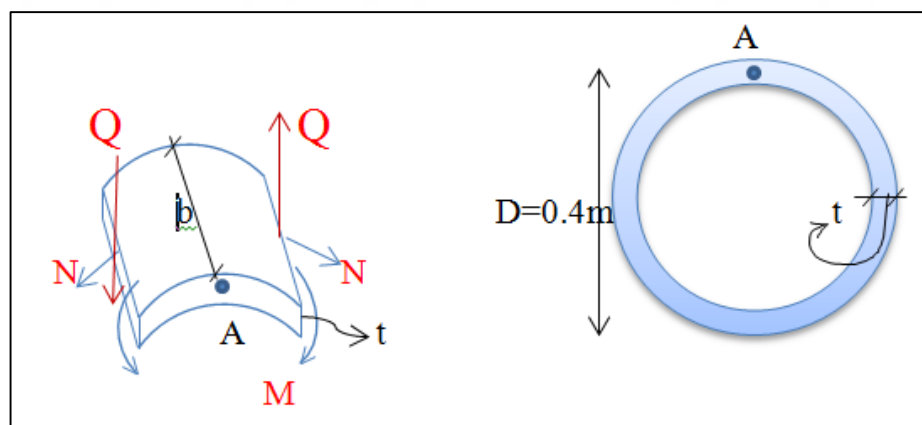
Figure 4.19: Schematic representation of axial force, shear force and bending moment applied on pipe.

Figures 4.20, 4.21 and 4.22 show the maximum and minimum values of axial force, shear force and bending moments in pipe using the plate option of PLAXIS. The values of the mentioned parameters can be obtained for each calculated phase (Plastic and Dynamic) seperately. By selecting the Envelop bottom in Output, the maximum values can be derived, and these values can be used for evaluating the pipe failure considering the pipe properties.

71

Axial forces N (scaled up 0.0500 times)

Maximum value = 0.000 kN/m (Element 4 at Node 622)

Minimum value = -12.83 kN/m (Element 24 at Node 645)

Axial forces N (scaled up 0.0500 times)

Maximum value = 1.083 kN/m (Element 16 at Node 350)

Minimum value = -23.21 kN/m (Element 26 at Node 648)
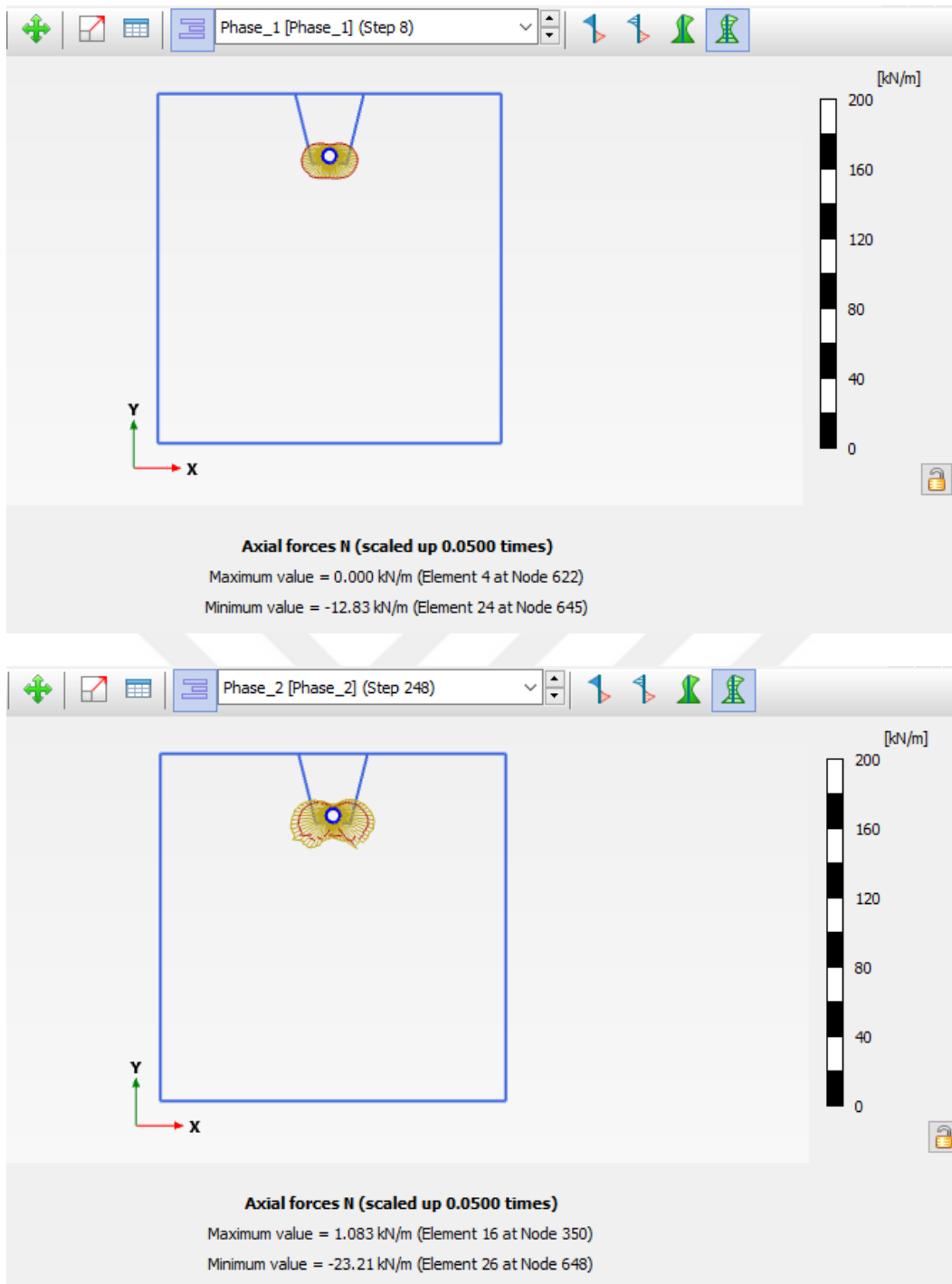
Figure 4.20: Configuration of axial forces in pipe in two phases.

As Figure 4.21 shows, the maximum and minimum shear force impose more change under dynamic load. Difference between two phases represents that the effect of earthquake on the shear force is considerable and significant in comparison to axial force and bending moment.
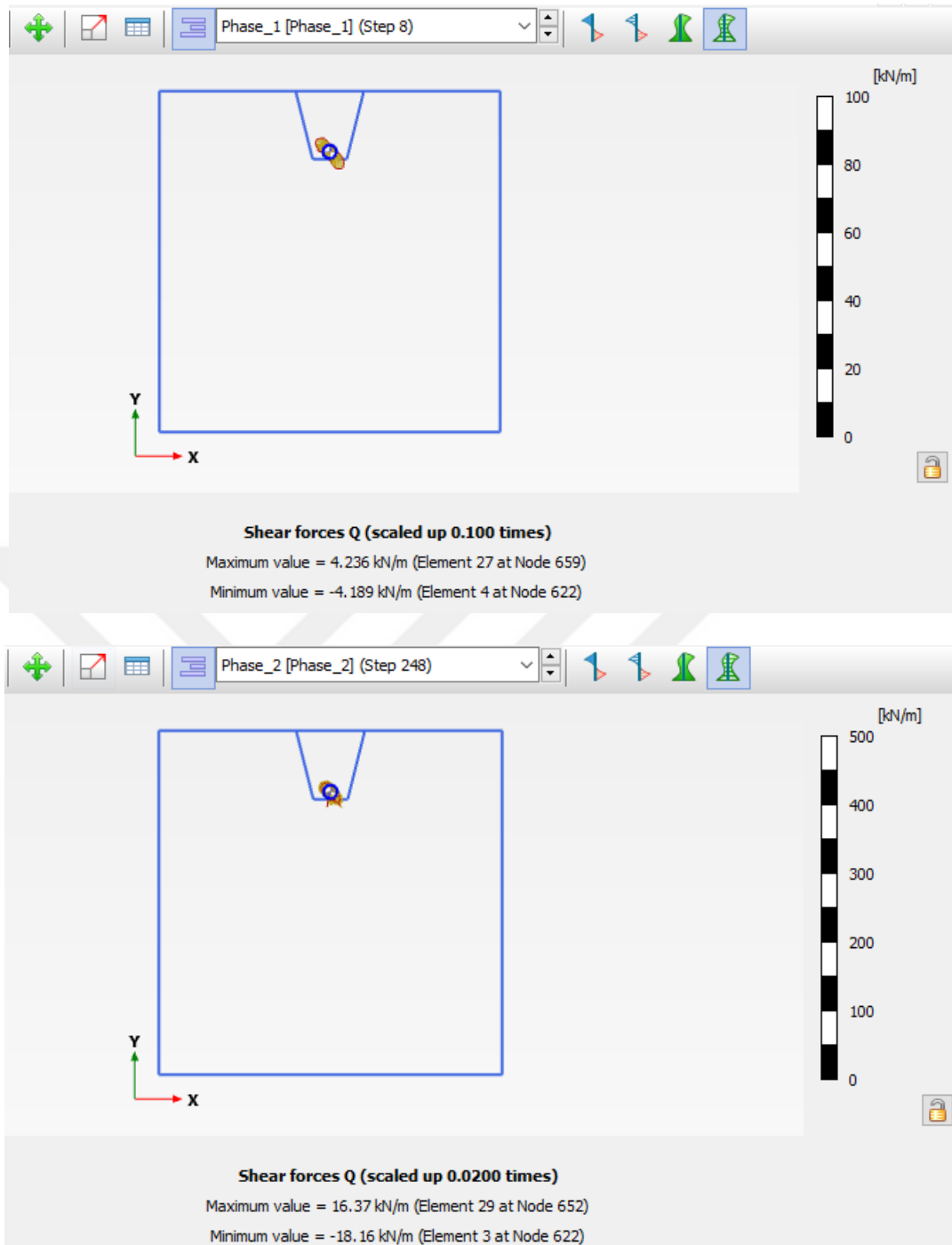
Figure 4.21: Configuration of shear forces in pipe in two phases.

The same as axial force, bending moment has the same increase in quantity in dynamic phase, around two-times of plastic value in first phase.(Figure 4.22)
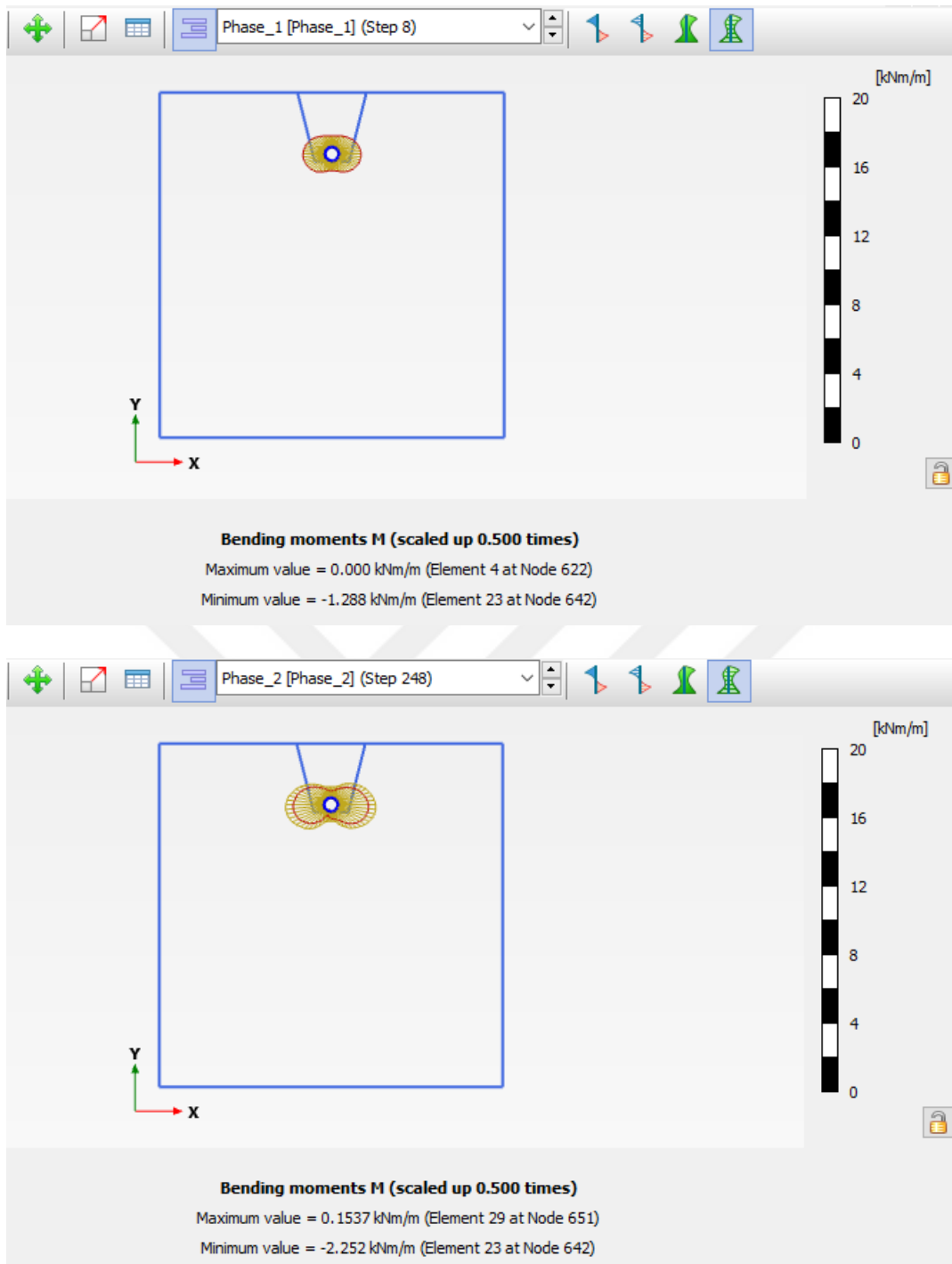
Figure 4.22: Configuration of bending moments in pipe in two phases.

Table 4.5 gives data about the values of Axial Forces, Shear Forces, and Bending moments at the points located on the pipe as plate material in PLAXIS. It can be seen that the critical point on pipe is C that has greater values in comparison to other points B and D. Also for the cited point, the values increase in dense sand, so failure probability in denser soil is higher.

Table 4.5: The values of N, Q and M on pipe in four cases.

Case	Point	N	N_{min}	N_{max}	Q	Q_{min}	Q_{max}	M	M_{min}	M_{max}
Loose Sand Soft Backfill	B	-7.67	-10.20	0.00	0.35	-1.75	2.76	-0.41	-0.80	0.00
	C	-13.28	-16.39	0.00	1.44	-1.40	2.54	-1.49	-1.73	0.00
	D	-1.51	-4.28	0.00	-0.43	-1.51	1.20	-0.54	-0.80	0.00
Loose Sand Stiff Backfill	B	-6.54	-9.01	0.00	-0.84	-2.33	3.13	-0.47	-0.88	0.00
	C	-13.27	-15.26	0.00	-0.08	-2.35	2.40	-1.38	-1.55	0.00
	D	-1.26	-4.19	0.00	0.19	-1.95	2.58	-0.50	-0.75	0.00
Loose Sand Soft Backfill	B	-7.85	-9.21	0.00	0.84	-4.48	7.19	-0.25	-0.51	0.03
	C	-15.32	-17.91	0.00	1.73	-1.75	4.78	-1.81	-2.14	0.00
	D	0.12	-2.08	1.34	-0.13	-3.05	3.55	-0.40	-0.63	0.00
Dense Sand Stiff Backfill	B	-7.41	-8.86	0.00	-0.87	-6.02	6.54	-0.33	-0.57	0.00
	C	-15.50	-18.92	0.00	1.35	-2.23	4.90	-1.77	-2.20	0.00
	D	-0.32	-2.38	0.92	-0.19	-3.32	4.10	-0.40	-0.64	0.00

According to the above data , by evaluation of all the values of N, Q and M for the four soil condition, it can be concluded that ,dense sand with stiff backfill has significant values.

4.4 Pipe Failure Analysis

The structure was modeled as elasto-plastic, in order to simulate the pipeline break PLAXIS account for plasticity through a yielding bending moment My and hoop force Ny. For the HDPE, these yielding internal forces define a rhombus shape domain in the M-N plane. On the basis of the yielding stress f_y, these stress characteristics were evaluated as (Beer et. al., 2015):

$$N_{\max allowable} = F_y * b * t \tag{4.1}$$

$$Q_{\max allowable} = F_y * b * t * 0.6 \tag{4.2}$$

$$M_{\max allowable} = \frac{b.t^2}{4} . F_Y \tag{4.3}$$

Where the base of the equivalent rectangle was b=1m and the height is the thickness t, as required by the PLAXIS input.

$N_{\max allowable}$ =(3200/0.145) *1*0.012= 264.82 kN

$Q_{\max\,allowable}$ =(3200/0.145) *1*0.012*0.6=158.90 kN

$M = \dfrac{b.t^2}{4} .F_Y$ Fy= 3200 psi (Tensile Strength Yield of pipe)

$M= \dfrac{1*(0.012)^2}{4}$ *(3200/0.145) = 0.79 kN.m/m

According above calculation the values of maximum, axial force, shear force and bending moment for each point located in pipe are 264.82 kN, 158.90 kN and 0.79 kN.m/m respectively, so if there is the greater moment of this , it would be caused to reach yielding stress and then appearing the any type of deformation and breaking.

5. CONCLUSION

The performance of buried pipeline systems in areas subjected to seismic load is an important engineering consideration for natural water, wastewater, gas and oil utility owners, because the failure of these systems can affect the public property and safety. The present study investigates the behavior of High-density polyethylene (HDPE) buried pipeline subjected to harmonic and earthquake loads using PLAXIS-2D program software, where the acceleration, displacement, spectral response acceleration and force values have been plotted against different parameters like bedding and backfill material properties, harmonic and earthquake loads. Based on the results of the figures, the following conclusions have been made.

1- Earthquake can induce significant damage to pipeline in two different processes: permanent ground deformation (PGD) and wave propagation. According to the literature and analytical investigation, it was observed that the failure caused by wave propagation in comparison to PGD is negligible.

2- Considering the fact that the amount of damping at backfill material surrounding the pipe is higher than the bedding material, the energy loss around the pipe is high. Consequently, smaller values of horizontal displacement are for soft soils, in comparison to the other points (further the backfill).

3- Under a certain harmonic loading, PSA maximum spectral acceleration response in points located at surface and free field is close to the value of PSA at the bottom of model as input motion.

4- The maximum acceleration response is observed in dense sand with stiff backfill and vice versa. The minimum acceleration response is illustrated in loose sand with soft backfill.

5- The maximum horizontal displacement values for all soil position, (different bedding and backfill) are approximately the same. However, for the points located on the pipe, there is more displacement for the point located just on the bedding, compared with the points located in other positions.

6- Unlike the horizontal displacement, the vertical displacement in loose sand is significant, regardless of the backfill materials (nearly four times more than dense value).

7- It can be said that any increase in the bending moment, above the level of maximum allowable moment, can cause failure in the pipe. This is while axial force and shear force do not have significant effect in pipe failure.

8- The comparison of two selected points close in pipe and soil (backfill) shows that relative displacement of two points is high in dense sand, so the more the slippage, the more damage will occur in denser sand.

9- By examining the amount of strain as an important factor in the assessment of the behavior of the pipes buried under the effect of dynamic weights, based on the figures indicated in the PLAXIS application, the study can conclude that the level of horizontal and vertical strain in loose sand is higher than that of dense sand.

In this study, the behavior of buried pipeline under dynamic loads was evaluated 2D software. The internal forces in pipeline can change depending on the orientation of buried pipelines according to permanent ground deformation and wave propagation direction. It can be suggested for future works, 3D model can be used to perform finite element analysis of buried subjected seismic loads.

REFERENCES

American Lifeline Alliance (ALA), 2001. Guidelines for the design of Buried steel pipe, American Society of Civil Engineering.

American Society of Civil Engineering (ASCE) (2001). Guidelines for the Design of Buried Steel Pipe. American Lifelines Alliance.

Beer, F. P., Johnston, E. R., Dewolf, J. T. and Mazurek, D. F., (2015). "Mechanics of Materials", McGraw-Hill Education, Chapter 7.

Benz. T., (2007). Small-Strain of Soils and its Numerical Consequences. University Of Stuttgart.

Brinkgreve R. B. J., (2010). Validation of empirical formulas to derive model parameters for sands.

Brinkgreve, R. B. J., (2015). Ground response analyses in PLAXIS-2D Delft University of Technology &PLAXIS, The Netherlands.

FEM-233, (1992). Earthquake Resistant Construction of Gas and Liquid Fuel Pipeline Systems Serving, or Regulated by, the Federal Government, Earthquake Hazard Reduction Series 67.

IITK-GSDMA, (2007). Guidelines for seismic design of buried pipelines.

Hall, W. and Newmark, N. (1977). Seismic Design Criteria for Pipelines and Facilities, Current State of Knowledge of Lifeline Earthquake Engineering, ASCE, New York, pp. 18-34.

Hamada, M. and O'Rourke, T. D. (1992). Large Ground Deformations and Their Effects on Lifelines, Japanese Case Studies of Liquefaction and Lifeline Performance during Past Earthquakes. Technical Report NCEER-92-0001, Multidisciplinary Center for Earthquake Engineering Research, Buffalo, New York.

Jos D. G., (2015). Interaction between pipelines and flood defenses subject to induced earthquake loads in Groningen**.**

Karamitros, D. K., Bouckovalas, G. D. and Kouretzis, G. P. (2007). Stress Analysis of Buried Steel Pipelines at Strike-slip Fault Crossings. Soil Dynamic and Earthquake Engineering, 30, 1361–1376.

Kennedy, R. P., Chow A. W. and William R. A., (1977). Fault Movement Effects on Buried Oil Pipeline. Transportation Engineering ASCE, 103, 617–633.

Kobayashi, T., Nakane, H., Suzuki N. and Shikawa, M. I., (1989). Parametric Study on Flexibility of Buried Pipeline Subject to Ground Displacement. Proceedings of second Japan-U.S. Workshop on Liquefaction, Large Ground Deformation and Their Effects on

Multidisciplinary Centre for Earthquake Engineering Research, Buffalo, New York, 348-362.

Liu, A. W. et al., (2004). An Equivalent-Boundary Method for the Shell Analysis of Buried Pipelines under Fault Movement. Acta Seismologica Sinica Vol.17, 150-156.

Liu, X. and O'Rourke. M., (1997). Seismic Ground Strain at Site with Variable Subsurface Conditions. Computer Methods and Advances in Geomechanics, (J X Yunan, Editor), AA Balkema, 2239-2244.

Newmark, N. M. and Hall, W. J. (1975). Pipeline Design to Resist Large Fault Displacements. U.S. National Conference on Earthquake Engineering Ann Arbor, Michigan, 416-425.

Meyersohn, W. D., (1991). Analytical and Design Considerations for the Seismic Responseof Buried Pipelines, Thesis, Graduate School of Cornell University.

O'Rourke, M. J., (1989). Approximate Analysis Procedures for Permanent Ground Deformation Effects on Buried Pipelines. Proceedings of the Second U.S.-Japan Workshop on Liquefaction, Large Ground Deformation and Their Effects on Lifelines, Buffalo, New York, Technical Report NCEER, 336-347.

O'Rourke, T. D. and Lane, P. A., (1989). Liquefaction Hazards and their Effects on Buried Pipelines. Technical Report NCEER-89-0007, National Center for Earthquake Engineering Research, Buffalo, New York.

O'Rourke, T. D. and Tawfik, M. S., (1983). Effects of Lateral Spreading on Buried Pipelines during the 1971 San Fernando Earthquake. Earthquake Behavior and Safety of Oil and Gas Storage Facilities, Buried Pipelines and Equipment, PVP-77, ASME, 124132.

O'Rourke, T. D., and Palmer, M. C., (1996). Earthquake Performance of Gas Transmission Pipelines. Earthquake Spectra 20(3), 493-527.

O'Rourke, M. J. and Ayala, G. (1993). Pipeline Damage Due to Wave Propagation. Journal of Geotechnical Engineering 119(9), 1490-1498.

O'Rourke M. J. and Liu, X., (1994). Failure Criterion for Buried Pipe Subject to Longitudinal PGD: Benchmark Case History. Proceeding of 5th U.S.-Japan Workshop on Earthquake Resistant Design of Lifeline Facilities and Countermeasures Against Soil Liquefaction, Tech, 639-651.

O'Rourke, M. J. and Liu, X. (1999). Response of Buried Pipelines Subjected to Earthquake Effects. MCEER Monograph No.3. University at Buffalo, New York.

PLAXIS-2D, (AE)(2014), Tutorial manual., www.plaxis.nl.

Radan, I., (2000). Analysis of Jointed Pipelines Crossing Faults by a Purpose-Made Specialized Program. No.7, 203-212.

Rajkumar, R. and Ilamparuthi, K., (2008). Experimental Study on the Behavior of Buried Flexible Plastic Pipe. EJGE 13: 1-10.

Ramberg W. and Osgood W. R., (1943). Description of Stress-Strain Curves by Three Parameters. Technical Note No. 902, National Advisory Committee For Aeronautics, Washington DC.

Toprak, S. and Taskin, F., (2006). Estimation of Earthquake Damage to Buried Pipeline Caused by Ground Shaking. Natural Hazards, 40, 1-24.

Suzuki, N., Arata, O. and Suzuki, I., (1988). Parametric Study of Deformation Analysis of Welded Pipeline Subject to Liquefaction-Induced Permanent Ground. Proceeding of first Japan-US Workshop on Liquefaction, Large Ground Deformation and their effects on Lifeline Facilities, 155-162.

Takada, S., Liang, J. and Li, T. (1998). Shell-Model Response of Buried Pipelines to Large Fault Movements. Journal of Structural Engineering. JSCE, 44, 1637-1646.

Trautmann, C. H. and O'Rourke, T. D. (1985). Lateral Force–Displacement Response of Buried Pipe. Geotechnical Engineering, ASCE 111(9), 1068-1075.

Tsai, J. S., et al., (2000). Damage to Buried Water Supply Pipelines in the Chi-Chi (Taiwan) Earthquake and a Preliminary Evaluation of Seismic Resistance of Pipe Joints. Journal of the Chinese Institute of Engineering, Vol.23, Issue 4, 395-408.

USGS, (2008). Oil and Gas Pipeline. The Shakeout Scenario Supplemental Study Circulation 1150, report 25, version 1.0, 207 version 1.0.

Wai-Fah C. and Charles S., (2003). Handbook of Structural Engineering. CRC PRESS Boca Raton.

Wang, L. R. L. and Yeh, R. (1985). A Refined Seismic Analysis and Design of Buried Pipeline for Fault Movement. Earthquake Engineering and Structural Dynamics, Vol. 13, 75-96.

Wells, D. L., and Coppersmith, K. J. (1994). Updated Empirical Relationships among Magnitude, Rupture Length, Rupture Area and Surface. Displacement, Bulletin of the Seismological Society of America, Vol. 84, No. 4, 974-1002.

CURRICULUM VITAE

Name Surname: Ehsan YAHYAVI ZANJANI

Place and Date of Birth: Iran,Zanan 21.03.1979

E-Mail: eyahyavi@itu.edu.tr

B.Sc.: Civil Engineering , Azad University Of Zanjan